Alma Mater Studiorum - Università di Bologna

Facoltà di Scienze Matematiche Fisiche e Naturali

Scuola di Dottorato in Scienze Biologiche, Biomediche e Biotecnologiche

Dottorato di Ricerca in Biologia Funzionale dei Sistemi Cellulari e Molecolari

Ciclo XX

Settore scientifico disciplinare di afferenza: BIO/10

Il centro di reazione fotosintetico batterico
in ambiente nativo ed artificiale:
effetti sul trasferimento elettronico

(The photosynthetic bacterial reaction center in native and artificial

envirnoments: effects on light-induced electron transfer)

PhD student: *Tutor:*
Dott. ssa MANUELA DEZI   **Chiar. mo Prof. GIOVANNI VENTUROLI**

PhD Coordinator:
Chiar. mo Prof. VINCENZO SCARLATO

Academic Years 2005/2007

Alma Mater Studiorum - Università di Bologna

Facoltà di Scienze Matematiche Fisiche e Naturali

Scuola di Dottorato in Scienze Biologiche, Biomediche e Biotecnologiche

Dottorato di Ricerca in Biologia Funzionale dei Sistemi Cellulari e Molecolari

Ciclo XX

Settore scientifico disciplinare di afferenza: BIO/10

Il centro di reazione fotosintetico batterico in ambiente nativo ed artificiale: effetti sul trasferimento elettronico

(The photosynthetic bacterial reaction center in native and artificial environments: effects on light-induced electron transfer)

PhD student:
Dott. ssa MANUELA DEZI

Tutor:
Chiar. mo Prof. GIOVANNI VENTUROLI

PhD Coordinator:
Chiar. mo Prof. VINCENZO SCARLATO

Key Words: reaction center, core complex, electron transfer, cardiolipin, trehalose

Academic Years 2005/2007

C o n t e n t s

1   INTRODUCTION

1.1   Photosynthetic bacteria

Sun light is one of the most important energy source on earth. Plants together with particular bacterial and algal groups can perform conversion of the light energy, gained by the absorption of a photon, in chemical energy. They store this energy in the form of phosphoester bonds at high quantum yield (larger than 98%). In order to catch photons energy a sophisticated photosynthetic machinery was developed involving pigment-protein complexes organized in cellular membranes. Though the different strategies used, common features can be recognized in photosynthesis in plants, algae and bacteria. It is established, in fact, that the primary photochemistry involves the transfer of an electron from an excited chlorophyll (Chl) or bacteriochlorophyll (BChl) molecule to some sort of electron acceptor molecule (A) and the $Chl^+ A^-$ state initiates the subsequent electron transfer processes. The maximum photon absorption is achieved thanks to the antenna protein structures, containing a high concentration of pigments whose primary function is to collect photons and funnel excitation energy to the reaction center (RC), the pigment-protein complex involved in the primary electron transfer event. Chlorophyll a/b/c are the main photosynthetic pigments and absorb blue and red light. Other pigments, like carotenoids or phycobilins, called accessory pigments, absorb light at different wavelengths. They do not participate directly in photosynthetic reactions but are able to pass their energy to chlorophyls. Purple and green bacteria contain bacteriochlorophyls that absorb in the infrared region at wavelength above 700 nm. The combination of all of the pigments increases the spectral range that photosynthetic organisms can use in photosynthesis.

Photosynthetic organisms can be divided in two main groups depending on the electron source utilized to reduce the CO_2: the oxygenic photosynthetic organisms like plants and algae that utilize water releasing oxygen in the atmosphere, and the anoxygenic photosynthetic organisms that oxidize other inorganic or organic molecules. Different electron transfer chains correspond to different photosynthetic apparatuses. Being characterized by a relatively simple apparatus, the photosynthetic bacteria offer the most useful model system for studying the primary events of photosynthesis, *i.e.*

excitation energy transfer within the RC-antenna system and the electron transfer steps catalyzed by the RC.

Anoxygenic photosynthetic bacteria have been previously classified into three families of purple bacteria and two families of green bacteria, but in a more recent classification based on ribosomal ribonucleic acid studies, purple bacteria and their relatives have been grouped in the new class of Proteobacteria, subdivided into four sub-groups, called α, β, γ, δ (Woese, 1987). Purple bacteria have been studied intensively, offering a number of advantages to the experimentalists: they contain a single photosystem, they can grow photoheterotrophically or chemotrophically in darkness under aerobic conditions and, most importantly, pigment-protein complexes can be isolated to a high degree of purity. In this group of bacteria most of the photosynthetic proteins are located within the invagination of the intra cytoplasmic membrane (ICM) that are physically connected to, but functionally distinct from the cytoplasmic membrane (CM). These invaginations network can assume different shape like vesicles, tubules, thylakoid-like flat lamellae (Oelze *et al.*, 1972). Following cell disruption procedures, the connection between the invaginations breaks up and single vesicles or lamellae with an inverse orientation of the membrane components respect to the CM can be obtained, called "chromatophores". The amount of chromatophores is strictly tuned by the oxygen tension and the light intensity: the extension of the ICM systems increases under semiaerobic condition in the darkness or switching to phototrophic growth condition but at low light intensity (Holt *et al.*, 1965). The presence of light partially inhibits the synthesis of the respiratory chain enzymes located in the CM. The respiratory capacity represents an alternative resource when photosynthetis is unfavoured by environmental conditions.

1.2   The photosynthetic bacterial reaction center

As mentioned in the previous chapter the photosynthetic apparatus of purple bacteria is located in the ICM. *Rhodobacter (Rb.) sphaeroides*, a purple-non sulphur bacterium, member of the proteobacteria α-subgroup, is one of the best-characterized photosynthetic organisms and its photosynthetic apparatus has become a reference

model in studying the primary processes of photosynthesis. The reaction center is the key protein in the photosynthetic machinery as upon direct excitation by light or transfer of the energy from the antenna systems, an excited singlet state of the primary electron donor is created. This event leads to the subsequent electron transfer processes coupled to the pumping of protons across the energy transducing membrane. The resulting electrochemical potential of protons drives the synthesis of ATP via a chemiosmotic circuit, enabling the transformation of electromagnetic energy into chemical energy (Cramer *et al.* 1990). The crystal structure of the RC from *Rb. sphaeroides* has been determined at atomic resolution (Allen *et al.*, 1987a and b). Following these pioneering studies a number of x-ray structures at improved resolution, obtained using different crystallization protocols, have been reported (Ermler *et al.*, 1994; Katona *et al.*, 2003).

1.2.1 Structure

The central core of the RC is composed of two proteins both containing 5 trans-membrane α-helices (named A, B, C, D and E), called L (light) and M (medium) according to their apparent molecular weight of 21 and 24 kDa respectively (see **Fig. 1.1**). At the cytoplasmic side a third subunit, H (heavy, 28 kDa) characterized by a large globular domain, is anchored by a membrane spanning helix to the LM complex. The function of the H subunit has not been fully clarified. It is most likely involved in: (a) protection of the Q_A-binding site from a cytoplasmic contact; (b) stabilization of the RC structure; and (c) H^+ uptake and transfer associated with electron transfer to the quinones. There are, also, evidences of an involvement in reaction center assembly (Chory *et al.*, 1984). The L and M subunits bind the photosynthetic pigments (cofactors) that are: 2 bacteriochlorophyill molecules forming the so called "special pair" (P), 2 accessory bacteriochlorophyll molecules, 2 bacteriopheophytin molecules, one ubiquinone which acts as first electron acceptor Q_A, and a second ubiquinone Q_B which is the final electron acceptor. Cofactors are arranged around the axis of a 2-fold symmetry in two branches forming a sort of triangular disposition with a vertex in the special pair close to the periplasmic side, and the quinone molecules at the opposite cytoplasmic side. Halfway between quinones a non-heme iron atom is located, coordinated by four His residues belonging to the D and E helices of both L and M subunits (see **Fig. 1.1**). The 2-fold symmetry axis connects the center of the special pair

P with the Fe atom. Not all the pigments are involved in the light-driven electron transfer and, according to the nomenclature proposed by Hoff (1988), we distinguish the A (active) branch close to the L subunit from the B (inactive) branch. In branch A cofactors exhibit a spatial organization that confers them a higher rigidity possibly favouring the forward electron transfer reactions.
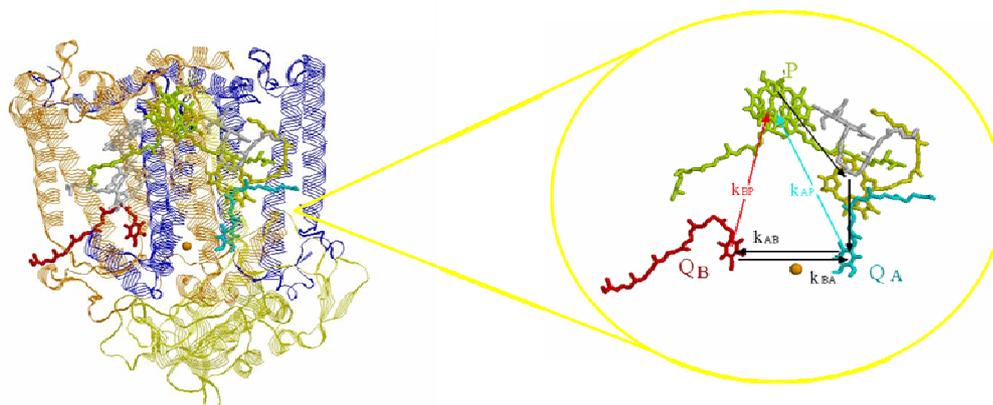
Fig. 1.1 Cartoon model of RC structure with its subunits: the L in blue, M in brown, H in dark yellow; the cofactors belonging to branch A are shown enlarged on the right. P is the special bacteriochlorophyls pair, the accessory bacteriochlorophyls is the grey molecule, while the bacteriopheophytin is yellow, Q_A (cyan) and Q_B (red) are the quinone acceptors molecules. The arrows indicate pathway of the electron transfer.

Within the RC, the bacteriochlorophyll special pair (P), facing the periplasmic side of the membrane, acts as the primary electron donor: upon light excitation it delivers an electron, via a bacteriopheophytin molecule to Q_A. The primary charge separated state ($P^+Q_A^-$), generated in about 200 ps, is then stabilized by electron transfer from Q_A^- to a second ubiquinone molecule bound at the Q_B site of the RC. This process occurs over a time scale of 20-200 μs. *In vitro*, when no physiological or artificial electron donor is available to re-reduce flash generated P^+, the electron on Q_B^- recombines with the hole on P^+, restoring the initial ground state of the RC. *In vivo*, the photoxidized donor, P^+, is rapidly re-reduced by a soluble c-type cytochrome, so that a second charge separation can take place across the RC, leading to the double reduction and protonation of Q_B to ubiquinol (QH_2) (Okamura *et al.*, 2000). The ubiquinol molecule leaves the RC and is replaced at the Q_B site by oxidized ubiquinone (UQ) from a pool present in stoichiometric excess over the RC.

1.2.2 *The light-induced electron transfer reactions*

The charge separation and recombination events following light excitation in the isolated RC can be described by the following reaction scheme (Kleinfeld *et al.* 1984b; Rubin *et al.* 1984):

$$PQ_AQ_B \underset{k_{AP}}{\overset{h\nu}{\rightleftarrows}} P^+Q_A^-Q_B \underset{k_{BA}}{\overset{k_{AB}}{\rightleftarrows}} P^+Q_AQ_B^- \qquad (1.2.1)$$

$$k_{BP}$$

The state $P^+Q_A^-Q_B$ can either recombine yielding the ground state PQ_AQ_B with a rate constant $K_{AP} \approx 10$ s^{-1} or, in the presence of ubiquinone bound at the Q_B site, yield $P^+Q_AQ_B^-$. Under physiological conditions, the state $P^+Q_AQ_B^-$ is stabilized with respect to $P^+Q_A^-Q_B$ by 70 meV and, since $(k_{AP} + k_{BA}) \approx 10^4$ s^{-1} $>> k_{AP}$, electron transfer to Q_B occurs with an extremely high quantum efficiency (Kleinfeld *et al.*, 1984b). The state $P^+Q_AQ_B^-$ recombines slowly (lifetime ≈ 1 s) essentially via the intermediate $P^+Q_A^-Q_B$ state, with the direct route (k_{BP}) being negligible at room temperature (Kleinfeld *et al.*, 1984b; Labahn *et al.*, 1995). Under the condition k_{AB}, $k_{BA} >> k_{AP,}$ scheme 1.2.1 predicts an observable rate constant k for charge recombination given by:

$$k = \frac{\left(k_{AP} + k_{BP}L_{AB}\right)}{\left(1 + L_{AB}\right)} \qquad (1.2.2)$$

Where $L_{AB} = k_{AB}/k_{BA}$ is the equilibrium constant for electron transfer from Q_A^- to Q_B.

As deeply discussed in detail by Shinkarev and Wright (1993), the back reaction is also affected by the binding equilibrium of the quinone at the Q_B site. In fact several observations occur to indicate that a fast quinone exchange occurs at the Q_B site (Shinkarev *et al.*, 1993). In particular, it has been shown that the rate constant k of charge recombination decreases when the concentration of ubiquinone in equilibrium at the binding site increases (Mallardi *et al.*, 1997) To better understand the role of the quinone exchange on the electron transfer processes, the previous simplified scheme 1.2.1 can be modified as shown in scheme 1.2.3 (Wraight, 1981; Wraight and Stein,

1983; Schinkarev *et al.* 1984), in which the binding of quinone at the Q_B site is explicitly considered:

$$PQ_AQ_B \underset{k_{AP}}{\overset{hv}{\rightleftarrows}} P^+Q_A^-Q_B \underset{k_{BA}}{\overset{k_{AB}}{\rightleftarrows}} P^+Q_AQ_B^-$$

with k_{BP} above, and vertical equilibria k_{BQ}^*/k_{QB}^* and k_{BQ}/k_{QB} down to:

$$PQ_A \underset{k_{AP}}{\overset{hv}{\rightleftarrows}} P^+Q_A^-$$

(1.2.3)

The rate constants k_{BQ} and k_{BQ}* are the true first-order rate constants, while k_{QB} and k_{QB}^* are the pseudo-first-order rate constants for binding of pool quinones to the Q_B site, *i.e.*, $k_{QB} = k_{QB}'[Q]$ and $k_{QB}^* = k_{QB}^{*'}[Q]$, being $[Q]$ the ubiquinone concentration. When the quinone exchange is fast at the Q_B site (Palazzo *et al.*, 2000, Shinkarev *et al.*, 1984b), and electron transfer between Q_A and Q_B is much faster than all other reactions of the scheme (so that a quasi equilibrium between $P^+Q_A^-Q_B$ and $P^+Q_AQ_B^-$ is established (Croft *and* Wraight 1983; Kleinfeld *et al.* 1984b; Okamura *et al.* 2000)), scheme 1.2.3 predicts an observed rate constant for charge recombination given by:

$$k \cong \frac{\left(k_{AP} + k_{BP}L_{AB}\dfrac{K}{1+K}\right)}{\left(1 + L_{AB}\dfrac{K}{1+K}\right)}$$

(1.2.4)

where $K = k_{QB}'[Q]/k_{BQ}$ is the dimensionless equilibrium constant of quinone binding at the Q_B site in the $P^+Q_A^-$ state. According to eq. 1.2.4 an increase in the quinone concentration associated with the RC will result in a decrease of the observed rate constant k, when $k_{BP} < k_{AP}$ (a condition which has been shown to be largely satisfied (Schmid and Labhan, 2000)). Under saturating quinone concentration, *i.e.* for $[Q] \rightarrow \infty$, the rate constant will approach a minimal value, which coincides with that given by eq. 1.2.2. From the observations summarized above it appears that the analysis of the charge recombination processes can yield a wealth of information, on the energetics of

the electron transfer events involving Q_A and Q_B on the binding of quinone at the Q_B site.

The protein environment and the electrochemical properties of Q_A and Q_B differ substantially. Q_A is tightly bound to the protein and acts practically as a prosthetic group while Q_B can freely exchange with the pool in the membrane bilayer. Under physiological conditions Q_A accepts only a single electron while Q_B is doubly reduced. The protonation of the doubly reduced UQ at the Q_B site takes place in two separated steps during the transfer of the second electron from Q_A to Q_B. Both the primary and the secondary acceptors are buried inside the RC, bound at the level of the lipid headgroups at the cytoplasmic side of the membrane and do not have any contact with the aqueous environment. Protons are delivered from the cytoplasm to Q_B mainly along two pathways composed of hydrogen-bond networks involving titratable residues and water molecules (Koepke *et al.*, 2007). These "proton channels", ending respectively close to the glutammic acid residue L212 and the aspartic acid L213, each delivers a proton to Q_B after its reduction. The first electron transfer from $P^+Q_A^-$ to Q_B is coupled to protonation of the residue L212, due to electrostatic interactions (Maroti *et al.* 1988, McPherson *et al.*, 1988), while the first protonation of the reduced quinone occurs during the second electron transfer from Q_A^- to Q_B forming the intermediate $(Q_BH)^-$. The second protonation involves internal transfer of a proton from L212 to $(Q_BH)^-$ leading to the formation of Q_BH_2.
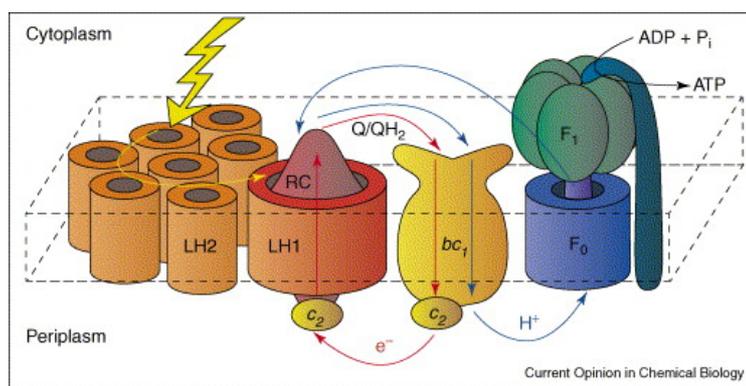

Fig. 1.2 ICM representation. Scheme of the integral protein complexes involved in the coupled electron-proton transfer across the membrane of *Rb. sphaeroides* (from Scheuring, 2006a).

In vivo, the UQH_2 molecule and oxidized cyt c_2 generated by the RC are utilized by the cytochrome bc_1 complex as reductant and oxidant, respectively, resulting in a cyclic electron transfer chain which pumps protons from the cytoplasmic to the periplasmic side of the membrane (Crofts *et al.*, 1983b; Cramer *et al.*, 1990) as represented schematically in **Fig. 1.2**.

1.3 The coupling between electron transfer and RC internal dynamics

Proteins are characterized by a complex conformational dynamics. The wide range of internal motions they experience at physiological temperatures originates from rugged energy landscapes (**Fig. 1.3**), which feature an extremely large number of minima corresponding to different conformational substates (Frauenfelder *et al.*, 1991; Frauenfelder *et al.*, 1994; Gafert *et al.*, 1995; Parak *et al.*, 2003; Hofmann *et al.*, 2003b). The ability of the protein to perform structural fluctuations among many different conformational substates appears to be intimately connected to protein function (Frauenfelder *et al.*, 1998; Fenimore *et al.*, 2002; Bourgeois *et al.*, 2003).
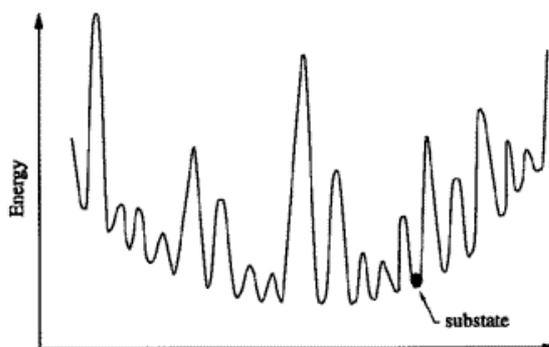
Fig. 1.3 A highly simplified one-dimensional cross section through the energy landscape of a protein. The abscissa corresponds to a conformational coordinate. Each valley represents one particular conformation, called a conformational substate. Fluctuation between a number of substates occur at physiological temperatures (from Frauenfelder *et al.*, 1998).

The photosynthetic reaction center from purple bacteria is becoming a paradigmatic system in the study of the relationship between electron transfer processes and protein conformational dynamics. In fact, a large number of experimental findings indicates that the electric field generated by light induced charge separation within the RC perturbs substantially the protein giving rise to conformational changes, which in

turn affect the electron transfer kinetics (see e.g. ref. Arata *et al.*, 1981; Kleinfeld *et al.*, 1984a; Nabedryk *et al.*, 1990; Brzezinski *et al.*, 1995; McMahon *et al.*, 1998). A basic strategy to gain insight into the coupling between electron transfer and protein motions consists in modulating the rate of conformational relaxations and the interconversion among protein conformational substates by changing the temperature. Fundamental information was obtained by comparing the kinetics of electron transfer in RCs frozen at cryogenic temperatures in the dark and under illumination. These studies have unambiguously shown that RCs can be trapped at cryogenic temperatures in a *dark-adapted* and a *light-adapted* conformation, which drastically differ in the stability of the primary charge separated state $P^+Q_A^-$. Each conformation is characterized by a large distribution of substates, as inferred from the strongly distributed, non exponential kinetics of $P^+Q_A^-$ recombination at cryogenic temperatures (Kleinfeld *et al.*, 1984b; McMahon *et al.*, 1998). According to the dynamic model proposed by Nienhaus and coworkers (McMahon *et al.*, 1998), at physiological temperatures, the RC protein, following light-induced transition to the $P^+Q_A^-$ state, relaxes rapidly from the *dark-adapted* to the *light-adapted* conformation by solvating the altered charge distribution.
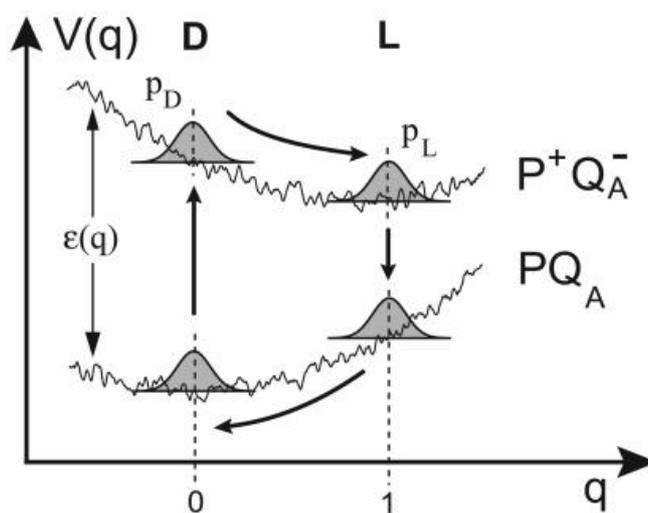

Fig. 1.4 Schematic depiction of the rugged energy surfaces in the neutral (PQ_A) and charge-separated ($P^+Q_A^-$) states of RCs. The energy gap, ε, which controls the electron transfer rates, varies as a function of the conformational coordinate, q (modified from McMahon *et al.*, 1998).

As shown in **Fig. 1.4**, this relaxation is accompanied by a decrease in the energy gap between $P^+Q_A^-$ and the neutral state PQ_A, which is reflected in a decrease of the electron transfer rate, *i.e.* in a stabilization of the charge separated state. At room temperature, the RC protein rapidly samples the distribution of conformational substates and averaging of the corresponding rate distribution over the time scale of charge recombination gives rise to an almost exponential kinetics of $P^+Q_A^-$ recombination (McMahon *et al.*, 1998).

In the last few years several studies shed further light also on the coupling between RC dynamics and electron transfer from the photoreduced Q_A^- to Q_B. The rate of this process was found to be independent of the associated redox free energy change (Graige *et al.*, 1998), demonstrating that the reaction is not rate-limited by electron transfer itself, but gated by some other process. The structural basis for the conformational gating of interquinone electron transfer remain at present an unresolved issue, but a few structural aspects of the underlying energy landscape have been enlighten by recent studies combining structural, spectroscopic, mutational and computational approaches. X-ray diffraction structures purposely determined for reaction centers frozen in the dark and under the light have shown the secondary quinone Q_B in two distinct positions, the "distal" and the "proximal" site (Stowell *et al.*, 1997). In the "proximal" site Q_B had shifted by approximately 5 Å and undergone a 180° rotation of the headgroup, moving closer to Q_A This led Stowell *et al.* (1997) to propose the distal and proximal position as inactive and active conformations with respect to interquinone electron transfer. Other available X-ray diffraction structures of the Q_B site reported by different groups are distributed between these two positions with a tendency to concentrate around the distal and proximal site (Stowell *et al.*, 1997; Walden *et al.*, 2002; Rahaman *et al.*, 2004). A recent X-ray diffraction study, in which the best resolution ever reported for the RC was achieved (1.87 Å), has confirmed the existence of two different binding positions of the secondary quinone, a distal and a proximal one, observed in the neutral and in the charged separated state, respectively (Koepke *et al.*, 2007). However, at variance with what found by Stowell *et al.* (1997), a new orientation of Q_B in its distal position was observed, which shows no ring-flip compared to the orientation in the proximal position (**Fig. 1.5**).
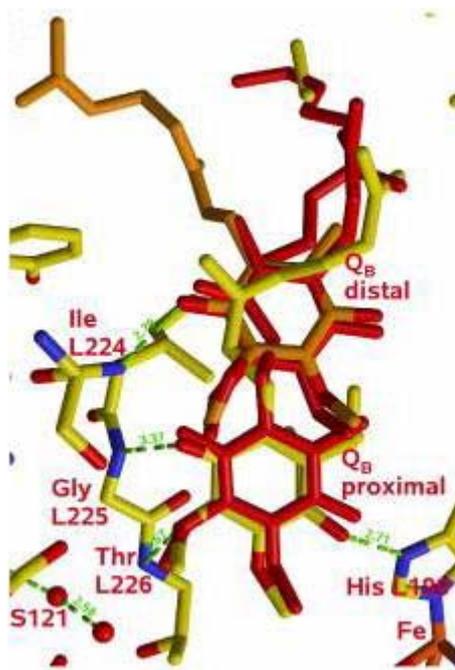
Fig. 1.5 Super position of the L-, D- adapted quinone position and colored in yellow and orange respectively with the structure from Stowell et al. (1997) of the same state and at the same pH, shown in red.

Computational works (Alexov *et al.*, 1999; Rabenstain *et al.*, 2000) have verified that electron transfer to Q_B is thermodynamically unfavorable in the distal compared to the proximal state and has suggested that migration of Q_B from the distal to the proximal position is related to the protonation state of two nearby residues (Grafton *et al.*, 1999) and to the orientation of residue L212 side chain (Walden *et al.*, 2002). A recent attempt to calculate a two dimensional potential energy surface for Q_B binding (Rahaman *et al.*, 2004) resulted in a rugged energy landscape displaying several minima, including a global minimum in good agreement with structural features of the proximal binding site and with FTIR data (Breton *et al.*, 2002). Although binding at the proximal position is likely to be a prerequisite for interquinone electron transfer, that the large quinone shift from the distal to the proximal position represents *per se* the rate-limiting conformational gating step is still an open question. For example, recent studies have shown that a RC mutant having Q_B locked predominantly in the proximal site (Kuglstatter *et al.*, 2001) still exhibit a significant energy barrier to electron transfer to Q_B (Xu *et al.*, 2002), suggesting that motion other than quinone translation must be rate limiting. Moreover

Fourier transform infrared spectroscopy has shown that the H-bonding pattern and Q_B interactions do not change upon photoreduction, arguing against a large scale translation in the position of Q_B as the gating step for interquinone electron transfer (Breton *et al.*, 2004).

It appears at present that different types of reorganization in addition to the movement of Q_B are likely to affect significantly the energetics of electron transfer to Q_B and to play a predominant role in gating the electron transfer process. They include small scale dielectric responses of protein residues, internal proton displacements, changes in site occupancy and orientation of water molecules in the channels connecting Q_B to the RC surface and rearrangements in intraprotein networks of hydrogen bonds (Stowell *et al.*, 1997; Graige *et al.*, 1998; Alexov *et al.*, 1999; Cherepanov *et al.*, 2001; Xu *et al.*, 2002a; Xu *et al.*, 2002b).

1.4 The antenna system

As in most species of photosynthetic purple bacteria, in *Rb. sphaeorides* the light harvesting system is made up of two light harvesting antenna complex (Cogdell *et al.*, 2006): the inner light-harvesting complex (LH1 complex) and the peripheral antenna (LH2 complex). The secondary antenna complex, LH2, and the RC surrounded by the primary antenna complex,*i.e.* RC-LH1, can be isolated by a mild solubilization (Octyl glucoside (OG) and Sodium Cholate (NaCholate)) of the ICM membranes (Francia *et al.*, 1999). The antenna pigment-protein complexes are fundamental for the conversion of light energy into an electrochemical transmembrane potential difference of protons. They, in fact, harvest sunlight and, through a series of energy transfer within and between complexes, they make the excitation energy available to the RC protein. Recently, by exploring single-molecule fluorescence techniques, the energy transfer process has been observed in a single self-aggregated photosynthetic unit formed by a peripheral antenna complex LH2 from *Rhodopseudomonas* (*Rps.*) *acidophila* and a RC-LH1core complex from *Rb. sphaeroides* (Hofmann *et al.*, 2003a).

In the ICM the LH1 is present in a fixed stoichiometry with the RC forming the so called *core* complex. On the contrary the LH2 level varies with the irradiance and oxygen tension, so that the ratio between LH2 and RC-LH1 strongly depends on the

growth conditions. The availability of high–resolution crystallographic structures of the peripheral antenna complexes LH2 from the purple bacteria *Rps. acidophila* and *Rhodospirillum (Rs.) molischianum* (McDermott *et al.*, 1995, Koepke *et al.,* 1996 and Papiz *et al.*, 2003) has greatly contributed to the understanding of the photosynthetic light-harvesting mechanism. It also allowed to develop model structures for LH2 systems of different species, for which crystal diffracting at high resolution have not yet been obtained. Although there are no crystal structures of the LH2 from *Rb. sphaeroides*, the Atomic Force Microscopy (AFM) images of two-dimensional crystals (Scheuring *et al,.* 2003) and homology to the LH2 complex of *Rps. acidophila* allow to construct a reasonable model for the LH2 antenna of *Rb. sphaeroides*.

Both the LH2 and LH1 antenna complexes are assembled from very similar building units containing non-covalently bound carotenoid and bacteriochlorophyll a (BChl *a*) molecules. Bchl molecules are characterized by transition dipoles which due to an appropriate relative orientation, can promote extremely fast resonance energy transfer across relatively long distance. The major singlet transition dipoles, differing due to the asymmetry of the conjugated structure, are denoted Q_x and Q_y.

1.4.1 The LH2 complex

The LH2 antenna structures are oligomers of two hydrophobic low molecular mass (5-7 kDa) apo-proteins called α and β (the α-polypeptide on the inner and the β-polipeptide on the outer side of the complete ring structure, see below), both of which have a single membrane-spanning helix. In *Rb. sphaeroides* the peripheral antenna LH2 is arranged as a symmetric ring formed by 9 (α,β) units each containing one carotenoid and three BChl *a* molecules. Two spectral forms of bachteriochlorophyls are present due to their different protein environment: these two forms are called B800 and B850 according to their absorption maxima. The 18 B850 bacteriochlorophyll molecules, coordinated by highly conserved His residues, close to the C-terminal of the (α,β) apo-proteins form a ring of tightly coupled pigments. Their tetrapyrrolic planes are perpendicular to the membrane plane. The B800 bacteriochlorophyll molecules are close to the cytoplasmic side of the membrane, located between the N-terminus transmembrane helices of neighboring β apo-protein, and form a second ring of nine

weakly interacting pigments, with their tetrapyrrolic structures parallel to the membrane plane (**Fig. 1.6**).
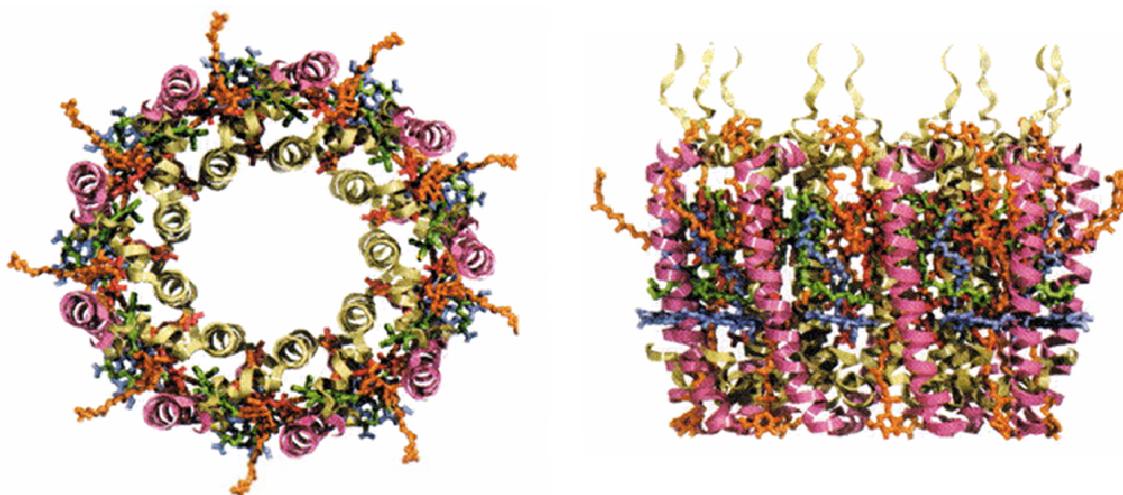

Fig. 1.6 Structure of the LH2 antenna system Schematic representation of the overall structure of the LH2 from *Rps. acidophila*, based on 2.0 Å resolution x-ray diffraction (Cogdell *et al.*, 2003). The left picture shows a view along the normal to the membrane plane. On the right a view of the complex from "within the membrane", looking along the membrane plane, is shown. Between the α- (dark yellow) and the β- (purple) polypeptides there are the B800 ring (blue), the B850 (alternatively red and green) and the carotenoid molecules (orange) are visible.

Different types of carotenoid molecules were isolated from different strains of *Rb. sphaeroides*: spheroidene in the anaerobically grown 2.4.1 strain, spheroidenone in the semiaerobically grown 2.4.1 strain, neurosporene in the G1C strain, a mix of neurosporene, chloroxantin and 3,4-dihydrospheroidene in Ga strain. The structure of the binding site of the carotenoid molecules is highly dependent on the bacterial strain and on the chemical nature of the molecule itself (Gall *et al.*, 2003). Carotenoid molecules have both a functional and a structural role in the antenna systems. They primarily act by collecting, absorbing photons and transferring excitation energy to the BChl molecules. A photon-induced transition from the ground state (S_0) to the first singlet state (S_1) is optically forbidden, so the absorption band in the visible region are due to a transition from the ground state to the second excited singlet state ($S_0 \rightarrow S_2$). Carotenoid singlet excitation energy transfer mainly occurs from the S_2 state with more than 90% transfer efficiency and the remainder from the carotenoid S_1 state after radiationless relaxation from $S_2 \rightarrow S_1$, (Freer *et al.*, 1996). The energy transfer processes

involve both B850 and B800 BChls but the final acceptor state is the B850 Q_y level, the lowest singlet excited state in the complex (**Fig. 1.7**).

Under redox conditions in which the quinones are reduced, or in RCs lacking quinones, the primary photochemistry is blocked, and RCs can form a triplet state on P. The triplet state that forms on P is quenched by the bound carotenoid, and this is an essential function of this molecule. Indeed, in general, when BChl triplet states are formed by illumination in an aerobic environment, a singlet state of oxygen may be produced. This state of molecular oxygen is a powerful oxidizing agent capable of killing cells by inducing damage to proteins, lipids, and DNA. Carotenoids prevent oxidative destruction by rapidly quenching the sensitizing triplets before they can initiate this route of photo-impairment.
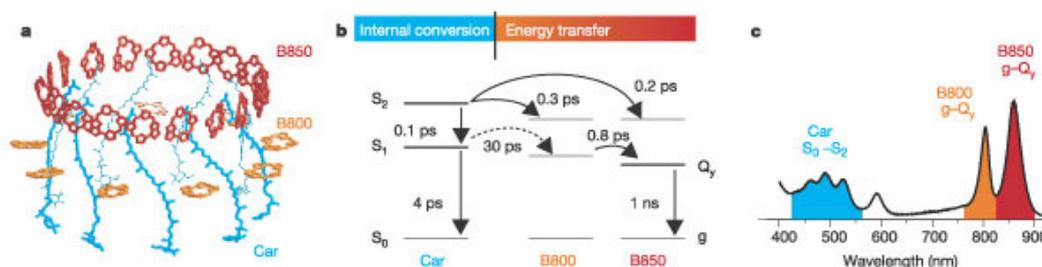
Fig. 1.7 Carotenoid BChls Energy Transfer. a) Geometrical arrangement of carotenoids (blue) and BChls (red and orange) in the LH2 system. b) Scheme of the energy transfer pathways from carotenoids to BChls. c) Absorption spectrum of the LH2 system (from Herek *et al.*, 2002).

Besides these functional roles, carotenoids are fundamental in maintaining the LH2 tertiary structure as they have an extended S-shape conformation that span the entire depth of the complex, making many important and intimate contacts with the phytyl systems of both the B800 and B850 pigments, and making specific interactions with several polar residues on the cytoplasmic side. The absence of coloured carotenoids destabilizes the wild-type LH2 of *R. sphaeroides* R-26 strain (Clayton, 1963; Davidson and Cogdell, 1981); under this condition α- and β- polypeptides are synthesized, but they are rapidly degraded and are not stably integrated into the membrane (Lang *et al.*, 1994). The structurale role of carothenoids is further supported by the observation that the mutant R-26, which does not synthesize coloured carotenoid,

also lacks the LH2 complex. The R-26 strain can revert to the strain R-26.1 which contains a modified LH2 complex (Braun and Scherz 1991). Carotenoids seem to be important in protecting the LH1 complex structure against the detergent destructive effect (Bahatyrova *et al.*, 2004b). The morphology of the membranes is also affected in carotenoidless strains of *Rb. sphaeroides*: the absence of the LH2 complex results in long tubes instead of the vesicular structure that characterizes the *wt* (Jungas *et al.*, 1999).

1.4.2 *The RC-LH1 complex*

The RC and the LH1 complex form the so called "core complex". Pioneering studies of Miller *et al.* (1982) showed the presence of a RC surrounded by the internal antenna complex LH1 in the native membrane of *Blastochloris (Blc.) viridis.* This notion has been confirmed by medium resolution structures of core complexes from different species subsequently obtained. In all photosynthetic bacteria the LH1 is composed of pairs of hydrophobic apo-proteins (α,β) as the LH2, and each couple binds non covalently two BChl a molecule and a carotenoid. AFM, x-ray analysis and electron microscopy have revealed several details of the interactions and assembly of RC, LH1 and additional subunits. In particular *Blc. viridis, Rhodospirillum (Rsp.) photometricum, Rsp. rubrum* and *Phaeospirillum (Phsp.) molischianum* appear to share a core-complex architecture characterized by a RC encircled by a closed LH1 ring composed of 16 (α,β) units. In *Rhodopseudomonas (Rps.) palustris* the RC seems to be surrounded by 15 (α,β) LH1 subunits plus a different transmembrane subunit named W. Cryo-Electron Microscopy (EM), crystallography and AFM has shown that in *Rhodobacter* strains a small transmembrane protein similar to the W, and called Puf X, is present in a 1:1 stoichiometry with the RC. The tightly fixed stoichiometry is consistent with the fact that the *puf X* gene is transcribed as part of the same operon of the RC genes *pufL* and *pufM*. Both *Rb. sphaeroides* and *Rb. blasticus* present a dimeric core complex structure composed of two open LH1 of 14 and 13 (α,β) subunits respectively. Each open ring contains a Puf X protein. The dimeric S-shaped antenna houses 2 RC proteins (see **Fig. 1.8** Structure of the RC-LH1 core complex for a review see Scheuring *et al.*, 2006). All the core complex monomers, notwithstanding the different characteristics, present an elliptical shape, which results from the interaction between the RC and the LH1. Indeed,

in mutants of *Rb. sphaeroides* lacking the RC protein (Bahatyrova *et al*., 2004b), circular but even elliptical, polygonal ring shapes, as well as arcs were revealed by AFM images, indicating a considerable flexibility and the lack of structural coherence of the LH1. These studies also evinced a certain variability in LH1 aggregation in the membrane when both RC and Puf X were absent, suggesting that the antenna needs a guide or a template (as the RC) to correctly perform the assembly in the membrane. The presence of open rings could be the consequence of the relatively weak association of the protomers in the LH1complexes as compared to the stable LH2 ring, due to the different H-bonding patterns that stabilize binding of the BChls to the protein. Anyhow, it seems clear that the instability of the $\alpha_1\beta_1BChl_2$ protomers allow the passage of quinone (Q or QH_2) from the Q_B site of the RC across the barrier formed by the LH1 ring. This process is essential because the exchange of Q and QH_2 mlecules between the RC and the cytochrome (cyt) bc_1 complex is required to promote a full turnover of the cyclic electron transfer chain. This Q/QH_2 exchange is likely to be facilitated by the lower rigidity of the LH1 with respect to the closed ring of the LH2.

The cryo-EM and AFM analyses performed by Scheuring *et al*. (2004) and more recently by Qian *et al*. (2005) have yielded interesting details of the core complex structure in *Rb. sphaeroides*. These studies have shown the presence of dimeric complexes formed *in vitro* by the purified proteins. This structure reflects the *in vivo* structure of the RC-LH1, as described in membranes by AFM (Bahatyrova *et al*., 2004). The *puf X* gene has been found only in the members of the genus *Rhodobacter*. Puf X$^-$ deletion mutants have been studied in the closely related species *Rb. capsulatus* and *Rb. sphaeroides*. The role and the position in the core complex of this small transmembrane protein is still a question of debate.

Puf X is a 9 kDa protein, essential for the photosynthetic growth; it is required for a fast QH_2/Q exchange between the Q_B site in the RC and the cyt bc_1 complex in the membrane (Farchaus *et al*., 1992; Lilburn *et al*., 1992) and has a strong tendency to interact with α polypeptide of the LH1 (Recchia *et al*., 1998). These data have suggested that Puf X associates with the inner α-ring of LH1 and interrupts the LH1 assembly preventing the closure of the ring.
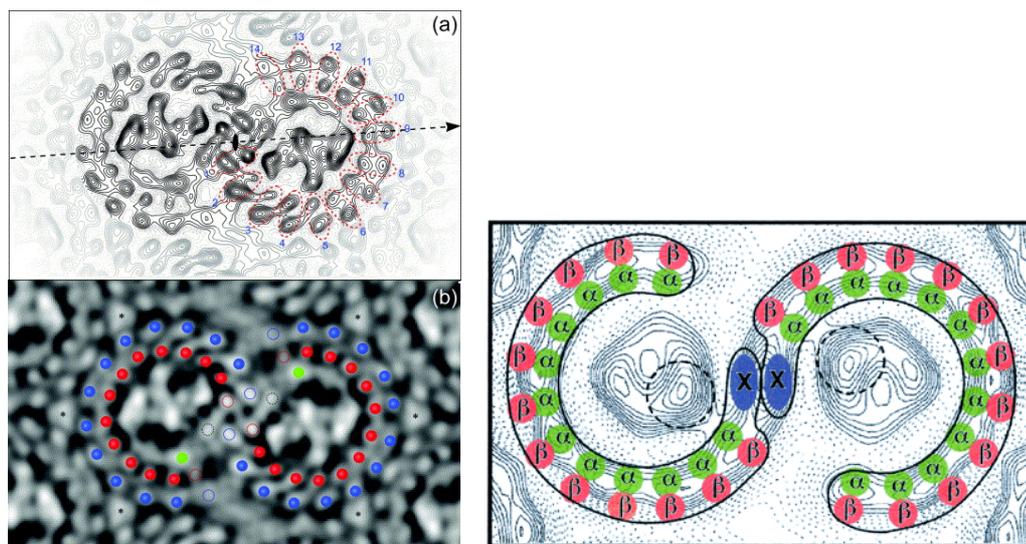
Fig. 1.8 Structure of the RC-LH1 core complex from *Rb. sphaeroides*. Panel on the left show: (panel a) the averaged projected density (at 8.5 Å resolution) of the core complex 2D crystal, and (panel b) the grey level of the projection density (Qian *et al.*, 2005). LH1 α and β are marked in red and blue respectively. Open red and blue circles are the terminal subunits of each LH1 arc. High density which do not arise from LH1 or the RC are marked with green and open black circles. The density marked in green could be accounted for by the Puf X transmembrane domain. The asterisk (*) indicates additional density found between dimeric complexes. The right panel shows the projection map (at 26 Å resolution) of the core complex with a superimposition of colored circles corresponding to α and β polypeptides (green and red respectively) and Puf X proteins (blue) as obtained by Scheuring *et al.*, (2004). The maximum densities of the RCs are circled with a dotted line, indicating a preferred orientation.

Two locations have been tentatively proposed for Puf X (**Fig. 1.8**). Qian *et al.* (2005) localized Puf X within the major arc of the LH1 as they found a density region that could well correspond to that of an α-helix. They also propose that Puf X-Puf X interactions, necessary for a Puf X-induced dimerization of the core complex (Francia *et al.*, 1999), are still possible through their respective N or C termini. However, they do not exclude the possibility that some of the densities in question arise from ordered lipids or quinones within the core complexes as suggested by Aklujkar *et al.* (2006). In fact, working on *Rb. capsulatu*s, a species closely related to *Rb. sphaeroides*, Aklujkar *et al.*, obtained evidences that Puf X interacts with the RC, and that its presence effects the efficiency of energy transfer to the RC. These authors have proposed that Puf X binds bacteriochlorophyll and takes part in the transfer of excitation energy delocalized over the entire LH1 complex (Comayras *et al.*, 2005a). Consistently with these functional properties, a different position is suggested for the Puf X protein, *i.e.* at the

junction region of the dimer as originally proposed by Scheuring *et al.* (see **Fig. 1.8**). These authors based their opinion on low resolution structural studies of *Rb. sphaeroides* (Scheuring *et al.*, 2004) and *Rb. blasticus* (Scheuring *et al.*, 2005a) dimeric RC-LH1-PufX core complexes. In this position Puf X would form a central homodimeric component of the core complex. On the basis of comparative structural studies performed on the Puf X from *Rb. sphaeroides* and the related species *Rb. veldkampii*, it has been suggested that dimerization of the LH1 complex is due to a specific structural motif, which is present in the *sphaeroides* Puf X, but not in *capsulatus* and *veldkampii* Puf X proteins. This would explain the absence of RC-LH1 dimers in the latter species, in spite of the presence of Puf X (Busselez *et al.*, 2007). It seems clear, however, that the presence of Puf X, both in the monomeric or dimeric form, facilitates the Q/QH_2 exchange between the RC and the cytochrome bc_1 complex (Gubellini *et al.*, 2006), most likely due to an interruption of the LH1 ring. This fits the specific orientation of the RC inside the antenna with the Q_B site facing the $\approx 25\text{Å}$ wide gap, as observed in the core complex structure from *Rps. palustris* (Scheuring *et al.*, 2005a).

1.4.3 *The topologycal organization of the chromatophore membrane*

The occurrence of a supramolecular organization of the photosynthetic complexes in the chromatophore membranes was first suggested by Jungas *et al.* (1999). They observed that a LH2-deficient *Rb. sphaeroides* strain produces tubular instead of vesicular chromatophore membranes as found in the *wt* strain. These tubular structures induce the formation of LH2 2D crystal native membrane allowing *in vivo* EM studies. The 20 Å projection map obtained from these strains revealed long array of dimeric core complexes. In this study the presence of a cyt bc_1 complex, closely associated with a RC-LH1-Puf X dimer, was supposed, although its limited contribution to the projection map renders the assignment questionable. The alignment of core complexes into regular arrays in *Rb. sphaeroides* has been proved to be due to the presence of the Puf X protein (Frese *et al.*, 2000 and 2004). Unfortunately a direct localization of the cyt bc_1 complex *in vivo* is still absent notwithstanding the great number of AFM and electron microscopy analyses performed directly on native membranes from various bacterial

strains (for a review see Sturgis *et al.*, 2007). In *Rb. blasticus* the ordered organization of the antenna complexes appears to be randomized, with a considerable mixing of LH2 and dimeric core complexes (Scheuring *et al.*, 2005a). In *Rsp. photometricum* membranes (see **Fig. 1.9**) a dense, scarcely ordered packing of photosynthetic units has been seen by AFM. Interestingly, in cells grown under high light intensity the membranes are predominantly characterized by randomly distributed LH2 and monomeric core complexes, while under low-light intensity, as a consequence of chromatic adaptation, domains of hexagonally packed LH2-only region arise (Scheuring *and* Sturgis, 2005b). The same overall arrangement of chromatophore membranes was observed in *Phaeospirillum molischianum*, were two separated regions coexist: one characterized by a paracrystalline hexagonally packed LH2 arrays and the other exhibiting mixed domains of LH2 and core complexes (Gonçalves *et al.*, 2005). In *Rps. palustris*, as well, hexagonal lattices of peripheral antenna complexes and regions with a random distribution of LH2 and core complexes exist in cells grown under low light intensity. At high light intensity a unique, apparently crystalline core complex region was observed (Scheuring *et al.*, 2006b). Finally, in *Rb. sphaeroides* a recent AFM analysis of native patches of membranes (Bahatyrova *et al.*, 2004) revealed the presence of two types of specialized domains. A first region composed of linear arrays of several, continuous, dimeric core complexes separated by sequences of 10-20 nonameric LH2 complexes, some of which are in close physical association with the RC-LH1-Puf X complexes. This arrangement is expected to facilitate the energy transfer to the RC. A second region was seen, consisting of clusters of isolated LH2, which probably represents the variable antenna formed in response to low light intensity. Importantly, both at high and low light intensity, the core-core interactions (*i.e.* between RC-LH1 complexes) are preserved. Secondly, extensive physical continuity between individual LH2 complexes and between LH2 and core complexes is also maintained. The LH2 rings seem to form an extended array for collecting photons and transfer excitation energy downhill to a dimeric core complex.
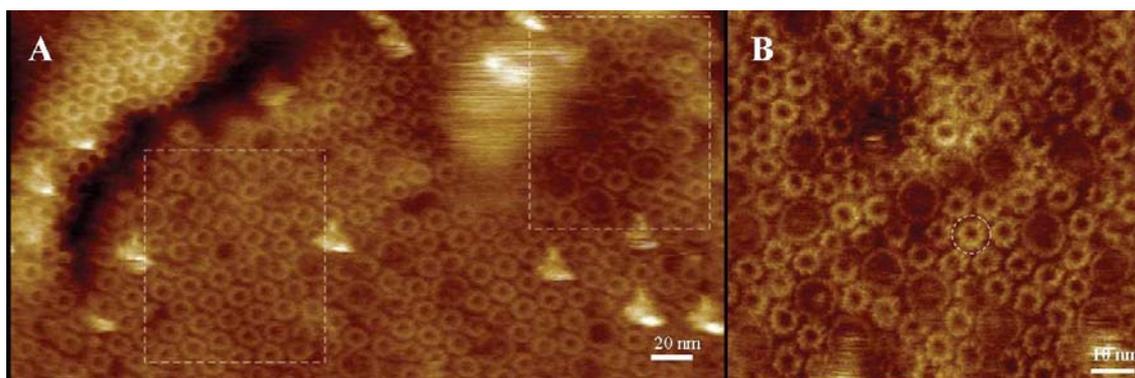
Fig. 1.9 AFM images from low- (A) and high-light (B) adapted photosynthetic membranes of *Rsp. photometricum*. (A) Medium resolution topograph of a native low-light adapted photosynthetic membrane. In the outlined box on the left is an example of a paracrystalline LH2 domain, while the box on the right show a more disordered region in which core complexes are still in contact. (B) High resolution topograph of a high-light adapted membrane in which core complexes are homogeneously distributed (Scheuring *et al.*, 2005b).

The linear array of core complex cooperate in the energy trapping process, as the excitation can migrate along a succession of such dimers until an "open" RC is reached. "Open" is a RC available for receiving a photon while "closed" is a RC undertaking photochemical charge separation. As supposed by Bahatyrova *et al.* (2004), a close packing of complexes is thought to reduce the lateral mobility of each component. Diffusional dynamics of the photosynthetic units have been recently analyzed in membranes of *Rsp. photometricum* (Scheuring *and* Sturgis 2006c). It was found that disordered region, with mixed LH2 and core complexes, are much more dynamic than the ordered antenna domains. Moreover, it resulted that in the paracrystalline region, proteins occupy $\approx$ 91% of the total surface area, while a lower fraction, around 73%, is occupied by the complexes in the disordered region. In the light of these results, the authors proposed that such an organization of the photosynthetic membrane could optimize the structural and functional properties of the system, as compared to the supramolecular organization of Jungas *et al.* (1999). Since the cyt bc_1 complex has not yet been detected in the native membranes, Scheuring *and* Sturgis suggest that the disordered dynamic region allow the quinone and quinole migration in the space between the complexes until the cyt bc_1 is reached. At variance metabolically active quinones would be excluded from the large, static, crystalline LH2 domains. The latter assumption is supported by studies performed in *Rb. sphaeroides* where quinone

molecules appear to be confined in the vicinity of the core complexes (Francia *et al.*, 2004; Comayras *et al.*, 2005a and b; Dezi *et al.*, 2007). According to the partitioning of the ICM in regions differing in fluidity is essential for the perfect functioning of the photosynthetic apparatus. In fact, cyclic electron energy transfer, and therefore proton translocation and transduction require that proteins and/or cofactor can diffuse within the membrane bilayer crowded with proteins. On the other side, an efficient energy transfer requires a dense, rather ordered packing of the complexes in the membrane, promoted by strong protein-protein interactions.
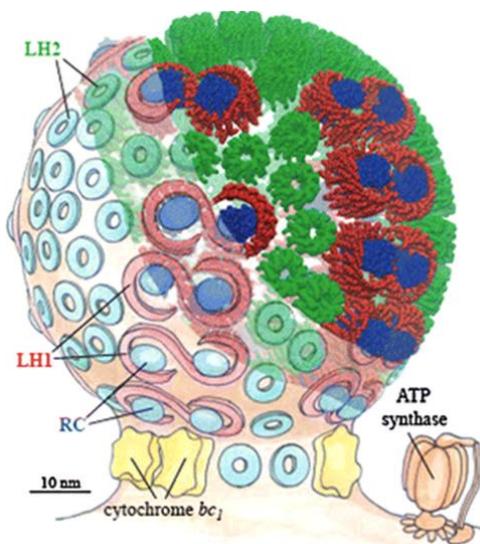
Fig. 1.10 Model of a chromatophore vesicle. Cytoplasmic surface of an *in situ* chromatophore vesicle of *Rb. sphaeroides* as modelled by Sener *et al.* (2007). The vesicles have an average internal diameter of 60 nm as determined from AFM (Bahatyrova *et al.*, 2004) and linear-dichroism data (Frese *et al.*, 2004). At the upper right LH2 and the LH1-RC. Complexes are reported in green and red, respectively. The cytochrome bc$_1$ and the ATPase are depicted at the vesicle neck but additional bc$_1$ complexes may be located closer to the core complexes.

Combining recent AFM and linear dichroism studies Frese *et al.* (2004) have proposed a model for the supraorganization of the chromatophore membrane from photosynthetically growth *Rb. sphaeroides*. As shown in **Fig. 1.10** the chromatophore is depicted as a quasi-spherical vesicle in which, core RC-LH1 complexes are organized in arrays with interdispersed LH2 complexes. The RC has a fixed orientation within the LH1 ring. These authors also suggest that the LH2 are more abundant in curved

domains. The bc$_1$ and the ATPase complexes are tentatively located at the basis of the vesicles. More recently the same authors (Frese *et al.*, 2007) demonstrated that the presence or absence of Puf X, the appearance of core complexes domains and the membrane curvature are strictly associated. They found that the interplay of membrane crowding and the asymmetries in the size and shape of integral membrane protein alone could account for both domain formation and the local membrane curvature responsible of the invagination and budding of membrane. This observation suggests that the membrane organization and shape are governed by a general, unique mechanism.

1.5 The photosynthetic reaction center in physiological and artificial environment

1.5.1 *The physiological lipid-protein environment of the reaction center*

Photosynthetic complexes are embedded in a lipid bilayer. The standard model of the membrane architecture was developed by Singer and Nicholson (1972) who proposed the idea of membranes like a sea composed of lipids of the same thickness with a low concentration of proteins dispersed within. This model has been modified during the last decades and the membrane is presently conceived as an association of lipid patches, crowded with proteins, and with a bilayer varying considerably in thickness (for a review see Engelman, 2005). In this context, protein motion and membrane fluidity must be considered differently because, although some proteins can undergo relatively free diffusion, a variety of restrictions on the motion and additional constraints can be imposed by protein-lipid interactions and by lipid segregation in specific regions. Biological membranes play many different, fundamental roles in living cells, providing specialized permeability barriers and giving rice to protein-lipid interactions which are essential for processes like respiration, photosynthesis, solute and protein transport, signal transduction and motility.

Lipid structures effects on membrane protein functions can be described in terms of specific molecular interactions and physical parameters of the bilayer (e.g. lipid fluidity, membrane tension; see Lee, 2004). Specific protein-lipid interactions may be necessary for structural stability, integrity and proper function of the protein, as shown

in particular for several membrane proteins involved in energy trusduction processes. Phospholipids are essential for the activity of the cytochrome bc_1 complex as proved by the observation that an increased delipidation of this enzyme gradually leads to a loss of activity (Lange *et al.*, 2001). It has been found that two molecules of cardiolipin are tightly bound to the bc_1 complex and that digestion of these lipids inactivates the complex. The effect can be reversed, since addition of cardiolipin reactivates the enzymatic activity (Gomez *et al.*, 1999). It is well documented that the LHCII complex (the major light-harvesting complex present in chloroplasts) engages in key interactions with lipids; in particular it has been established that its trimeric form is closely associated with phospatidyl glycerol. Gradual delipidation of the protein causes dissociation of the trimers into monomers (Nußberger *et al.*, 1993). Varanesi *et al.* (2006) verified that alteration of the lipid environment of the Cytochrome C Oxidase in *Rb. sphaeroides*, which most likely affects the lipid binding sites of subunit III, leads to the inactivation of the complex.

Evidence that specific lipid molecules are closely associated with protein subunits is provided by an increasing number of high resolution x-ray structures of membrane complexes (Byrne *et al.*, 2002). Lipids interacting with membrane proteins can be distinguished in three groups. The first is represented by the *annular shell* of lipids at the protein-bilayer interface. The second group includes lipid molecules immersed in cavities and clefts, and frequently at the interfaces of multi-subunit complexes. These lipids are generally referred to as *non-annular surface lipids*. The last group is represented by the *integral protein* lipids. These lipid molecules, present within the protein in unusual position, are supposed to play a role in folding and assembly of membrane proteins (Palsdottir *et al.*, 2004).

The majority of the identified lipids are endogenous and co-purify with the protein independently of the specific-detergent purification protocol used, confirming the notion that membrane proteins are actually isolated as proteo-lipid complexes. Among the several X-ray crystal structure of membrane proteins associated with lipids, a significant proportion is represented by photosynthetic complexes (for a review Jones, 2006). The similarities in position of bound lipids in the three types of RCs (bacterial RC, photosystem I (PSI) and photosystem II (PSII) from cianobacteria and plants)

reflect the structural important similarity which characterizes these complexes, in spite of their different level of complexity (Fyfe *et al.*, 2004). As shown in **Fig. 1.11** in the bacterial RC a cardiolipin molecule is attached to the intra-membrane surface between the Puf L (L) and Puf M (M) subunits. Correspondingly, in the PSII complex a monogalactosyldiacylglycerol (MGDG) interacts with residues from two α-helices at the D_1/D_2 subunit interface. In the PSI complex the PsaA polypeptide, corresponding to the D1 subunit in the PSII complex, contains binding sites for MGDG and phosphatidylglycerol (PG) approximately in the same locations seen in the PSII complex.

The lipids resolved in the above described crystal structures could in principle play structural roles, stabilizing the multimeric complexes, as well as affect function, rendering more rigid or flexible specific protein regions. In particular it has been proposed that in the bacterial RC, a particular pattern of lipids facilitates the quinone/quinole binding/debinding at the Q_B site, a key process in protein traslocation (Jones, 2006). In summary, several structural and functional studies, indicate that important biophysical and biochemical properties of these proteins are determined by the lipid environment.

The intracytoplasmic membrane of *Rb. sphaeroides*, is composed of phosphatidylcholine (PC), phosphatidylglycerol (PG), phosphatidylethanolamine (PE) and cardiolipin (CL) or diphosphatidyl glycerol, and two glycolipids, *i.e.* sulfoquinovosyl diacylglycerol and glucosylgalactosyl diacylglycerol (Benning, 1998). The relative composition of the membrane can vary depending on the growth condition, while the fatty acid chains are predominantly composed of C_{16} and C_{18} satured and mono unsaturated methyl esters and trace amount of smaller chains (Casadio *et al.*, 1979). The lipid composition of chromatophore vesicles does not differ from that of the not invaginated regions of the cytoplasmic membrane. Birrell *et al.* (1978), using lipid spin-labels, showed that the antenna complexes preferentially associate with negatively charged lipids like PG and CL.
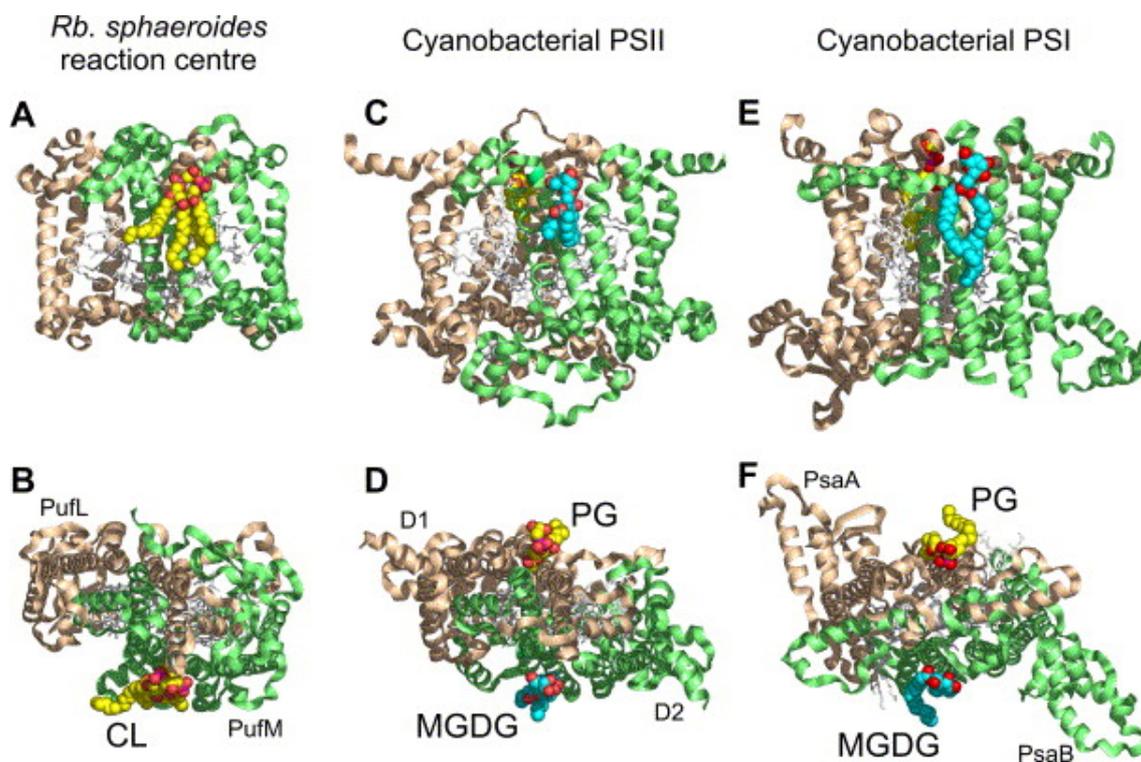
Fig. 1.11 Lipids bound to photosynthetic reaction centers. Protein heterodimers are shown as ribbons, electron transfer cofactors as white sticks and lipids as spheres. (A) The PufL/M heterodimer of bacterial RC (beige and green, respectively), with CL shown with yellow carbons. (B) Top view of the complex in A. (C) The D1/D2 heterodimer of PSII (beige and green, respectively). MGDG – cyan carbons, PG – yellow carbons. (D) Top view of complex in C. (E) The heterodimer formed by the C-terminal regions of the PsaA and PsaB polypeptides of PSI (beige and green, respectively). MGDG – cyan carbons, PG – yellow carbons. (F) Top view of the complex in E. Phosphorous in lipid molecules is represented as red sphere (from Jones, 2006).

As shown in **Fig. 1.11**, a cardiolipin molecule is bound to the RC (Mc Auley *et al.*, 1999). Two additional lipid molecules have been subsequently identified in the RC structure, *i.e.* the glycolipid glucosylgalactosyl diacylglycerol (GGDG) and a phosphatidylcholine (Camara-Artigas *et al.*, 2002). The three lipids bind at distinct sites as also confirmed by x-ray crystallography of RC complexes supplemented with brominated lipids (Roszak *et al.*, 2007). Thanks to the characteristic strong x-ray scattering from the bromine atoms, Roszak *et al.* unequivocally identified three lipid binding sites distinct from that of the cardiolipin molecule (named site C). One of the sites is located in the hydrophobic surface close to the tail of the ubiquinone Q_A (site A), the second is close to the tail of ubiquinone Q_B (site B) and the last one is located in the groove containing Q_A surrounded by the helices of all three protein chains L, M and H (site D), close to the site where cardiolipin was found (**Fig. 1.12**).
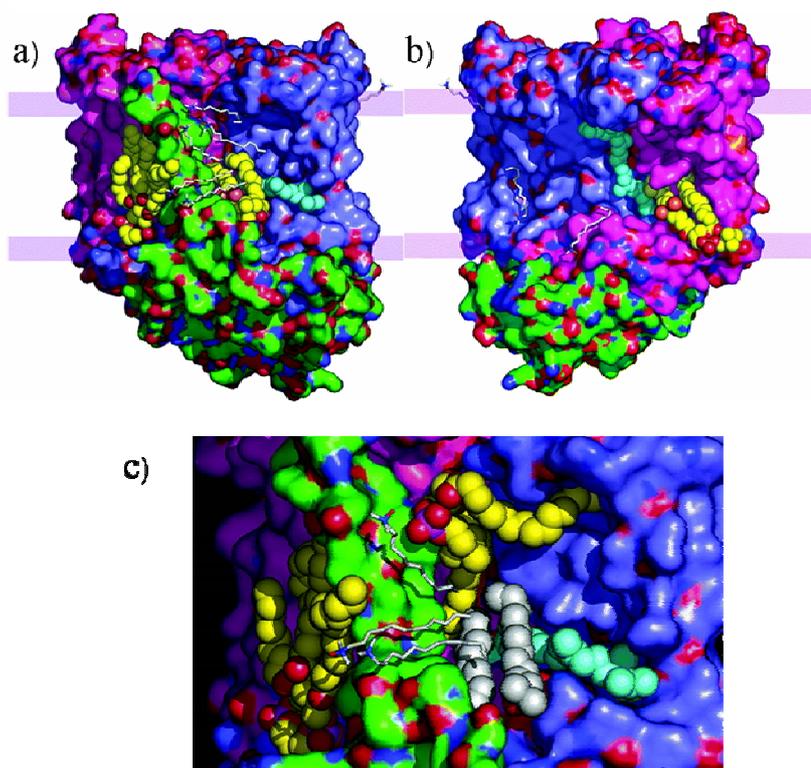
Fig. 1.12 Lipid binding sites of *Rb. sphaeroides* RC a) Site A and C; b) Site B; c) Site D. In all the figures, the M chain (including pigments) is shown in pink, the L chian in blue and the H chain in green. The brominated lipid is represented in yellow (C atoms), red (O atoms) and orange (Br and P atoms). UQ_A is drawn as cyan spheres and LDAO molecules are shown as white-stick-style models (from Roszak *et al.*, 2007).

1.5.2   *The reaction center in artificial environment*

Electron transfer studies, performed in RCs incorporated into artificial matrices, have provided useful information on the role of the RC dynamics and of protein-solvent interactions in governing the rate of electron transfer processes. Among non liquid matrices, glassy matrices obtained by dehydration of RC-saccharide solution (see par. 3.11.1), have been extensively characterized.

Glassy matrices of saccharides exhibit an outstanding ability in protecting against adverse environmental conditions, such as potentially detrimental freezing, heating and dehydration (Crowe *et al.*, 1996; Crowe *et al.*, 1998). Saccharide glasses are employed by several organisms that can survive for long periods under extreme drought and high temperature, entering a state of suspended metabolism (anydrobiosis), which is preceded by a massive synthesis of specific carbohydrates (Crowe *and* Crowe, 1984;

Hirsh, 1987; Crowe, 2002). Among sugars, the disaccharide trehalose (**Fig. 1.13**) appears to be the most effective protectant (Crowe *et al.*, 1983; Colaço *et al.*, 1992; Uritani *et al.*, 1995; Sun and Davidson, 1998). Its ability in preserving the structural and functional integrity of biostructures is largely employed in food, pharmaceutical and biotechnology sciences to optimize long term storage of biological samples (Roos, 1995; Eroglu *et al.*, 2000; Eroglu 2002; Walkers *et al.*, 2003). Notwithstanding the large efforts devoted, neither the nanoscopic mechanisms through which trehalose (or other saccharides) prevent biomolecules from denaturation, nor the reason for the higher effectiveness of trehalose have been fully understood (Carpenter and Crowe, 1989; Belton and Gil, 1994; Sampedro and Uribe, 2004).
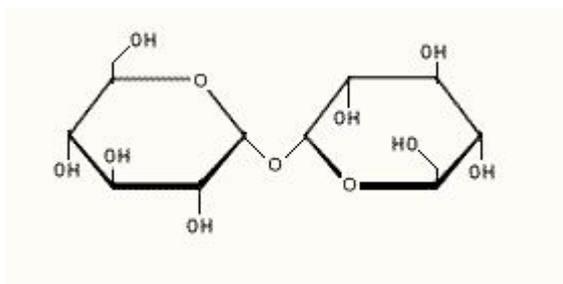
Fig. 1.13 In the figure the chemical structure of the trehalose is shown. Trehalose is a non reducing sugar formed from two glucose units joined by a 1-1 alpha bond giving it the name of α-D-glucopyranosyl-(1→1)-α-D-glucopyranoside.

Spectroscopic studies, as well as molecular dynamics simulations, performed on soluble proteins embedded into amorphous water-trehalose matrices, have shown that the room temperature conformational dynamics of proteins is severely hindered in such systems (for a recent review see Cordone *et al.*, 2005). This reduction in the motional freedom would be basically responsible for biopreservation, by preventing transitions to non-native conformations and denaturation. More specifically, it has been proposed that the reduction of protein dynamics evidenced in saccharidic glassy matrices is due to the formation of structures which confine the protein within a network of hydrogen bonds, connecting protein groups, residual water molecules and sugar molecules (Cottone *et al.*, 2002; Giuffrida *et al.*, 2003; Giuffrida *et al.*, 2004). These putative structures are expected to be protein- and matrix- specific, being determined by the propensity of the matrix molecules to establish an hydrogen bond network matching the protein surface to the matrix environment. This view is supported by several findings, which suggest that

such a specificity could also explain the peculiar efficacy of trehalose in biopreservation. Among them: (i) molecular dynamics simulations of sucrose- and trehalose-coated carboxymyoglobin (MbCO) have shown that the fraction of hydrogen-bound water molecules shared between the protein and the sugar is lower in sucrose than in trehalose, pointing to a lower protein-matrix coupling in sucrose (Cottone *et al.*, 2005); (ii) Fourier transform infrared (FTIR) spectrosocopy measurements performed over the 300-20K temperature range on MbCO embedded in a number of different sugars (including sucrose) have indicated that the content of residual water in the sugar matrix modulates the amplitude of MbCO internal motions in a way which is peculiar for each sugar, and that, at all water contents investigated, the dynamical protein-solvent coupling is tighter in trehalose than in other sugars (Giuffrida *et al.*, 2006); (iii) an NMR study of protein mobility in lysozime-water-sugar amorphous systems has provided evidence that the protein and the sugar "phase separate" in lactose but not in trehalose matrices (Lam *et al.*, 2002).

In the following we summarize the results of studies (Palazzo *et al.*, 2002; ; Francia *et al.*, 2003; Francia *et al.*, 2004b; Francia *et al.*, 2004c) in which the relationships between electron transfer and protein dynamics were explored *at room temperature* by incorporating the RC into trehalose amorphous matrices and by studying the response of the electron transfer kinetics to dehydration of the embedding medium. It has been shown that the incorporation of the RC into a dehydrated amorphous trehalose matrix severely restricts the RC conformational dynamics *at room temperature* as judged from the effects on the kinetics of specific electron transfer processes (Palazzo *et al.*, 2002; Francia *et al.*, 2003; Francia *et al.*, 2004b; Francia *et al.*, 2004c). This approach provides an attractive, complementary alternative to investigations in which the slowing down of the protein dynamics is obtained by lowering the temperature (see par. 1.3). In fact, in *trehalose-coated* RCs the coupling between RC dynamics and electron transfer can be examined *at physiological temperatures*, thus uncoupling, in principle, temperature from solvent effects.

A progressive dehydration of trehalose-coated RCs first affects Q_A^- to Q_B electron transfer, causing its block in an increasing fraction of the RC population. This reversible inhibition has been ascribed to a large increase (*non-homogeneous* through the sample)

of the energy barriers which govern the conformational transition gating electron transfer (Francia *et al.*, 2003). Upon further dehydration (below ~ 0.8 water molecules per trehalose) the kinetics of $P^+Q_A^-$ recombination after a flash accelerate abruptly and become broadly distributed, mimicking, at room temperature, those observed at cryogenic temperatures in a glycerol-water mixture (Palazzo *et al.*, 2002). This similarity indicates that in extremely dehydrated trehalose-water matrices thermal fluctuations between conformational substates, as well as relaxation from the *dark-adapted* to the *light-adapted* state, are largely hindered at room temperature over the time scale (10^{-1} s) of charge recombination. It has been suggested that, as proposed for small, soluble proteins, also in the case of a large membrane protein complex as the RC, a network of hydrogen bonds involving residual water molecules locks the protein surface to the trehalose matrix, determining a tight structural and dynamical coupling between the RC and the water-sugar matrix (Palazzo *et al.*, 2002; Francia *et al.*, 2003; Francia *et al.*, 2004c; Cordone *et al.*, 2005). This is in line with the observation that both interquinone electron transfer and $P^+Q_A^-$ recombination are marginally affected in RC films obtained in the absence of trehalose, even at extreme dehydration (Palazzo *et al.*, 2002; Francia *et al.*, 2003). In this respect we also note that incorporation of RCs into strongly dehydrated trehalose glasses fully preserves at room temperature their native structure and photochemical activity at least for several weeks (Palazzo *et al.*, 2002).

2 AIM OF THE RESEARCH

As outlined in the Introduction, the reaction center purified from the photosynthetic bacterium *Rhodobacter sphaeroides* has become a reference model in the study of protein electron transfer because both its structure and photochemical reactions are known in great detail.

A more limited information is available on the supramolecular organization of the photosynthetic unit of which the reaction center is the central component. In particular the effects that the *in vivo* environment of the RC has on the light-induced electron transfer have not been deeply studied. This point has recently attracted a large attention, not only in view of its physiological relevance, but also because solvent-protein interactions are emerging as one of the important factors which determine the mechanisms of electron transfer in proteins. In fact, the internal, conformational protein dynamics, which is strongly affected by the solvent, appears to play a central role in governing several electron transfer processes.

The main purpose of the present thesis has been therefore to contribute to clarify these interconnected questions, studying the kinetics of electron transfer processes catalyzed by the RC complex, when inserted into the physiological core complex and when embedded into artificial matrices.

The results obtained and the relative discussion paragraphs are presented in three chapters (4-6), each dealing with the effects of a particular environment.

In Chapter 4 the kinetics of charge recombination are compared in purified RCs and in core complexes formed by the RC and by the LH1 antenna. In the latter, more intact system, a large stabilization of the charge separated state has been observed only at physiological pH values. The lipid and quinone complements tightly associated with the RC-LH1 core complex have been analyzed and compared with those coupurifying with the peripheral LH2 antenna and with those found in intact membranes. This analysis indicated an *in vivo* anisotropic distribution of both quinone and lipids, evidenced by a large confinement of quinone and cardiolipin to the core complex. The specific composition of the core complex lipid phase, as well as the high quinone

concentration found in association with the RC-LH1 complex, have been proposed to contribute to the stabilization of light-induced charge separation.

In capter 5 the role of the solvent dynamics on electron transfer catalyzed by the RC has been examined by incorporating the RC protein into non-liquid amorphous matrices formed by different saccharides, *i.e.* glucose, sucrose and trehalose. Upon dehydration, suspensions of the RC in these sugars form glassy matrices, whose dynamics can be modulated by varying the content of residual water. This approach allows to control at room temperature the RC protein dynamics and to examine its effects on the kinetics of specific electron transfer processes. A much tighter protein-matrix structural and dynamical coupling has been found in the case of trehalose, a disaccharide which exhibits an extraordinary efficacy in protecting biomolecules against potentially detrimental conditions (high temperature, extreme dehydration). The analysis of thermal denaturation of the RC incorporated in the different sugar matrices confirmed the conclusion that in the trehalose matrix, at very low water contents, the RC dynamics is strongly inhibited. On the contrary, when the RC is embeeded in a glass formed by the homologous saccharide sucrose, a very weak protein-matrix coupling was observed and the resistance against thermal denaturation was not enhanced as compared to a RC film dehydrated in the absence of any sugar. An intermediate RC-matrix coupling was found in the case of glucose.

In capter 6, we studied the effects of incorporation of the RC protein into a different artificial environment, formed by multilayers of polyelectrolytes (PEM). The purpose of this study was twofold: on one side, we checked the stability of the protein in such an unusual environment, and studied the effects of dehydration on electron transfer; on the other side we tested the response of the system to herbicides, determining binding constants and kinetics for different inhibitors of Q_A^- to Q_B electron transfer. These studies show that RC polyelectrolyte multilayers are a promising system in the development of an herbicide biosensor.

3 MATERIALS AND METHODS

3.1 Bacterial strains and growth conditions

RC-LH1 core complexes were purified from genetically modified strains of the green spontaneous *Rb. sphaeroides* (Ga) strain. The so called *wt* and the ΔX strain (Puf X deleted strain) were obtained from a ΔQ-X/g strain in which the *puf* operon was completely substituted with a Kanamicine resistance cartridge isolated from the transposon Tn5 (Jorgensen *et al.*, 1979). The photosynthetically competent ΔQ-X/g(prKX) (Francia *et al.* 1999), or *wt* strain was obtained from the ΔQ-X/g strain complemented with a derivative of the prK404 (Ditta *et al.* 1985) plasmid carrying the puf operon construct. The photosynthetically deficient ΔX phenotype, ΔQ-X/g(p2T) (Barz *et al.* 1994), was constructed from the ΔQ-X/g using a plasmid with a *puf* operon lacking the pufX gene (prKXmut2T) (Farchaus *et al.* 1990a), complementing the ΔQ-X/g strain yielded. All the strains were grown in Sistrom's minimal medium (Table 1a). Vitamins and amminoacids (5 ml/L, Table 1b) were added after sterilization in autoclave (30 min at 110°C) while kanamycin (25 μl/mL) and tetracycline (2 μL/mL) were added depending on the strain.

Table 1a

Composition of Sistrom medium	
1 M Potassium Phosphate pH 6.8	20 mL/L
10% Potassium Succinate pH 6.8	20 mL/L
Solution C (table 1c)	20 mL/L
5% NaCl solution	10 mL/L
10% $(NH_4)_2SO_4$ solution	5 mL/L
Yeast extract	1g/L

Table 1b

Amminoacids plus vitamins solution composition	
2% L-Aspartic Acid pH 6.9	2 mL/L
5% L-Glutammic Acid pH 6.9	2 mL/L
100 μg/mL Biotine pH 7.0	0.1 mL/L
500 μg/mL Thiamine pH 7.0	1 mL/L

Biotine stock solution: 1 mg/mL in NaOH.

Table 1d

Table 1c

Composition of Solution C	
$CaCl_2$ x 2 H_2O	3.34 g/L
$FeSO_4$ x 7 H_2O	0.099 g/L
$(NH_4)_6Mo_7O_{24}$ x 4 H_2O	0.00925 g/L
Nicotinic Acid	0.05 g/L
Nitrilotriacetic Acid	10 g/L
$MgSO_4$ x 7 H_2O	29.5 g/L
Trace elements (Table 1d)	50 mL/L
KOH	To reach pH 6.9

Trace elements solution composition	
$Co(NO_3)_2$ x 6 H_2O	0.248 mg/L
$CuSO_4$ x 5 H_2O	0.392 mg/L
H_3BO_3	0.114 mg/L
EDTA	2.5 mg/L
$FeSO_4$ x 7 H_2O	5 mg/L
$MnSO_4$ x H_2O	1.54 mg/L
$ZnSO_4$ x H_2O	10.95 mg/L

RCs lacking the antenna system were purified from the carotenoidless-mutant R-26, grown in RCV medium (Table 2a). Vitamins (0.04 mL/L) were added after sterilization in autoclave for 20 min at 120°C.

Table 2a

Table 2b

Composition of RCV medium	
10% $(NH_4)_2SO_4$	10 mL/L
10% DL Malic Acid	40 mL/L
1% EDTA	2 mL/L
20% $MgSO_4$ x 7 H_2O	1 mL/L
Trace elements (Table 2b)	1 mL/L
7.5% $CaCl_2$ x 2 H_2O	1 mL/L
0.5% $FeSO_4$ x 7 H_2O	2.4 mL/L
0.2% Nicotinic Acid	1 mL/L
0.2% para Ammino Benzoic Acid	1 mL/L
Yeast extract	0.6 g/L
10% Phosphate buffer pH 6.8	15 mL/L

Trace elements in 250 mL	
$MnSO_4$ x 2 H_2O	0.3975 g
H_3BO_3	0.7 g
$Cu(NO_3)2$ x 3 H_2O	0.01 g
$ZnSO_4$ x 7 H_2O	0.06 g
$NaMo_4$ x 2 H_2O	0.1875 g

The vitamin solution is composed by 1 g thiamine plus 10 mg biotine in 20 mL 50% ethanol.

Solidified medium was obtained adding 15 g/L of Agar before sterilization. Bacteria were grown photosynthetically at 30°C in Roux bottles exposed to two 100W tungsten lamps and cells were harvested in the late-log phase.

Rb. capsulatus FJ2, a kind gift of Prof. F. Daldal, is a mutant strain deleted in both the cyt c_2 and the membrane-bound cyt c_y (Jenney *et al.* 1993). It was grown semi aerobically in the darkness using YPS medium (Table 3) supplemented with spectinomycin and kanamycin (both 10 μg/mL), added after the sterilization in autoclave (120°C, 20 min).

Table 3

Composition of 1L YPS medium, pH 6.8	
$CaCl_2$ x 2 H_2O	2mM (294 mg)
$MgSO_4$ x 7 H_2O	2mM (492 mg)
Pepton	3 g
Yeast extract	3 g

3.2   Chromatophore isolation

Chromatophore vesicles were isolated from intra-cytoplasmic membranes of *Rb. sphaeroides* Ga and ΔX strain as essentially described in Baccarini-Melandri *et al.* (1971).

a) Harvesting of cells from at least 5L coltures;

b) Washing cells at least twice resuspending them in 200 ml of 50 mM MOPS, pH 7.4, 0.1 M KCl and centrifuging at 10000 rpm for 10 min at 4°C in a JA14 rotor (Beckman);

c) Resuspension of the pellet in 60 mL of buffer and disruption of the cells by passing them twice through a French press at a 1000 psi pressure;

d) Centrifugation of the cells extracts at 27000g for 35 min at 4°C in a JA25.50 rotor (Beckman);

e) Collection of the supernatant and centrifugation at 40000 rpm for 1 h 30 min at 4°C in a 50.2Ti ultracentrifuge Beckman rotor;

f) Resuspension of the pellet in 50 mM Glygly, pH 7.8 in a potter;

g) Storage of the preparation at -80°C in aliquots aliquots (containing 30 mg of protein for core complexes preparation) after freezing in liquid nitrogen.

3.3   Purification of RC-LH1 and LH2 complexes

Membranes were washed in a NaBr solution to eliminate peripheral proteins and to avoid the presence of ribosomal particles contamination (Fraker *et al.*, 1971). Photosynthetic complexes were extracted by a mild solubilization of membranes and separated by centrifugation on a sucrose density gradient in the presence of detergents, essentially as described by Francia *et al.*(1999). The detailed procedure is summarized in Scheme 1.

Scheme 1

a. Chromatophore membrane washing
-Dissolve a chromatophore aliquot (30 mg protein) in 50 mL of 50 mM Glygly, pH 7.8, and add 50 mL of the same buffer supplemented with 4 M NaBr, 0.4 M Sucrose, and shake the solution in ice in the darkness on a rotatory plane for 30 min.
-Add 100 mL of buffer to dilute the NaBr and ultracentrifuge at 40000 rpm for 1h at 4°C in 50.2Ti Beckman rotor.
-Collect and re-suspend the pellets in a potter with 50 mM Glygly, pH 7.8, in the smallest volume as possible to avoid excessive dilution of the sample.
-Measure the protein concentration and adjust it at 11.1 mg/mL.
-Freeze in liquid nitrigene and store the washed chromatophores at -80°C.
b. Purification of photosynthetic complexes
-Add to an aliquot of washed chromatophores a volume of detergent solution (30% w/v n-octyl-ß-D-glucopyranoside (OG), 5% w/v Sodium Cholate) corresponding to 1/11 of the sample volume and keep it under stirring in ice in the darkness for 10 min
-Centrifuge the sample for 1h at 45000 rpm in a 50.2 Ti Beckman rotor and collect the supernatant.
-Prepare a continuous sucrose gradient mixing in a gradient maker a 40% w/v and a 10% w/v sucrose solutions in buffer 50 mM Glygly, pH 7.8 in the presence of 0.6% w/v OG and 0.2% w/v Sodium Cholate.
-Load an aliquot of the supernatant on each gradient tube and centrifuge for 19 hours and 30 min at 45000 rpm in a 41.14 Kontron rotor or 16 hours at 36000 rpm in a 50.2Ti Beckman rotor, without using the brake to stop the centrifuge.

After the centrifugation, several bands are visible in the sucrose gradient (**Fig. 3.1**). They can be extracted through the use of a capillary glassy tube connected to a peristaltic pump. Sucrose was eliminated by passing the proteins through a Sephadex G-25 column (PD10, Pharmacia, Sweden) eluted with 50 mM glycilglycine, pH 7.8, 0.6% w/v OG, 0.2% w/v Sodium Cholate. The sugar-free complexes were concentrated by ultrafiltration with a 100 KDa cutoff Centricon concentrator (Amicon, Witten, Germany).
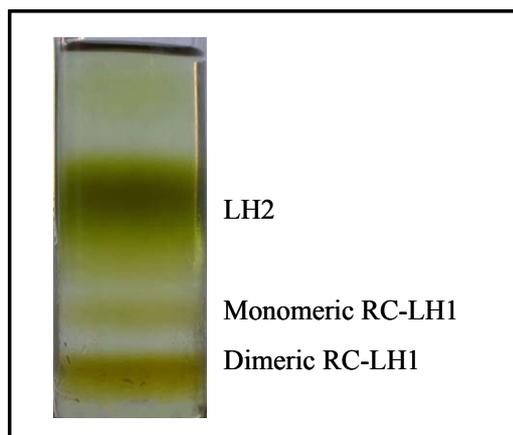

Fig. 3.1: Zonal centrifugation gradient. Protein separation by rate zonal centrifugation of detergent extracts from photosynthetic membrane complexes of *Rb. sphaeroides* Ga strain.

3.4   Purification of RC complexes

RCs deprived of the LH1 antenna complex were purified from chromatophores of *Rb. sphaeroides* R-26 strain as described in Gray *et al.* (1990). According to this protocol, chromatophores were solubilized in two steps at increasing concentration of the detergent Lauryl-DimethylAmine-N-Oxide (LDAO). The RCs extracted by solubilization, were subsequently purified in a DEAE column washed with salt solutions at increasing concentration. A fraction of the collected RCs (usually 30% of the whole population) is deprived of the secondary ubiquinone molecule bound at the Q_B site, as shown by kinetic analysis of charge recombination following a flash of light (see Introduction, par. 1.2.2). The RC can be totally deprived of or reconstituted with the secondary quinone acceptor Q_B, in order to obtain homogeneous preparations (see par. 3.4.3, 3.4.4). To study the kinetics of charge recombination at pH<7, LDAO was exchanged with 0.6% Octyl-β-D-glucopyranoside (OG) and 0.2% Sodium Cholate. In

fact at acidic pH values, LDAO suspensions of RC undergo a progressive emulsification, resulting in increase of turbidity and some alteration of the recombination kinetics (Piazza *et al.*, 2003, Palazzo *et al.*, 2004). In the following the purification and Q_B reconstitution/depletion procedures are described.

3.4.1 Preparation of chromatophores for the purification of RCs

The protocol for chromatophore isolation is almost the same of that previously described (par. 3.2) except for the buffer used and for storage condition. 20 mM TRIS-HCl, pH 8, is used as buffer both for washing and resuspending the cells before French press disruption. Chromatophores are stored in 100 mL aliquots at a concentration corresponding to 50 A optical density at 870 nm wavelength.

3.4.2 RC purification

In order to optimize the protocol, the isolation and purification of RCs is generally carried out over three days period. During the first day, the following steps are performed.

a) Chromatophore are diluited in a final 100 mL volume at a final optical density of OD_{870} = 50 A in the presence of 125 mM NaCl, 1 mM Na-Ascorbate, 0.5 mM Phenylmethylsulfonyl fluoride (PMSF) and 0.25% w/v LDAO. The suspension is stirred in the darkness at room temperature for 45 min;

b) The suspension is subsequently centrifuged at 40000 rpm at 4°C for 1h and 30min (50.2Ti Beckman rotor), resuspending the pellet in 20 mM TRIS-HCl, pH 8, 125 mM NaCl, 0.35% w/v LDAO, to a final volume of 100 mL;

c) After stirring of 30 min in the darkness on ice, the solution is again centrifuged under the same conditions; the supernatant, which is enriched in RCs, is diluted 1:1 with 20 mM TRIS-HCl, pH 8, to halve the salt and detergent concentrations;

d) The obtained RC suspension is loaded on a DEAE column equilibrated with 10 mM TRIS-HCl, pH 8, 0.08% w/v LDAO, leaving the sample to completely adhere to the resin and then washing it overnight with 10 mM TRIS-HCl, pH 8, 0.08% w/v LDAO, 80 mM NaCl, at a flow of 1-1.5 mL/min.

During the second day the sample in the column is washed with 10 mM TRIS-HCl, pH 8, 0.08% w/v LDAO, 135 mM NaCl, at a flow rate of 2-2.5 mL/min for at least 4 hours. Subsquently the column is washed again with the same buffer, but with 280 mM NaCl,

at a flow rate of 1-1.5 mL/min. This causes elution of the blue band containing the RC. The collected RC (usually around 40 mL volume) is dialyzed against 5 L 10 mM TRIS-HCl, pH 8, 0.025% w/v LDAO, for 12 hours.

During the third day, the resulting RC solution can be concentrated by ultrafiltration with a 100 KDa cutoff Centricon concentrator. Alternatively the RC solution can be loaded on a DEAE column and eluted by washing with 10 mM TRIS-HCl, pH 8, 0.08% w/v LDAO, 280 mM NaCl,. This step is skipped if the RC has to be reconstituted with or deprived of the secondary quinone acceptor (see further). The collected RC is frozen in liquid nitrogen and stored at -80°C.

3.4.3 *Removal of the secondary quinone acceptor*

Following the procedure set up by Okamura *et al.* (1975), a solution containing 150 nmoles of RC is loaded onto a previously equilibrated DEAE column (10 mL volume) with 10 mM TRIS-HCl, pH 8, 0.1% w/v LDAO, and washed with 70 mL of 10mM TRIS-HCl, pH 8, 1% w/v LDAO, 1mM Orto-phenantroline (O-phen). O-phen binds at the Q_B site, displacing ubiquinone. The column is washed with 40 mL of 10 mM TRIS-HCl, pH 8, 0.1% w/v LDAO and the RC is eluted with 1M NaCl. After collection, the RC is dialyzed two times for 12 hours against 10 mM TRIS-HCl, pH 8, 0.025% w/v LDAO using 100 volumes of buffer.

3.4.4 *Reconstitution of the secondary quinone acceptor*

The Q_B site was reconstituted following the protocol described in van Mourik *et al.*, (2001). The RC was loaded on a DEAE column (10 mL volume) previously equilibrated with buffer 20 mM TRIS-HCl, pH 8, 0.025% w/v LDAO, containing UQ-10 in excess. To overcome the low solubility of UQ-10 in aqueous buffer, 10mg of UQ-10 are solubilized overnight in a 1 mL solution of 30% LDAO. The sample is washed extensively (250-300 mL) the sample with the same buffer and the reconstituted RC eluted with 400 mM NaCl and dialyzed over-night.

3.4.5 *Detergent exchange in purified RC*

To exchange the LDAO detergent with OG and Sodium Cholate, the RC solution is first diluted below the LDAO critical micellar concentration (0.025% w/v) and dialyzed against the appropriate buffer containing 0.06% w/v OG and 0.02% w/v

Sodium cholate for 36 hours. Following this exchange the sample is concentrated by ultrafiltration with a 100 KDa cutoff Centricon concentrator, loaded on a PD10 column and eluted with buffers containing 0.6% OG and 0.2% Sodium cholate.

3.5 Determination of bacteriochlorofill content

The BChl in purified complexes and chromatophore was estimated spettrophotometrically following pigment extraction (Clayton *et al.*, 1966). The pigments were extracted from 20-50 μL of sample by mixing with 1 mL of acetone/metanol 7:2 (v/v), kept in the darkness and in ice for 30 min. Before measuring the absorption spectrum between 650 and 785 nm, the suspension is spinned in a microcentrifuge at maximum speed (15000 g) for 8 min to eliminate insoluble material. The BChl concentration can be evaluated on the basis of the Lambert-Beer law using an extinction coefficient, $\varepsilon = 75$ mM^{-1}cm^{-1} at 772 nm. When determining the concentration of the peripheral antenna in LH2 suspensions, a number of 27 BChl molecules per complex has been assumed (Mc Dermott *et al.*, 1995).

3.6 Extraction and analysis of phospholipids

The total phospholipids content of preparations was detrmined on the basis of phosphorous measurements by Inductively Coupled Plasma Atomic Emission Spectroscopy (ICP-AES) or by a spectrophotometric assay. In order to determine the lipid composition, lipids were extracted using the Bligh and Dyer method slightly modified as determined in 3.7.2. The relative phospholipid composition was evaluated by TLC and by ^{31}P-NMR analysis.

3.6.1 Phosphorous content

The total phospholipid complement associated with the purified complexes (RC, RC-LH1, and LH2) and the phospholipid/RC ratio in the chromatophore membranes have been determined on the basis of the phosphorous content measured directly on the untreated preparations by ICP-AES. Purified complexes were diluted with water to concentrations ranging between 10 and 50 nM and chromatophores to about 2 μM BChl. Diluted samples were directly pumped into the nebulizer of a Spectro Ciros

apparatus (Spectro A.I. Inc., Malborough, MA, USA) and analyzed for phosphorous content.

Phospholipid determination on lipid extracts resuspended in chloroform was performed spettrophotometrically as described in Rauser *et al.* (1970). The procedure includes the following steps:

a) Lipid samples are transferred into clean glass tubes and the solvent is completely evaporated;

b) The samples are supplemented with 0.65 mL perchloric acid (65%) and the tubes are heated at about 150°C for about 30 min (or until the yellow colour has disappeared);

c) After cooling at room temperature, 3.25 mL of water, 0.5 mL of molybdate solution (2.5g in 100 mL water) and 0.5 mL of an ascorbic acid solution (10g in 100 mL of water) are added. The solution is vortexed and placed in a boiling bath for 5 min;

d) The absorbance of cool samples (including the standards) are read at 800 nm. Standards) are prepared by diluting aliquots ranging from 1 to 5 mg P in 3.3 mL water and 0.65 mL perchloric acid. Digestion is not necessary before adding reagents. Classically, 5 μg P give an absorbance of 0.9. In order to have a solution containing 100μg P/mL, 439 mg of KH_2PO_4 in 1 L of water.

3.6.2 *Lipids extraction*

Before lipid extraction it is fundamental to decrease as much as possible the detergent concentration from the purified complexes. To this end, purified complexes are collected from the sucrose gradient and concentrated until a sample volume of 1.5 mL is obtained at protein concentrations ranging from 1.7 to 3 μM. The chromatophore suspensions at concentrations ranging between 1 and 2.5 mM BChl are directly extracted in the organic solvent mixture without any previous treatment.

In the case of the purified complexes, the detergent is partially removed by passing each sample twice through a PD10 column, eluting with 50 mM glycylglycine buffer, pH 7.8 and by diluting (at least 6 times) the collected fractions with the same buffer and centrifuging for 16 h at 180000 g. The lipid extraction is performed by:

a) Resuspending in 2 mL of the sample in a mixture of chloroform and methanol at a $H_2O/CH_3OH/CHCl_3$ ratio of 0.8:2:1 (v/v) in a final volume of 9 mL;

b) Shaking the suspension for 15 min and centrifuging for 10 min at 1200 g.

This extraction is repeated twice. The suspensions recovered after each extraction are collected in a separator funnel and supplemented with H_2O and $CHCl_3$ to obtain $H_2O/CH_3OH/CHCl_3$ ratios equal to 1:0.9:1 (v/v) which enable the H_2O/CH_3OH phase form the $CHCl_3$. The lower $CHCl_3$ phase , enriched in lipids, is collected and dried using the Rotavapor (maximum bath temperature 45°C, pressure at 460 mbar) or under nitrogen flow. The obtained lipid extracts are resuspended in chloroform and stored at minus 20°C.

3.6.3 *TLC analysis of lipid extracts*

TLC plates are obtained as described in detail in Scheme 2.

Scheme 2 TLC of phospholipids extracts

-Draw a line at 3 cm from the bottom where the sample will be loaded and a second line at 13 cm from the first as a run stop on a silica plate (20 cm x 20 cm x 0.25 mm thickness, 60 Å).

-Wash the plate twice with chloroform/methanol 1:1 (v/v) and activate it charring at 120°C in a oven for 2 hours.

-Prepare a solvent mixture of chloroform/methanol/acetic acid/water, 75:13:9:3 (v/v) as mobile phase and pour it in the chamber, and leave it closed in the cold room for at least 2 hours.

-Load (possibly under nitrogen flow) the sample in order to have no more then 100 μg of lipids extracts keeping in mind that the lipid extract contain pigments too.

-Put the plate in the chamber taking care to position it perpendicularly to the chamber bottom. Let the mobile phase to run up until it reaches the run stop line.

-Take out the plate from the chamber and let it dry for a while under the fume hood, then spray it with a 5% sulphuric acid or Molibdenum Blue solution and charry at 120°C for 30 minutes.

Quantitative analyses of the phospholipid contents were performed by densitometry using Total Lab software (Nonlinear Dynamics Ltd, Newcastle upon Tyne, UK). The lipid standard curves were linear in the range 0.5- 10 μg. Phospholipid used as standards were PC, PG, PE and CL.

3.6.4   NMR analysis of lipid extracts

For ^{31}P-NMR measurements, lipids (extracted as described above) have been dried under nitrogen flow and re-dissolved in 1 mL of a solvent mixture previously prepared by mixing 10 mL of predeuterated dimethyl formamide (DMF-d$_7$), 3 mL of triethylamine (ET$_3$N) and 1 g of guanidinium hydrochloride (GH$^+$) according to Bosco *et al.*, (1997). NMR experiments were performed with a 400 MHz Varian Inova spectrometer equipped with a multinuclear switch probe operating at 161.844 MHz for the ^{31}P nucleus. The experiments were carried out at room temperature (20 °C) in 5 mm tubes; the DMF-d$_7$ present in the mixture ET$_3$N-DMF-GH$^+$ acts as lock solvent. To perform a quantitative analysis, ^{31}P-NMR proton decoupled spectra were acquired by exploiting an inverse gated pulse sequence to suppress the nuclear Overhauser effect and by using a 70° r.f. pulse (7 µs), a 1s acquisition time, a relaxation delay of 20 s and a number of scans sufficient to achieve the desired signal-to-noise ratio. The relaxation times T_1 of several phospholipids have been previously measured in ET$_3$N-DMF-GH$^+$, and range from 0.85 to 1.3 s (Bosco *et al.*, 1997); therefore the sum of the acquisition time plus the relaxation delay was always more than five times T_1. The quantitative analysis was carried out through fitting of spectra to get the peak areas by use of the software MestReC from Mestrelab Research (Santiago de Compostela, Spain).

3.7   Quinone extraction and determination

Quinones were extracted from chromatophores and from the purified complexes using the procedure described in Venturoli *et al.*, (1986), according to the following protocol:

a) Add 250 µL of sample in a conic glassy tube of 10 ml volume and, working in ice, add 3mL of a methanol/petroleum ether 3:2 (v/v) solution and shake vigorously for 30 sec on a vortex;

b) Centrifuge for 1 min at 1000 rpm to enable the separation of the two phases and collect with a Pasteur pipette the upper one (petroleum ether) enriched in quinones;

c) Repeat the extraction two times more and collect all the phases containing quinones in the same tube, dry under nitrogen flux and resuspend in 500 ml of 2-propanol.

To quantify the quinone content, the extracts redissolved in isopropanol were injected into the HPLC apparatus (Jasco Pu-1580). A C-18 reverse phase column (Waters Spherisorb 5 μm ODS2, 4.6 x 250 mm) was used, connected to a Jasco UV 970 detector operating at 275 nm. The mobile phase (flow rate 1mL/min) was a mixture of 99.5% ethanol, 0.5% pure water plus 1 mL/L HClO$_4$ 65%. The calibration curves were made injecting aliquots of UQ$_{10}$ in ethanol at the appropriate concentrations, determined spectrophotometrically using ε_{275}=14.7 mM^{-1} cm^{-1}.

3.8 SDS and Blue Native polyacrylamide gel electrophoresis

In order to separate proteins according to their size, Schägger and von Jagov (Schägger *et al.*, 1987) SDS-PAGE has been used, at 15% or 20% of acrylamide and bisacrylamide concentration. In tables 4, 5 and 6 the composition of separating and stacking tricine gels are summarized. All the solution were prepared using bidistillated (BD) water. The Ammonium Persulfate (APS) must be freshly prepared.

Table4

15% Resolving gel, 10 mL	
Gel Buffer	3.33 mL
30% Acrylamide, 30:1	5 mL
BD H$_2$O	1.6 mL
25% APS	30 μL
Temed	10 μL

Table 5

20% Resolving gel, 10 mL	
Gel Buffer	3.33 mL
30% Acrylamide, 30:1	6.66 mL
BD H$_2$O	---
25% APS	30 μL
Temed	10 μL

Table 6

4% Stacking gel, 5 mL	
Gel Buffer	1.25 mL
30% Acrylamide	0.8 mL
BD H$_2$O	2.95 mL
25% APS	30 μL
Temed	10 μL

Other details of the gel electrophoresis are given in the following.

Gel Buffer: 3M TRIS-HCl, pH 8.45, 0.3% w/v SDS

Loading Buffer: 8% w/v SDS, 24% v/v Glycerol, 100 mM TRIS-HCl, 8% v/v β-mercaptoethanol, 0.02% w/v Serva Blue G R250

Anode Buffer: 0.2 M TRIS-HCl, pH 8.9

Cathod Buffer: 0.1 M TRIS-HCl, 0.1 M Tricine, pH 8.25, 0.1% w/v SDS.

Run conditions: 15 min 30 V constant to concentrate the sample at the edge of the running gel, then 110 V constant at least for 2 h, at room temperature.

The best resolution of the bands is achieved by loading the sample at a concentration of 1.6 μM. Diluted samples can be concentrated as follows.

a) Add to one volume of the protein solution ten volumes of cold Acetone/Methanol 7:2 (v/v) solution and keep it in ice;

b) Shake vigorously on a vortex and spin in microcentrifuge at maximum speed (15000g) for 8 min;

c) Carefully discharge supernatant and retain the pellet; dry the pellet at 30°C and resuspend it in the loading buffer.

Membrane native-protein complexes were resolved in a nondenaturing PAGE, a technique developed by Schägger *and* von Jagow (1991), called Blue Native (BN) electrophoresis which allows the separation of complexes without dissociating them into their constituents. The electrophoretic mobility of the protein depends on the binding of negatively charged Coomassie dye to the protein. The presence in the gel buffer of the zwitterionic salt amino-caprionic acid aids the extraction of protein complexes without damaging the sopramolecular structure. Purified protein complexes were analyzed in a BN PAGE in order to verify the presence of impurities in the preparation or their aggregation.

Samples were concentrated at 3 - 4 μM and 1/20 of the sample volume of 5% Serva Blue G-250 was added before loading in the gel. Slices containing protein complexes may be subsequently analyzed by SDS-PAGE which denatures the complexes and separates them into their respective subunits. The native gel, as in SDS PAGE, is composed by a stacking and a separating gel. The former was prepared from a solution of 4% acrylamide concentration. The separating gel was prepared as a gradient with an exponential concentration of acrylamide ranging from 5 to 12%, in order to resolve complexes with molecular weight ranging between 900 and 100 kDa. The solutions were loaded in the gradient maker (**Fig. 3.2**) chambers in order to have the 12% solution at the side of the outlet valve connected to a thin (4 mm diameter) 40 cm

long tube. At the end of the tube a thin tip allow a slow and regular pouring of the gel. The wells are formed using a spacer of 1.5 mm thickness. Gel polymerization was carried out at room temperature.

Fig. 3.2: The gradient maker used for BN polyacrylamide gel electrophoresis. The gradient maker is placed on a magnetic stirrer.

The solutions for the separating and stacking gels were prepared in separated beckers in ice adding the components in the order shown in table 7 and 8 respectively.

Table 7

	Separating 5%, 12mL	Separating 12%, 6mL
BD H$_2$O	6.5mL	1,6mL
Gel buffer 3x native	4mL	2mL
Acrylamide 40%, 29:1	1,55mL	1,8mL
Glycerol	no	0,6mL
Temed	5μL	3μL
APS 10%	15μL	10μL

Table 8

4% Stacking gel, 4 mL	
BD H$_2$O	2.267 mL
40% Acrylamide, 29:1	400 μL
Native 3X Gel Buffer	1.333 mL
25% APS	50 μL
Temed	5 μL

Glycerol was added only in the 12% separating gel solution which is the first to be loaded between the sandwiched glasses. APS and N,N,N',N'-Tetramethylethylenediamine (Temed) solutions must be added just before the preparation of the gel, when the solution are already in the gradient maker columns.

The stock solution composition is the following.

Gel Buffer 3X native: 1.5 M Aminocaprioic acid pH 7, Bis-TRIS 150 mM pH 7 in 100mL water

Loading buffer (SBG): 50 mg Serva Blue G 250 in 1 mL water

Anhod buffer: Bis-TRIS 50 mM in 2L water

Cathode Buffer: Bis-TRIS 15 mM pH 7, Tricine 50 mM pH 7 in 1L water

The gel was run at room temperature at 40 V for 20 min or until the samples were aligned at the interface between stacking and separating gels. Then the run proceeded at 80 V.

Both in the SDS and the Blue Native PAGE the protein bands were fixed and stained by Coomasie Brilliant Blue.

3.9   Time resolved absorption spectroscopy

The extent of photoxidizable RC and the charge recombination kinetics have been measured spectrophotometrically using a laser kinetic spectrophotometer of local design. A scheme of the instrument is shown in **Fig. 3.3.** The measuring beam (yellow line) is provided by an illuminator(1) equipped with a 100 W quartz tungsten halogen lamp. This beam is filtered by a double monochromator (2) and collimated by two focusing lenses (4). In the sample box (5) both a cuvette or a specifically designed, gas tight, sample holder can be placed. To avoid actinic effects due to the measuring light, the monitoring beam is gated shut until approximately 1 s before the laser pulse by an electromechanical shutter (3), placed between the monochromator and the lenses, controlled by an electronic delay line (12). The photomultiplier (6) is protected from scattered excitation light by 0.01% blocking, 10 nm bandwidth, interference filters centered at the measuring wavelenght. Rapid digitization and averaging of the amplified (13) photomultiplier signal is done by a Le Croy 9410 digital oscilloscope (14) controlled by an Olivetti M290 personal computer (15). Signal acquisition by the

oscilloscope is triggered by a photodiode (11) sensing the laser beam. Excitation, at 90°
with respect to the measuring beam, is provided by a frequency doubled Nd:YAG laser
(Quanta System, Handy 710) delivering 200 mJ pulses of 7 ns width (8), operated to a
power supply (9) and triggered by a pulse generator (10). The laser beam (green line)
hits the sample after reflection by two prisms (7).
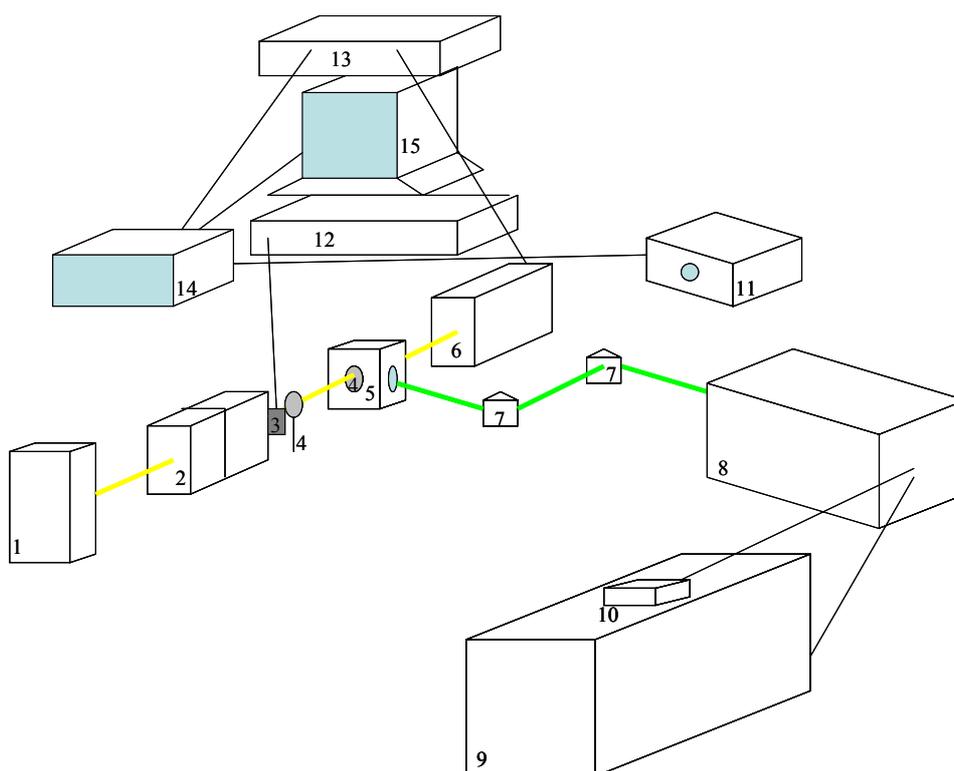
Fig. 3.3 Schematic representation of the laser kinetic spectrophotometer. Each component identified by
a numerical label, is described in the text.

When recording the charge recombination kinetics, saturation of a single
photoexcitation is close to 85% and larger than 90% for RC-only and RC-LH1
preparations, respectively. When repetitive photoexcitations are used to estimate the
total photoxidizable primary donor, the pulse energy is increased to 310 mJ. The sample
can be thermostated and the temperature of the sample is monitored by a Pt-100
resistance thermometer (Degussa GR 2105) immersed into or directly in touch with the
sample.

The kinetics of charge recombination following a single laser pulse is monitored at 422 nm as at this wavelength the light-dark differential spectrum of the RC exhibits a peak mainly due to photoxidation of the primary donor P; the remaining contribution (about 10%) is ascribed to formation of semiquinone on the acceptor complex (Slooten, 1972).

The concentration of photoactive RC is evaluated spectrophotometrically by measuring the concentration of the primary donor P photoxidized by a train of 6 laser pulses fired 100 ms apart. P^+ concentration is calculated from flash-induced absorbance changes measured at 600 nm using a differential extinction coefficient of $19.5 mM^{-1} cm^{-1}$ (Bowyer *et al.* 1981).

In kinetic spectrophotometric measurement, chromatophores are diluted at 50 μM BChl in 50 mM glcylglycine, pH 7.0, 50 mM KCl. Antimycin A (5 μM) and myxothiazol (0.5 μM) are added to inhibit the cyt bc_1 complex. The sample is also supplemented with 10 μM each of nigericin and valinomycin to collapse the transmembrane proton gradient and to avoid spectral interferences due to electrochromic effects. In chromatophores, measurements are routinely performed under two different conditions: (a) in the presence of 0.5 mM Na ascorbate to fully reduce the primary donor P in the dark; (b) in the presence of equimolar (0.5 mM) potassium ferro/ferricyanide to redox poise the system at 450 mV.

Most of the charge recombination kinetic measurements in purified RC-only and RC-LH1 core complexes have been performed in a buffer mixture containing 2-[N-Morpholino]ethanesulfonic acid (MES), glycilglycine and (3-[Cyclohexylamino]-1-propane sulfonic acid) CAPS, each at 20 mM (MGC buffer). In other measurements the following buffers were used at 10 mM concentration: piperazine-N,N^I-bis[2-ethanesulfonic acid] (PIPES) at 6.5<pH<7.7, tri[hydroxymethil]aminoethane (TRIS) at 7.7<pH<9.0 and 2-[N-cyclohexylamino]ethane sulfonic acid (CHES) at pH>9 adjusting the ionic strength at the desired value by additions of KCl. The value of pH was varied by small additions of KOH and HCl. To measure the recombination kinetics of the $P^+ Q_A^-$ state electron transfer from Q_A^- to Q_B was inhibited by adding o-phenanthroline at concentrations between 2.5 and 10 mM depending on the preparation examined.

Fitting of kinetic traces has been performed by non linear least-square minimization routines based on a modified Marquardt algorithm. Confidence intervals of fitting parameters have been estimated by an exhaustive search method.

3.10   Preparation of artificial RC containing matrices

3.10.1 RC embedded in saccharidic matrices

Glassy saccharidic matrices, containing trehalose or sucrose in a fixed sugar/RC protein rate equal to 10^4, were prepared according to the following procedures. RCs were diluted to 40 μM in 10 mM Tris, pH 8.0, 0.4 M sugar, 0.025 % LDAO. When preparing matrices for $P^+Q_A^-$ kinetic analysis, ortho-phenantroline was added at a final 10 mM concentration.
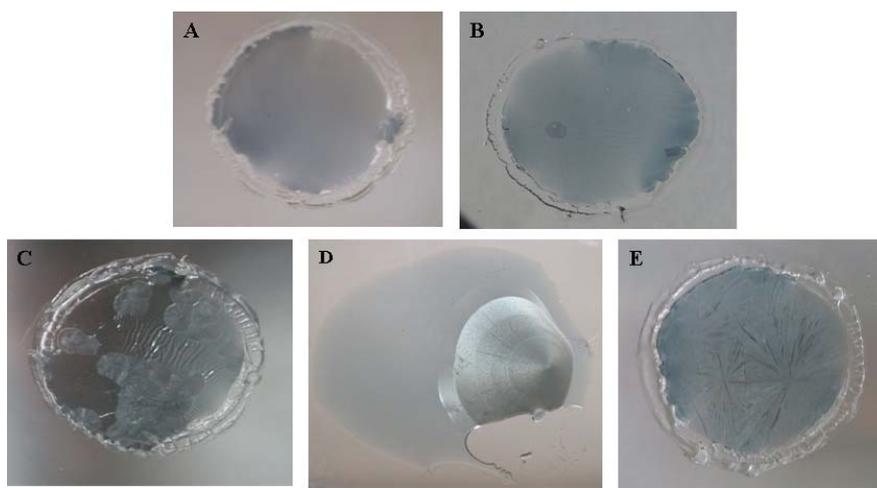

Fig. 3.4: Photographs of RC containing saccharidic matrices at different hydration levels. Panel A: a RC-trhalose plasticized matrix, after a few hours under nitrogen flux. Panel B: a RC-trehalose glassy matrix after a few days of drying, characterized by a 95% w/w sugar concentration. Panels C, D, E: RC-sucrose, RC-glucose and RC-trehalose glassy matrices, respectively, at extreme dehydration (over 97% w/w sugar concentration).

A thin layer (0.24 mL) of the liquid solutions, deposited on a 50 mm diameter optical glass window, was initially dried in a desiccator for ~ 8 hours under N_2 flow, at room temperature. At this time the sample has the characteristic aspect with of a plasticized, clear and transparent glass (see **Fig. 3.4 A**). Further drying of the trehalose matrices was obtained by leaving the samples under N_2 atmosphere at 30°C for ~ 12 hours (see **Fig. 3.4B**), then under vacuum for approximately the same time, and

alternating these treatments for several days depending on the sugar used. Typically a strong dehydration determines the formation of crystal-like structures in the matrix (see **Fig. 3.4 C**). Glucose matrices retained a plasticized character, even after this long dehydration protocol (see **Fig. 3.4D**). A similar procedure was used also for drying the sucrose matrices, which, however, reached maximal dehydration already after two days (see **Fig. 3.4E**).

To avoid water exchange with the environment during optical and near-infrared (NIR) measurements, the optical window on which the glassy sample was formed was inserted into a specifically designed, gas tight, sample holder, filled with dry N_2 (see **Fig. 3.5**).

Fig. 3.5 A RC-trehalose matrix inserted into the gas-tight sample holder used in spectrophotometric measurements.

3.10.2 Evaluation of the water content of the matrices

The water to RC molar ratio in dehydrated saccharidic matrices was evaluated by NIR spectroscopy. In the NIR spectral region, water has an important combination band at $\approx$ 1930 nm (due to the combination of scissoring and asymmetric stretching vibrations). The area S of the band, which is progressively reduced upon dehydration of the matrices, was used to evaluate the sample water content. Under the assumption that S is proportional to the water concentration and that glass formation and hardening does not affect the dipole strength of the transition, a proportionality constant, k = 100 (absorbance units) nm mM^{-1} cm^{-1} (Giustini *et al.*, 1996) was used (see eq.1). Since the optical path is not known and it likely depends on the water content we used the RC

absorption at 802 nm as an internal standard (see eq. 2). Assuming that the RC extinction coefficient at 802 nm (Straley *et al.*, 1973), $\varepsilon = 288$ mM^{-1}cm^{-1}, remains unchanged upon dehydration, we can calculate the relative glass composition as follows. The Lambert Beer law yields for the water and RC concentration:

$$S = k[H_2O]l \qquad (3.10.1)$$

$$A_{802} = \varepsilon[RC]l \qquad (3.10.2)$$

where k and ε have the values specified in the text. By dividing eq. 3.10.1 by eq. 3.10.2 we obtaine:

$$S^1 = \frac{S}{A_{802}} = \frac{k[H_2O]}{\varepsilon[RC]} \qquad (3.10.3)$$

From eq. (3), substituting the numerical values assumed for k and ε, the water/RC ratio can be obtained:

$$\frac{H_2O}{RC} = S^1 2880 \qquad (3.10.4)$$

The water/saccharide molar ratio is easily estimated from the water/RC ratio given by eq. (4), when considering that a ratio (sugar/RC = 104) has been used. Alternatively the level of dehydration can be expressed as in eq. (5).

$$\%saccharide = \frac{saccharide(w)}{saccharide(w) + H_2O(w)} = \frac{1}{1 + \dfrac{18}{saccharideMW}\left(\dfrac{H_2O}{saccharide}\right)} \qquad (3.10.5)$$

3.10.3 RC embedded in artificial matrices

Protein assembly by layer-by-layer adsorption of the negatively charged RC and the positively charged poly(dimethyldiallylammonium chloride) (PDDA) was performed on a glass or quartz slide (see **Fig. 3.6**). Substrates were negatively charged by using an oxidative cleaning in "piranha" solution (OLEUM H$_2$SO$_4$ and 30% H$_2$O$_2$ in a 3:1 ratio) for 15 min on ice (care should be taken in preparing and handling this solution, as the reaction is exothermic and the solution is highly corrosive) and subsequently left in Millipore water for 5 min. Finally, the substrates were rinsed with acetone and dried with nitrogen. To adsorb a polycation layer, the slide was immersed in a 2 mg/mL PDDA/water solution. Subsequently, it was washed in Milli-Q water and

a layer of negatively charged RC was adsorbed by dipping the specimen into 10 mM Tris-HCl buffer, pH= 8.0, containing 0.8% OG and 3 μM RC. After rinsing with Milli-Q water, the above described steps were repeated in order to obtain the required number of PDDA-RC multilayers. In this way both sides of the slide are covered with the same number of polyelectrolite multilayers. To reduce the possibility of RC desorption the last layer was always made by PDDA; adsorption and washing times were 30 min and 5 min, respectively; RC and polycation layers were grown in the dark at 4 °C. A sketch of the obtained multilayer is shown in **Fig. 3.6**.
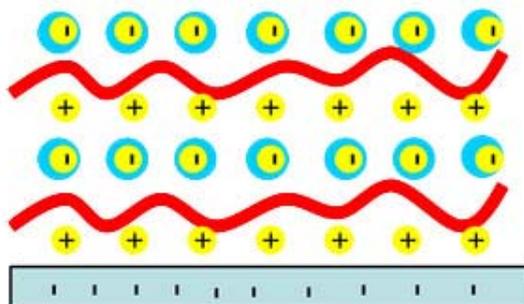

Fig. 3.6 Sketch of a PDDA-RC multilayer. The multilayer was assembled on a negatively charged glass support (the light cyan horizontal bar). The positively charged PDDA is represented by the red bended line while the RC protein layer is depicted by an array of cyan-yellow full spheres.

4 CHARACTERIZATION OF THE REACTION CENTER-LH1 ANTENNA COMPLEX

As described in par. 1.4, *in vivo*, the RC is intimately associated with the inner antenna LH1. Since the structure of the individual pigment-protein complexes which form the photosynthetic apparatus is essentially known, there is at present a growing interest in their supramolecular organization. Functional studies have led to the proposal of a "supercomplex" structure of the electron transfer proteins, associating two RCs, one bc_1 complex and one cytochrome c_2 (see Vermeglio and Joliot (2002) and references therein). An heterogeneous spatial distribution of the quinone pool has also been postulated on the basis of electron transfer studies performed in chromatophores (Drachev *et al.*, 1989; Comayras *et al.*, 2005a). A related question which has gained recently attention is the role of specific lipids not only in the structural stability and activity of individual membrane complexes, but also in the assembly and stability of supermolecular structures (Fyfe *et al.*, 2001; Palsdottir and Hunte, 2004; Jones, 2007). Crystallographic data have shown that the RC co-purify with tightly bound lipids which were structurally resolved (McAuley *et al.*, 1999; Camara-Artigas *et al.*, 2002).

The definition of a specific supermolecular architecture in the whole photosynthetic apparatus, its level of static (and/or dynamic) organization and its functional relevance are far from being clarified. When focusing on the behaviour of the LH1-RC core complex there is clear evidence, however, that the thermodynamics and kinetics of electron transfer processes within the RC are markedly affected by the degree of integrity of the system.

In this chapter, we describe and discuss results which concern the electron transfer properties and the ubiquinone and lipid complosition of RC-LH1 complexes. We have compared the kinetics of charge recombination of the $P^+Q_A^-$ and $P^+Q_B^-$ states induced by a single turnover photoexcitation in purified RC-LH1 complexes and in RCs deprived of the antenna. We found that the stability of the $P^+Q_B^-$ state is considerably enhanced in the core complex as compared to purified RCs in the absence of the LH1 complex. We also found that a large fraction (about 40%) of the endogenous membrane UQ pool is functionally retained in the purified RC-LH1 complex. However, analysis of the charge recombination, based on a kinetic model which considers rapid quinone binding

equilibrium at the Q_B site, indicated that the stabilization of the charged separated state in the core complex cannot be explained solely by a quinone concentration effect. The LH1 complex maintains within its ring structure a lipid domain whose interaction with the RC can in principle be responsible for stabilization of the charge separated state. To shed light on these points, we have: (i) examined the pH dependence of charge recombination in the RC-LH1 complexes; (ii) determined in parallel the quinone and lipid complements associated with the core complexes, comparing them with those of chromatophores; (iii) characterized the fractional composition of phospholipids copurifying with core complexes and compared it with that of the intact membrane and of purified LH2 complexes.

4.1   Results

4.1.1   *A comparison of the charge recombination kinetics in RC-only and RC-LH1 complex*

In a first series of measurements, we studied the recombination kinetics of the state $P^+Q_AQ_B^-$ induced by a laser actinic pulse at physiological pH value, varying the temperature. In a second step, the reaction was examined at constant temperature $294 \pm$ K, over a wide range of pH values. $P^+Q_AQ_B^-$ recombination has been extensively characterized in isolated RCs, yielding a wealth of information on the energetics of the electron transfer events involving the primary and secondary quinone acceptors (Kleinfeld *et al.*, 1984b; Mancino *et al.*, 1984; Palazzo *et al.*, 2000) and on the binding of the quinone at the Q_B site (Shinkarev *et al.*, 1997; Mallardi *et al.*, 1997). In **Fig. 4.1** the decay kinetics of P^+ generated by a laser pulse in RC-LH1 (trace a) and in RC-only (trace b) preparation are shown. In both cases the kinetics include two well-separated components and have been fitted to a fast exponential term plus a slowly decaying power law, according to eq. 4.1:

$$P^+(t)/P^+(0) = A_f \exp(-k_f\, t) + (1-A_f)\, (1 + k_0 t)^{-n} \qquad (4.1)$$

where A_f represents the fraction of reaction center (with the Q_B site empty or damaged during the purification procedure) that recombines from the state $P^+Q_A^-$ with a typical $k_f \approx 10$ s^{-1} (Feher *et al.*, 1989). The dominating slow component, attributed to $P^+Q_B^-$ recombination, deviates slightly but systematically from an exponential behavior

also in RC-LH1 preparations, as already reported for RC-only complexes (Francia *et al.*, 2003). The use of a power law to fit this kinetic phase implies a continuous distribution of rate constants (Kleinfeld *et al.*, 1984a; Palazzo *et al.*, 2002). The average rate constant, $<k>$, and the width, σ, of the rate distribution function are related to the parameters k_o and n in eq.4.1 by $<k>=nk_o$ and $\sigma^2=nk_o^2$ (Palazzo et al., 2002; see also below, par. 5.1.1). When fitting the kinetics to eq.4.1, we fixed the rate constant k_f of the fast phase to 8.2 s^{-1} as measured for $P^+Q_A^-$ recombination in suspensions of RC-only deprived of the secondary acceptor Q_B (Palazzo *et al.*, 2002). This in order to avoid effects of strong parameter correlation and in view of the relatively poor sampling of the fast kinetic component in traces recorded over several seconds. The validity of such an approach is justified by the fact that, in all preparations examined, leaving k_f as an adjustable parameter, yields values ranging between 8 s^{-1} and 10 s^{-1}, without any systematic difference between RC-only and RC-LH1 preparations. In agreement with this observation, when electron transfer to Q_B is inhibited by o-phenanthroline, essentially the same kinetics of $P^+Q_A^-$ recombination are measured in RC-only and RC-LH1 complexes, characterized by a rate constant $k\cong10$ s^{-1} at 298K (see below). The described fitting procedure yields in RC-LH1s purified from photosynthetically grown cells, an average rate constant ($<k>=0.29$ s^{-1}) 3.5 times smaller than in RC-only ($<k>=1.0$ s^{-1}). In both cases kinetics, at physiological pH, are moderately distributed with a comparable width of approximately 0.2-0.4 s^{-1} and the slow phase accounts for approximately 80% of P^+ decay (see **Fig. 4.1**). This relatively narrow distribution of rate constants agrees with the results of a previous analysis in RC-only (Francia *et al.*, 2003). Following the procedure exemplified in **Fig. 4.1**, the kinetics of P^+ decay after a laser pulse have been analyzed in a series of preparations of core complexes isolated from *wt* cells, grown under photosynthetic conditions, and from *wt* and X$^-$ strain cells, grown under semiaerobic conditions. Fitting parameters for the corresponding kinetics are summarized in **Table 1** which also includes two independent RC-only preparations.
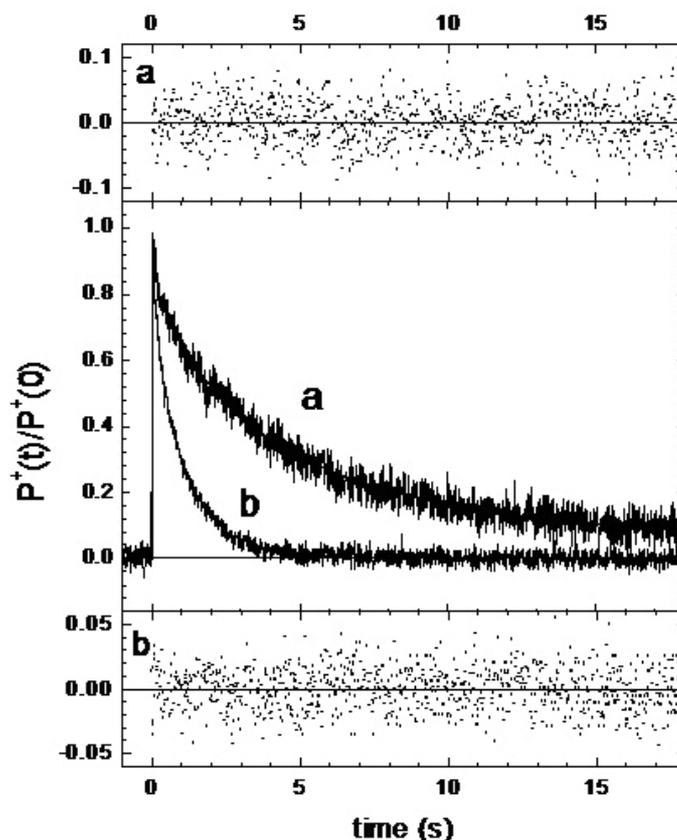
Fig. 4.1 Kinetics of charge recombination following flash excitation in dimeric RC-LH1 complexes purified from photosynthetically grown cells (trace a) and in RC-only complexes (trace b). Measurements, performed at T=298K, in the presence of 0.6%OG, 0.2% Na-cholate, are the result of 4 averages. P^+ decays recorded at 605 nm have been normalized to the maximal amplitude at the time of the laser pulse (t=0). Traces have been fitted to the sum of an exponential decay (fast phase) and a power law (slow phase) as described in detail in the text. This procedure yielded $<k>=0.28$ s^{-1}, $\sigma=0.22$ s^{-1} in the RC-LH1 complex and $<k>=1.01$ s^{-1}, $\sigma=0.35$ s^{-1} in RC-only. Residues for traces a and b are shown in the upper and lower panel respectively.

Drastic slowing down of the kinetic phase attributed to $P^+Q_B^-$ recombination appears to be a general feature of RC-LH1 core complexes as compared to RC-only. This slowing is however significatively more pronounced in *wt* preparations from semiaeobically grown cells than in complexes purified from photosynthetically grown *wt* cells.

In the former case the slow component of P^+ decay exhibit an average rate constant $<k>=0.21$ s^{-1}, four times smaller than in RC-only complexes ($<k>=1.0$ s^{-1}). In

core complexes purified from the PufX deleted strain the $<k>$ value is essentially coincident with that obtained in RC-LH1 from photosynthetically grown *wt* cells.

preparation	$<k> (s^{-1})$	$\sigma (s^{-1})$	A_f (%)	UQ_{10}/P^+	$BChl/P^+$
RC-LH1 from photosynthetically grown cells					
prep1	0.28	0.22	16.4	10.5 ± 0.7	35.0 ± 4.7
prep2	0.30	0.33	17.9	11.3 ± 0.5	34.0 ± 1.8
RC-LH1 from semiaerobically grown cells					
prep1	0.21	0.21	15.9	16.2 ± 0.6	23.5 ± 1.9
prep2	0.21	0.20	13.6	14.3 ± 3.0	27.2 ± 0.3
RC-LH1 from X$^-$ strain	0.29	0.21	6.5	$17.6 \pm ?$	36.9 ± 0.9
RC-only					
prep1	1.01	0.35	22.3	1.5 ± 0.3	4.5 ± 0.5
prep2	0.98	0.38	19.3	-	-

Table 1 Kinetic parameters of $P^+Q_B^-$ charge recombination and cofactor stoichiometries in RC-LH1 and RC-only preparations. Kinetics of charge recombination were measured at 605 nm at 25°C and fitted to the sum of a power law and an exponential decay with a fixed rate constant equal to 8.2 s^{-1} (see eq.4.1). See text for further details.

To safely attribute the extremely slow P^+ decay observed in core complexes to recombination of the $P^+Q_B^-$ state it is important to exclude the occurrence of side redox reactions which, on the time scale of several seconds, could contribute in principle to oxidize the light-generated semiquinone at the Q_B site thus inducing slow P^+ re-reduction by exogenous electron donors. The stability of the semiquinone formed upon laser excitation at the Q_B site has been therefore tested in the RC-LH1 complexes by monitoring the laser-induced formation of semiquinone at 446 nm, in the presence of added diaminodurene (DAD). This exogenous electron donor completely re-reduces the photoxidized P^+ in a few milliseconds, so that the $PQ_AQ_B^-$ and $PQ_A^-Q_B$ states are trapped (Vermeglio, 1977; Wraight, 1977). Under these conditions, in RC-LH1 complexes, the flash-generated semiquinone signal decayed by less than 10% over 20 seconds. This indicates that flash-induced Q_B^- is quite stable in core complexes over the time of P^+ decay measured in the absence of exogenous electron donors (**Fig. 4.1**). Assuming differential extinction coefficients $\Delta\varepsilon_{605} = 19.5 mM^{-1}$ and $\Delta\varepsilon_{446} = 8.5 \ mM^{-1}$ for P^+ and semiquinone respectively (Dutton *et al.*, 1975; Wraight *et al.*, 1975; Bowyer

et al., 1981), a Q^-/P^+ ratio close to one has been estimated, confirming the stability of the quinone acceptor radicals. These measurements unambiguously show that the very slow P^+ decay kinetics observed in LH1-RC complexes reflect a genuine charge recombination process.

The temperature dependence of $P^+Q_B^-$ recombination kinetics has been examined in LH1-RC complexes puified from photosynthetically grown *wt* cells over the range $275K \leq T \leq 305K$.
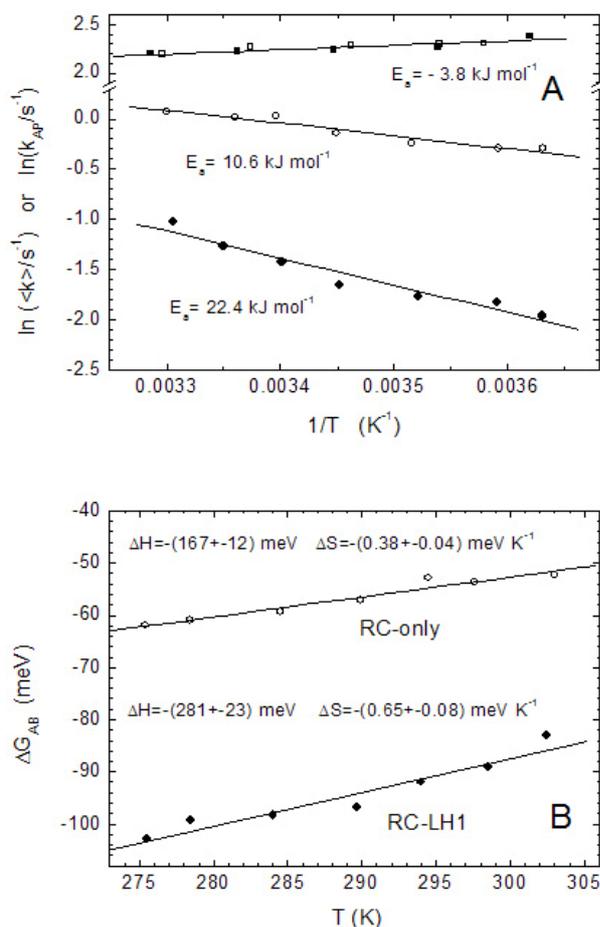

Fig. 4.2 Temperature dependence of $P^+Q_B^-$ (circles) and $P^+Q_A^-$ (squares) recombination kinetics in RC-LH1 (filled symbols) and RC-only complexes (open symbols). Panel A: Arrhenius plot of the the average rate constant $<k>$ of the slow kinetic component of P^+ decay ($P^+Q_B^-$ recombination) and of the rate constant k_{AP} measured in the presence of 10 mM o-phenanthroline ($P^+Q_A^-$ recombination). Panel B: Temperature dependence of the free energy difference ΔG_{AB} between the $P^+Q_AQ_B^-$ and the $P^+Q_A^-Q_B$ states evaluated from the data of panel A as described in the text (see Discussion, eqn.4.5). Best fitting straight lines correspond to $\Delta H= -(281\pm23)$ meV, $\Delta S= -(0.65\pm0.08)$ meV K^{-1} for RC-LH1 and $\Delta H= -(167\pm12)$ meV, $\Delta S= -(0.38\pm0.04)$ meV K^{-1} for RC-only.

Panel A of **Fig. 4.2** presents an Arrhenius plot of the average rate constant <k> determined by the above described fitting procedure in core complexes and in a RC-only preparation. A stronger temperature dependence is obtained in the former case, corresponding to an apparent activation energy of approximately 22 kJmol^{-1} as compared to 11 kJmol^{-1} in the RC-only complex. The kinetics of $P^+Q_A^-$ recombination were examined by measuring P^+ decay in the same RC-LH1 and RC-only preparations in the presence of 10 mM o-phenanthroline. Fitting the decays to a single exponential yielded very close values of the rate constant k_{AP} for $P^+Q_A^-$ recombination in the two systems. Rate constants vary in both preparations between approximately 10.8 s^{-1} at T=275K and 9.0 s^{-1} at T=305K (see **Fig. 4.2A**), exhibiting a small, negative, apparent activation energy of approximately –3.8 kJ mol^{-1}. The coincidence of k_{AP} values and the higher apparent activation energy measured for $P^+Q_B^-$ recombination in LH1-RC complexes strongly suggest that stabilization of the $P^+Q_AQ_B^-$ state with respect to the $P^+Q_A^-Q_B$ is increased in the presence of the LH1 antenna (see below in par. 4.2.2).

We have subsequently analyzed charge recombination in RCs deprived of the antenna and in the dimeric and monomeric forms of the core RC-LH1 complex as a function of pH (6.5<pH<11.5). **Fig. 4.3** shows traces recorded at two pH values in RC-only and in dimeric RC-LH1 complexes, at 294 ± 1 K. In agreement with previous measurements at pH=7.6 the recovery kinetics are drastically slowed in the core RC-LH1 complex as compared to the RC-only complex (panel A). In contrast, at alkaline pH values (panel B), kinetics do not differ substantially, being strongly and comparably accelerated in RC-LH1 and RC-only complexes. The kinetics, which exhibit a clear biphasic character, have been fitted to a fast exponential decay plus a slowly decaying power law, according to the eq. 4.1, which was previously shown to account satisfactorily for the kinetics measured at neutral pH values over a range of temperatures. To avoid the effects of parameter correlation, when fitting the kinetics to eq. 1 the value of k_f was fixed to 9.5 s^{-1}, as measured in RC-only and in RC-LH1 complexes at neutral pH values (see **Fig. 4.2A**). This fitting procedure was extended to the whole pH range investigated in view of the following observations:

(a) In the pH range between 6.5 and 9.0, where the two kinetic components are characterized by well separated time scales, leaving k_f as a free adjustable

parameter, yields values ranging between 8 and 10 s^{-1} in all the preparations examined.
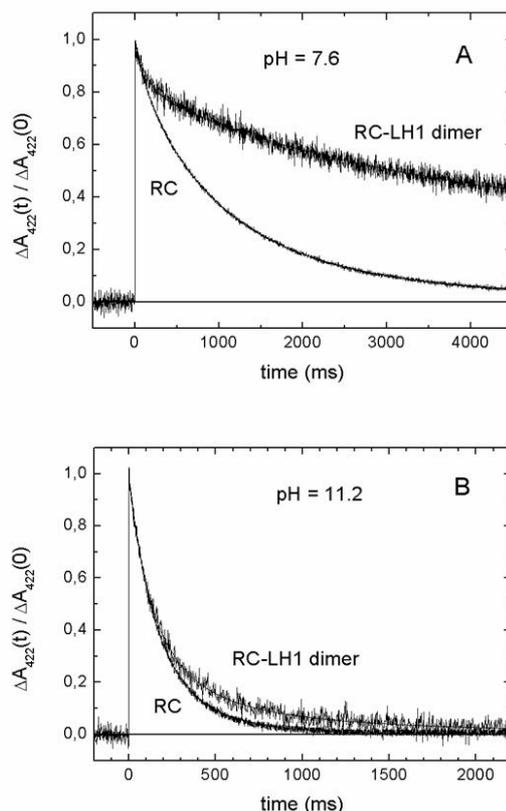

Fig. 4.3 Decay kinetics of P^+ generated by a laser pulse in RC-LH1 dimers and in RC-only complexes at pH=7.6 (panel A) and at pH=11.2 (panel B). Kinetics have been measured at 422 nm and normalized to the maximal absorbance change induced by the laser pulse fired at t=0. RC and RC-LH1 complexes were suspended in MGC buffer (see Materials and methods, par 3.9) at concentrations of 2.2 μM and 1.2 μM, respectively. Continuous lines represent best fits to eqn.1 corresponding to the following parameters. At pH = 7.6, $<k>$ = 0.97 s^{-1} (0.96, 0.98), σ = 0.48 s^{-1} (0.46, 0.49) for RC; $<k>$ = 0.22 s^{-1} (0.20, 0.24), σ = 0.23 s^{-1} (0.10, 0.32) for RC-LH1. At pH = 11.2, $<k>$ = 5.60 s^{-1} (5.42, 5.78), σ = 2.38 s^{-1} (2.04, 2.76) for RC; $<k>$ = 5.87 s^{-1} (4.48, 7.04), σ = 4.70 s^{-1} (3.02, 6.20) for RC-LH1. Values in parentheses represent the extremes of confidence intervals within two standard deviations. Although in panel A the trace measured in the RC-LH1 complex is shown over a 4 second time interval, the slow kinetics observed at pH < 10 were routinely sampled and fitted on a 20 s time interval.

(b) These values are consistent with those obtained for the kinetics of $P^+Q_A^-$ recombination in RC-only complexes in LDAO detergent over a large pH range (6.2< pH <11.8) (Kleinfeld *et al.*, 1984b).We have measured the kinetics of $P^+Q_A^-$

recombination in RC-LH1 core complexes and in RCs suspended in the same detergent (OG and Na-cholate) as a function of pH, by monitoring the decay of P^+ after a laser pulse in the presence of o-phenantrholine.

Interestingly, in RC-only preprations, o-phenanthroline blocks electron transfer to Q_B over the whole RC population at a concentration of 2.5 mM, as judged from the essentially monoexponential, fast decay of P^+ observed. At this inhibitor concentration, a considerable fraction of slow P^+ decay, reflecting $P^+Q_B^-$ recombination, is still present in RC-LH1 complexes and complete inhibition (single, fast exponential decay) is observed only at o-phenantroline concentrations higher than 10 mM. **Fig. 4.4** compares the rate constants obtained under these conditions in dimeric core complexes and in RCs. In both cases, the rate constant is pH independent, as found for the isolated RC in LDAO detergent (Kleinfeld *et al.*, 1984b). The same values are obtained within the experimental error in RC-LH1 and in RC-only complexes. No dependence on the ionic strength (between 20 and 100 mM) was observed. Essentially the same, pH independent, rate constant value was obtained in monomeric RC-LH1 from *wt* and PufX-deleted strains.
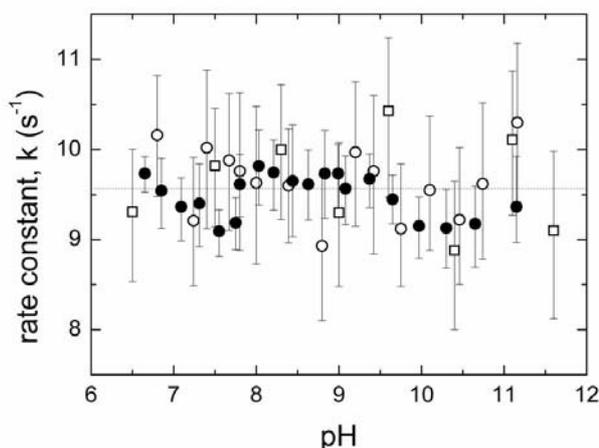
Fig. 4.4 The rate constant of $P^+Q_A^-$ recombination determined from the decay kinetics of flash generated P^+ in RC (closed circles) and in RC-LH1 dimers (open symbols) as a function of pH. Measurements in RCs were performed in the presence of 2.5 mM o-phenanthroline using PIPES, TRIS and CHES as buffers, depending on the pH range as described under Materials and methods (see paragraph 3.9), and adjusting the ionic strength to 100 mM. Kinetics in RC-LH1 suspensions were recorded in the presence of 10 mM o-phenanthroline in the same buffers (open squares) and in MGC buffer (open circles). The confidence intervals within two standard deviations are shown as vertical bars. The dotted horizontal line indicates the average of all the measured rate constant values.

Fitting to eq. 4.1 yields an accurate description of the kinetics of charge recombination over the whole pH range investigated (see continuous lines in **Fig. 4.3**). The fractional amplitude A_f of the fast phase is essentially pH independent, somewhat varying form preparation to preparations in a range between 0.1 and 0.3. In **Fig. 4.5** the values obtained for $<k>$ (panel A) and σ (panel B) in RCs and in different preprations of RC-LH1 core complexes are plotted as a function of pH.
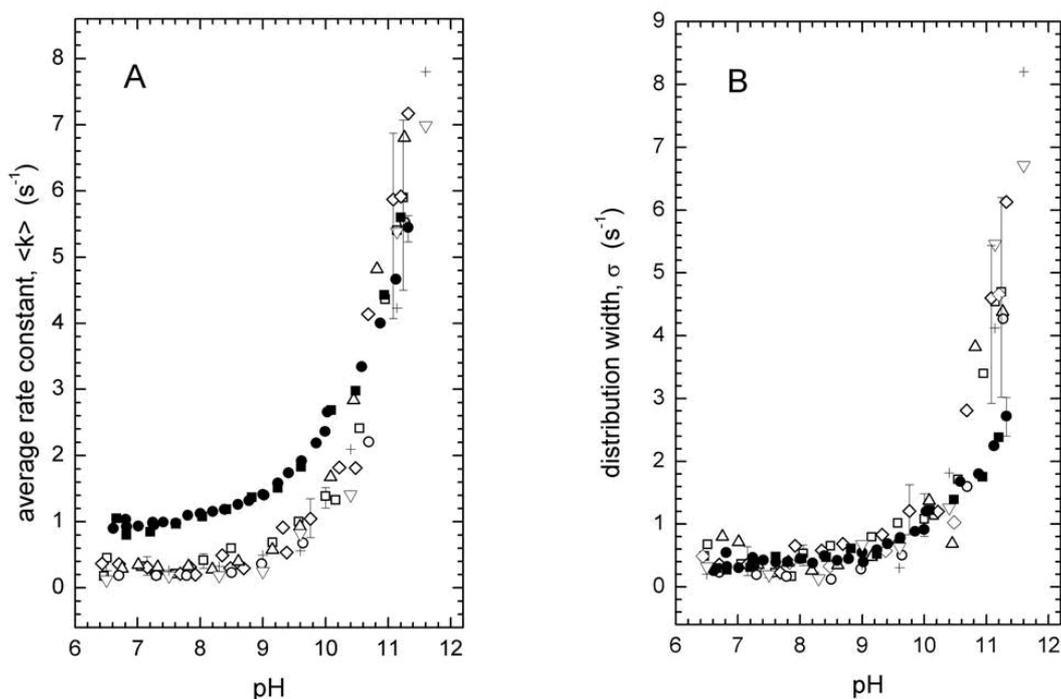
Fig. 4.5 The pH dependence of the average rate constant $<k>$ (panel A) and of the rate distribution width σ (panel B) for $P^+Q_B^-$ recombination in RC (closed symbols) and in a series of RC-LH1 core complex preparations (open symbols). Kinetic parameters were obtained by fitting P^+ decays following a laser pulse to eqn. (4.1) (see **Fig. 4.3** and text for further details). In RC suspensions, measurements were performed in 20 mM MGC buffer (closed squares) and using PIPES, TRIS and CHES as buffers at a final ionic strength of 100 mM (closed circles), as described in par. 3.9. Kinetics were monitored in MGC buffer in the dimeric (open squares) and monomeric (open diamonds) forms of RC-LH1 complexes purified from photosynthetically grown cells, in RC-LH1 dimers isolated from semiarobically grown bacteria (open circles) and in monomeric core complexes from the PufX-deleted strain (open triangles). Kinetics for the dimeric RC-LH1 complex from photosynthetically grown cells have been measured also using PIPES, TRIS and CHES as buffers at 10 mM each (open inverse triangles) and after adjusting the ionic strength at 100 mM with KCl additions (crosses). Titrations were carried out routinely from acidic to alkaline pH values. For each preparation data sets include experimental points obtained by titrating in the reverse direction after the high pH measurements. For visual clarity the confidence intervals within two standard deviations (vertical bars) are shown only for a selected number of measurements in the acidic, neutral and alkaline range of pH values.

To check whether the kinetics recorded at alkaline pH values were affected by possible partial denaturation of the complexes, after measurements at the highest pH values, samples were re-equilibrated at lower pHs and kinetics re-measured. Reversibility of the titrations was observed for all preparations. A further, minimal prerequisite for a physically meaningful interpretation of these results is that the supermolecular integrity of the core complexes is preserved over the whole pH range investigated. In fact, we cannot exclude a priori that the associations between the RC and the LH1 antenna and/or between two RC-LH1 monomers in the dimer are disrupted at alkaline pH values. To test these possibilities, we have re-loaded an already purified dimeric RC-LH1 complex on sucrose gradients equilibrated with buffers at different pH values. As shown in **Fig. 4.6**, the band attributed to the dimeric form of RC-LH1 (Francia *et al.*, 1999) is still present after ultracentrifugation at alkaline pHs (pH = 10.0 and 11.0). As previously found at pH = 7.8 (Francia *et al.*, 1999) re-loading of the dimer produces a partial monomerization, the extent of which however is not enhanced by alkalinization. From this observation we argue that core complexes preserve substantially their integrity during spectrophotometric measurements.
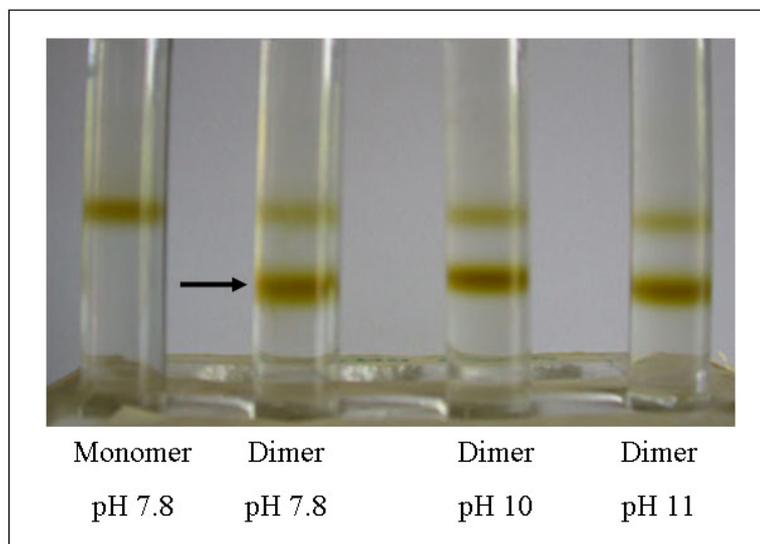
Fig. 4.6 Rate zonal centrifugation of previously separated monomeric (left tube) and dimeric forms of RC-LH1 complexes, reloaded on a sucrose density gradient (10-40% w/w sucrose) containing 0.6% OG and 0.2% sodium cholate in 20 mM MGC buffer (at pH 7.8) and 20 mM CAPS (at pH 10.0 and 11.0). The arrow indicates the position of the band corresponding to the dimeric complex. Determination of the UQ_{10} complement in the dimer fractions yields $UQ_{10}/RC \approx 25$ before and after sucrose gradient centrifugation at all pH values.

Since RC-LH1 complexes at pH 7.8 have been shown to copurify with a large fraction (about 40 %) of the native membrane quinone pool (see below, par. 4.1.2), we also measured the ubiquinone content of the dimeric fraction before and after re-loading on the sucrose gradient at different pHs. Essentially the same ubiquinone complement per photoxidizable RC was obtained at all pH values, indicating that UQ does not redistribute upon changing the pH. This observation is consistent with the finding that the fraction A_f of the fast phase in the kinetics of charge recombination does not depend upon the pH (see above), indicating the same occupancy of the Q_B site of the RC also at alkaline pH values.

As shown in **Fig. 4.5**, the kinetics of charge recombination have been analyzed in dimeric RC-LH1 complexes purified from *wt* cells grown both photosynthetically and semiarobically in the dark; also the monomeric forms isolated from photosynthetically grown *wt* cells and from the PufX-deleted strain have been characterized. Within the large experimental uncertainty, all the core complexes examined exhibit comparable values of the average rate constant <k>, with a similar pH dependence. Over the pH range between 6.5 and 9.5, the values of <k> in the core complexes are on average four times smaller than in the RC-only complex, in agreement with previous measurements at pH ≈ 8 (see above, **Fig. 4.1**). However, at higher pH values, for which the average rate constant increases, the marked stabilization of the $P^+Q_B^-$ charge separated state observed in the core complexes decreases progressively and vanishes at pH >11.

At pH values lower than approximately 9.0, the kinetics of the slow component of charge recombination are moderately and similarly distributed around <k> in all the core complexes examined and in RC-only complexes As shown in **Fig. 4.5B**, in fact, at pH < 9.5, the width of the rate distribution function, σ, fluctuates in the core complexes between 0.1 s^{-1} and 0.8 s^{-1}, a range comparable with the large uncertainty associated with the determination of this parameter. Within the experimental error, these values of σ coincides with those measured in the RC-only complexes, which fluctuate between 0.3 s^{-1} and 0.6 s^{-1}, in agreement with previous determinations at pH 7.8 (see **Table 1**). However when the pH increases above 9.5-10, the distribution width increases progressively both in the RC and in RC-LH1 complexes. In the latter, the effect is more

pronounced and σ increases by one order of magnitude, reaching values between 5 s^{-1} and 8 s^{-1} at pH > 11.

Most of the measurements described above have been performed in 20 mM MGC buffer (see par. 3.9). In this mixture, due to the dissociation equilibria of MES, glycyl-glycine and CAPS, the ionic strength of the sample varies over the pH range examined, increasing from about 20 mM at pH 6.5 to about 55 mM at pH=11.5. To check whether kinetics are affected by the ionic strength over this range of variation, measurements on RC-only complexes were performed both in 20 mM MGC buffer (closed squares in **Fig. 4.5**) and using three different buffers (PIPES, TRIS, CHES at 10 mM), adjusting the ionic strength at 100 mM, as described under Materials and methods, par. 3.9 (closed circles in **Fig. 4.5**). Under these two conditions essentially the same <k> and σ values were obtained over the whole pH range. A similar comparison was performed in RC-LH1 dimers, by examining the kinetics under three conditions: (i) in 10 mM PIPES, TRIS, CHES buffers (open inverse triangles in **Fig. 4.5**); (ii) in the same buffers, adding at each tested pH value the amount of KCl necessary to reach the corresponding ionic strength of the MGC buffer mixture (data not shown); (iii) in the same buffer, but adjusting the ionic strength to 100 mM over the whole pH range by the appropriate additions of KCl (crosses in **Fig. 4.5**). Essentially the same kinetic parameters (<k> and σ) were found within the experimental error under all conditions tested, concluding that the different forms of core complexes examined share essentially the same kinetics with a similar pH dependence (see open symbols in **Fig. 4.5A** and **B**); possible differences are within our experimental uncertainty.

4.1.2 *Ubiquinone and phospholipids complements associated with the purified core complex*

As analyzed in detail by Shinkarev and Wraight (1993) the kinetics of $P^+Q_AQ_B^-$ recombination can be considerably affected by the binding equilibrium of ubiquinone at the Q_B site when this process occurs rapidly over the time scale of $P^+Q_A^-$ recombination. Recent investigations performed on RC-only complexes in inverted micelles (Mallardi *et al.*, 1997) as well as in artificial lipid vesicles (Palazzo *et al.*, 2000) are indeed consistent with a fast quinone exchange at the Q_B site and indicate that the observed rate constant of $P^+Q_AQ_B^-$ recombination is sensitive to the concentration of quinone [Q] in

rapid equilibrium with the binding site (*i.e.* it decreases at increasing [Q], see Introduction, par. 1.2.2). This view clearly prompts for a determination of the quinone complement associated with the purified core complexes in which a marked slowing down of the recombination kinetics was observed.

The ubiquinone content of the examined core complex and RC-only preparations was determined by exhaustive extraction and HPLC analysis (see par. 3.7). **Fig. 4.7** shows the chromatogram of a pure ubiquinone-10 sample (dotted line) overlayed to a typical chromatogram of a RC-LH1 extract (continuous line). Spectral analysis of the eluates has confirmed the attribution to oxidized UQ_{10} of the peak at 6.4 minutes and has indicated that the components eluted at shorter times are mainly carotenoids. This analysis indicates also that the carotenoid contamination of the UQ_{10} fraction is lower than 10%.
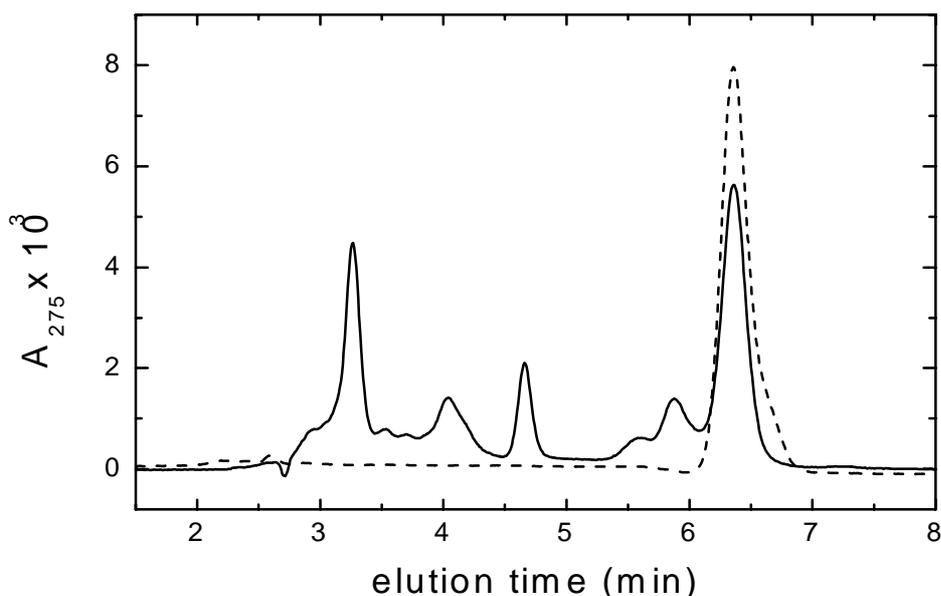
Fig. 4.7 HPLC chromatograms of the extract from a RC-LH1 preparation (prep1 from photosynthetically grown cells in **Table 1**) (continuous line) and of a standard solution of UQ_{10} corresponding to 150 pmoles (dashed line). The injected extract of the core complexes corresponds to 6.7 pmoles of photoxidizable reaction center.

In parallel measurements the total photooxidizable primary donor P was estimated by measuring the absorbance change induced at 605 and 542 nm (Dutton *et al.*, 1975; Bowyer *et al.*, 1981) by trains of actinic xenon flashes. In the case of purified RC-only

preparations, excitation by continuous light was used to achieve saturation (see par. 3.9). The stoichiometric ratios UQ_{10}/P^+ obtained on these basis are summarized in **Table 1**, which also includes the corresponding bacteriochlorophyls to P^+ ratios ($BChl/P^+$). As expectd determination of this stoichiometry in RC-only preparations yielded a value consistent with 4 BChl per RC, while a number of ubiquinone molecules per RC close to two was found, in agreement with previous measurements (Okamura *et al.*, 1975; Okamura *et al.*, 1982). In RC-LH1 core complexes purified from semiaerobically grown *wt* cells an average ratio of 25 BChl molecules per complex was obtained, in reasonable agreement with recent low resolution structural data which suggest the presence of 12 $\alpha\beta$ heterodimers per LH1 ring (Scheuring *et al.*, 2004). The $BChl/P^+$ ratio increases to approximately 37 in core complexes purified from the PufX deleted strain, a value consistent with previous observations (Mc Glynn *et al.*, 1994; Francia *et al.*, 1999) and with the notion that a closed ring of $\alpha\beta$ heterodimers surrounds the RC in the absence of the PufX protein. In RC-LH1 complexes purified from photosynthetically grown *wt* cells the number of BChl molecules per P^+ is close to 35, *i.e.* systematically and significatively larger than in complexes purified from semiaerobically grown bacteria.

Surprisingly in all the core complex preparations examined a large pool of ubiquinone-10 is detected; in fact the stoichiometry UQ_{10}/P^+ ranges from approximately 10 to 15 in RC-LH1 from photosynthetically and semiarobically grown *wt* cells respectively. An even larger pool (18 UQ_{10} molecules per photoxidizable RC) was determined in core complexes isolated from the X^- strain. The large ubiquinone complements associated with RC-LH1 represent a considerable fraction of the total ubiquinone present in the membrane phase. RC-LH1 complexes, exhibiting a UQ_{10}/P^+ ratio close to 11 were isolated from chromatophores characterized by a stoichiometry of 25 ubiquinone molecules per photoxidizable RC.

The high UQ_{10}/P^+ ratio found in RC-LH1 fractions are unlikely to be due to ubiquinone solubilized in a pure detergent phase. Analysis of the different fractions collected over the whole sucrose gradient used to separate photosynthetic membrane complexes has revealed sizable amounts of UQ_{10} in the top fraction of the gradient, where low density detergent micelles are expected to be layered. To further examine the

possibility that the large ubiquinone content of isolated core complexes is simply due to a strong preferential partion of UQ_{10} in the detergents with respect to the membrane phospholipids, we have determined the UQ_{10}/P^+ ratio in different fractions during the purification procedure. As shown in **Table 2**, chromatophores washed with 2M NaBr are characterized by an enrichment both in the number of BChl and of UQ_{10} per P^+, presumably due to inactivation of photochemistry in a fraction of RCs. Subsequent steps include detergent extraction with OG and NaCholate and ultracentifugation (see par. 3.3). The $BChl/P^+$ and UQ_{10}/P^+ stoichiometries have been determined in the pellet and in the supernatant which is loaded on the 10-40 % sucrose gradient for the isolation of the LH2 and RC-LH1 complexes. The number of BChl per photoactive reaction center is essentially unaffected in the supernatant and drastically reduced in the residual pellet indicating a good yield of detergent extraction of the photosynthetic complexes. The UQ_{10}/P^+ ratio decreases from 38 in the washed membrane fraction to 30 in the supernatant. At variance, a sizable increase of the UQ_{10}/P^+ stoichiometry is observed in the residual membrane pellet. These observations argue against a segregation of quinones in the detergent phase.

Sample	$BChl/P^+$	UQ_{10}/P^+
chromatophores	142 ± 8	25 ± 5
NaBr-washed chromatophores	175 ± 10	38 ± 3
supernatant	173 ± 7	30 ± 5
pellet	53 ± 6	43 ± 1

Table 2 Bacteriochlorophyll and ubiquinone-10 to P^+ stoichiometries determined in different fractions during the purification of core complexes. See text for details.

The concentration of the LH2 complexes purified on the same sucrose gradient from which the LH1-RCs were isolated, has been evaluated from the total BChl content by assuming 27 BChl molecules per complex (Mc Dermott *et al.*, 1995). On this basis, determination of ubiquinone in the LH2 fraction yields approximately 1.4 UQ_{10} molecules per LH2, well below the values obtained in RC-LH1. Since both LH2 and RC-LH1 fractions come from the same detergent extract, this observation again

indicates that the high UQ_{10} content of the RC-LH1 is not simply due to partition of ubiquinone in the detergents, but is a peculiar feature of the core complexes.

In order to confirm the analytical determinations of the ubiquinone to RC stoichiometries and to assess the functionality of the detected quinone molecules in accepting electrons at the Q_B site, we used an alternative quinone assay, based on the rapid oxidation of cytochrome c_2 by the RC under continuous illumination (Okamura *et al.*, 1982). In the presence of excess reduced cyt c_2 the number of turnover which the RC can sustain under continuous light is limited by the number of oxidized ubiquinone molecules available as electron acceptors at the Q_B site. More precisely when *n* ubiquinone molecules per RC are present in addition to the primary acceptor Q_A, ($2n$ +1) molecules of cyt c_2 per RC are expected to be oxidized under continuous illumination. **Fig. 4.8** shows the oxidation of exogenously added cyt c_2 (monitored at 551nm) by RC-LH1 and RC-only complexes exposed for 500 ms to continuous light excitation. Traces have been normalized on the basis of the total concentration of photoxidizable donor P present in the respective samples and a differential extinction coefficient $\Delta\varepsilon = 19.5$ mM^{-1}cm^{-1} at 551 nm has been used to evaluate the concentration of oxidized cyt c_2 (Dutton *et al.*, 1975). This can be measured from the plateau reached by the cyt c_2 oxidation trace, since oxidized cyt c_2 is stable on the time scale of the measurement. From the data in **Fig. 4.8**, total UQ_{10}/P^+ ratios of 14 and 1.5 can be evaluated in the case of RC-LH1 and RC-only respectively. These values well compare with the stoichiometries evaluated by HPLC that gave 11 and 1.5 UQ_{10}/RC respectively. This approach showed that the large UQ_{10} pool associated with the purified core complex is fully functional in accepting electrons at the Q_B site of the RC. Using a similar approach, Comayras *et al.* (2005a) have confirmed that an important fraction of the native quinone pool (25-30%) is retained in the isolated RC-LH1 complexes following mild detergent solubilization, with no difference between monomers and dimers. These findings have suggested a particular affinity of the quinones for core complexes, giving rise to an heterogeneous distribution of the quinone pool within the chromatophore membrane as previously observed. An *in vivo* confinement of the quinone pool over small domains has been proposed (Comayras *et al.*, 2005a).
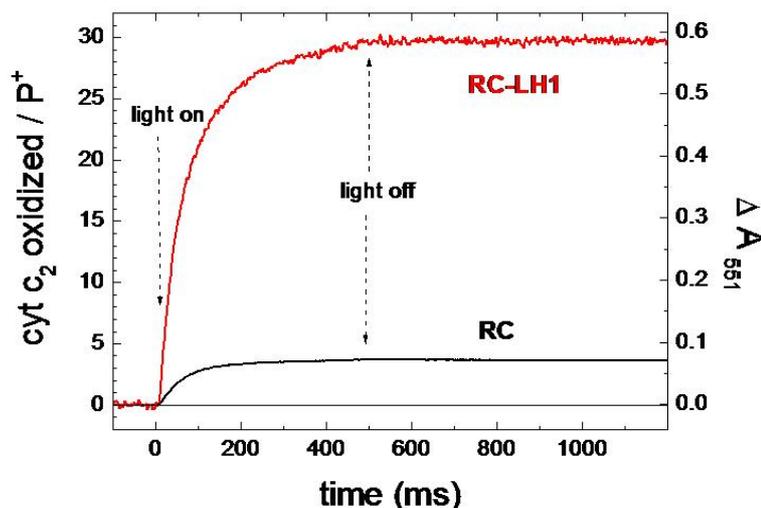
Fig. 4.8 Citochrome c_2 oxidation, measured at 551 nm, induced by continuous photoexcitation of RC-LH1 from photosynthetically grown *wt* cells (prep 2 in **Table 1**) (curve a) and of RC-only complexes (prep 1 in **Table 1**) (curve b). The P^+ concentration in the assays was 0.067 μM and 2.77 μM in RC-LH1 and RC-only samples respectively. Both signals have been normalized to a P^+ concentration equal to 1μM. Purified cyt c_2 was added at 50 and 10 times excess concentration over the photoactive RC in the RC-LH1 and RC-only sample respectively. The left scale gives the number of cyt c_2 oxidized per reaction center.

Clearly the relevant parameter in investigating the possible confinement of quinones in domains associated with the core complexes is not simply the UQ_{10}/RC ratio, but the effective quinone concentration in the lipid phase (*i.e.* the quinone/lipid ratio in the core complex preparations). To evaluate this parameter we have determined in parallel the quinone and phosporous complements (*i.e.* the UQ_{10}/RC and phosphorous/RC ratios) in dimeric and monomeric RC-LH1 complexes and in the chromatophores from which the core complexes were isolated. To have a further element of comparison we examined also the ubiquinone and phosphorous complement copurifying with the antenna LH2 complex. Phosphorus and quinone contents were evaluated by ICP-AES and by HPLC respectively, as described in par. 3.6 and 3.7. A homogeneous set of data is presented in **Table 3**.

As already observed and in agreement with previous determinations (Comayras *et al.*, 2005a), a large UQ_{10}/RC ratio is found in RC-LH1 complexes. The UQ pool associated with both the dimeric and monomeric forms of the core complex (≈15 UQ_{10}/complex) corresponds to about 45 % of the total endogenous ubiquinone pool in

the chromatophore membrane. By contrast, a low number of quinone molecules (approximately 2) is associated with the LH2 antenna complex. Since the phosphorous/complex ratios are comparable in RC-LH1 complexes and in the LH2 antenna (of the order of 10^2), a UQ_{10}/phosphorous ratio almost ten times larger is found in the core complexes as compared to the LH2 antenna.

sample	UQ_{10}/RC or UQ_{10}/LH2	phosphorous/RC or phosphorous/LH2	UQ_{10}/phosphorous
chromatophores	34.6 ± 7.4	2820 ± 780	$(1.2 \pm 0.4) \cdot 10^{-2}$
RC-LH1 dimer	15.8 ± 2.7	168 ± 26	$(9.4 \pm 2.2) \cdot 10^{-2}$
RC-LH1 monomer	15.2 ± 1.5	150 ± 10	$(10.1 \pm 1.2) \cdot 10^{-2}$
LH2	1.8 ± 0.4	164 ± 11	$(1.1 \pm 0.3) \cdot 10^{-2}$
RC	1.9 ± 0.3	37 ± 4	$(5.1 \pm 1.0) \cdot 10^{-2}$
RC-LH1 dimer from aerobically grown cells	26.4 ± 4.2	160 ± 17	$(16.5 \pm 3.2) \cdot 10^{-2}$
RC-LH1 monomer from PufX-deleted strain	25.2 ± 3.4	211 ± 29	$(11.9 \pm 2.3) \cdot 10^{-2}$

Table 3 Ubiquinone (UQ_{10}) and phosphorous content of chromatophores, core complexes, LH2 antenna and RC-only complexes. Monomeric and dimeric RC-LH1 preprations and LH2 antennas were obtained from the same chromatophore prepration isolated from photosynthetically grown *wt* cells. See Materials and methods for experimental details (see par. 3.6 and 3.7). Uncertainties were determined on the basis of standard deviations estimated from a minimum of 3 HPLC determinations of UQ_{10} and 5 ICP-AES measurements of phosphorous, respectively, and taking into account error propagation.

In purified complexes (RC-LH1, LH2) we can reasonably assume that the detected phosphorous comes essentially from phospholipids. These data indicate therefore that the quinone concentration in the lipid phase associated with the RC-LH1 complex is markedly larger than that of the antenna. Moreover, we have already demonstrated that the quinone enrichment found in RC-LH1 is unlikely to result artefactually from detergent solubilization of the complex. As shown in **Table 3**, RC-LH1 complexes (dimers) purified from aerobically grown cells and from the PufX-deleted strain (monomers) are also characterized by high UQ_{10}/complex ratios, resulting in high ubiquinone concentrations (UQ_{10}/phospholipids ratios larger than 10^{-1}).

In the chromatophore membrane, the obtained UQ_{10}/phosphorous ratio ($1.2 \cdot 10^{-2}$) is about eight times smaller than that determined in the core complex. Assuming that also in the chromatophore membrane the content of phosphorous can be attributed

mainly to phospholipids, this would indicate that the quinone concentration in the core complex is much larger than the average quinone concentration in the chromatophore membrane. Two aspects, however, have to be considered, when comparing the quinone concentration in intact membranes and in purified complexes. First, a considerable fraction of the phosphorous determined in chromatophore suspensions can be due to contamination by ribosomial particles rather than to the phospholipids (Fraker *et al.*, 1971). To quantify this possible contribution, we determined phosphorous/RC and UQ_{10}/RC ratios in chromatophores washed with a 2M NaBr solution. This treatment is known to yield preparations essentially free of ribosomal proteins (Schlueserner *et al.*, 2005; Klein *et al.*, 2005). A second point, relevant when comparing the quinone concentration in isolated complexes and in membranes, concerns the lipid complement associated with the purified complexes. Since a rather large lipid complement copurifies with the isolated complexes, which moreover has been found to vary considerably from preparation to preparation, it is likely that this complement includes a fraction of phospholipids weakly bound to the complexes (possibly organized in micellar structures involving or interacting with the detergent molecules) and a tightly bound fraction, in close interaction with the protein complexes. We measured therefore the phosphorous/complex and UQ_{10}/complex ratios also following detergent washing of the RC-LH1 and LH2 preparations (as described under Material and methods, see par. 3.6 and 3.7). When analyzing the composition of the phospholipids (see below), this treatment was routinely performed before lipid extraction to avoid detergent interference in TLC.

The results of the measurements described above are summarized in **Table 4**. A comparison of the phosphorous/RC ratio evaluated in untreated chromatophores and following NaBr washing indicates that a large fraction (about 60%) of the phosphorous detected in untreated chromatophores comes from (presumably ribosomal) contamination. The UQ_{10}/RC ratio is essentially unaffected by NaBr washing, resulting in a UQ_{10}/phosphorous ratio of $1.6 \cdot 10^{-2}$ in the washed membranes. In dimeric and monomeric RC-LH1 complexes purified from this chromatophore prepration an approximately two times larger UQ_{10}/phosphorous ratio is determined.

sample	UQ$_{10}$/RC or UQ$_{10}$/LH2	phosphorous/RC or phosphorous/LH2	UQ$_{10}$/phosphorous
chromatophores	24.8 ± 6.4	3480 ± 870	$(0.71 \pm 0.26) \cdot 10^{-2}$
NaBr washed chromatophores	23.2 ± 5.9	1490 ± 330	$(1.56 \pm 0.53) \cdot 10^{-2}$
RC-LH1 dimer	10.2 ± 2.1	250 ± 15	$(4.1 \pm 0.9) \cdot 10^{-2}$
Detergent-washed RC-LH1 dimer	10.0 ± 1.9	88 ± 6	$(11.4 \pm 2.3) \cdot 10^{-2}$
RC-LH1 monomer	9.5 ± 1.8	285 ± 13	$(3.3 \pm 0.6) \cdot 10^{-2}$
Detergent-washed RC-LH1 monomer	9.3 ± 1.4	81 ± 7	$(11.5 \pm 2.0) \cdot 10^{-2}$
LH2	1.6 ± 0.3	117 ± 8	$(1.4 \pm 0.3) \cdot 10^{-2}$
Detergent-washed LH2	1.2 ± 0.4	68 ± 6	$(1.8 \pm 0.6) \cdot 10^{-2}$

Table 4 The effects of NaBr washing of chromatophores and detergent washing of purified complexes on phosphorous and UQ$_{10}$ determinations. All complexes have been purified from the same chromatophore preparation of photosynthetically grown *wt* cells. Na-Br washing of chromatophores and the treatment for partial removal of detergent in the purified complexes are described in par. 3.6.2.

When the phosphorous content measured in the untreated chromatophore preparation of **Table 3** is corrected accordingly (assuming that only 40% of the detected phosphorous is contributed by phospholipids) a UQ$_{10}$/phosphorous ratio of $3.0 \cdot 10^{-2}$ is obtained, which is about one third of that determined in the purified core complex preparations. This seems to indicate that the quinone concentration in the RC-LH1 complex is only moderately increased with respect to the average concentration in the chromatophore membrane. However, the results obtained in the purified complexes following detergent washing yield additional information on this point. In fact, both in the monomeric and in the dimeric forms of the RC-LH1 complex, this treatment causes a considerable reduction of the phosphorous/complex ratios, but leaves unaffected the ubiquinone complement (UQ$_{10}$/complex). This is consistent with the idea that a large fraction of the lipids copurifying with core complexes are only weakly bound, probably in interaction with detergent molecules, and that, most importantly, the tightly bound

lipid fraction which remains associated with the core complex retains the entire quinone complement. The latter fact indicates that the large fraction of the membrane quinone pool associated with the core complexes is confined within a restricted lipid domain formed by less than 10^2 phospolipid molecules (see **Table 4**). As a result, the effective quinone concentration in the detergent washed core complexes is almost one order of magnitude larger than the average quinone concentration evaluated in chromatophores after NaBr washing.

4.1.3 *Lipid fractional composition in chromatophores and in the purified complexes*

The results previously described bring to light significative differences in the quinone/phospholipid ratios measurable in RC-LH1 complexes, LH2 antennas and chromatophore membranes. This conclusion led us to search for possible differences also in the fractional composition of the lipid complements associated with the purified core complexes, the peripheral antenna complex and intact membranes. The lipid fractional composition was examined by exploiting two independent techniques, namely thin layer chromatography (TLC) and ^{31}P-NMR spectroscopy. Both techniques allow the determination of the relative amounts of phospholipids but it should be noticed that TLC yields a weight-averaged composition (sulphuric acid staining is proportional to the molecular weight), while ^{31}P-NMR gives a composition averaged over the phosphorous nuclei. The two compositions will coincide only if the ratio (molecular weight/phosphorous atom) is the same for all the phospholipids.

An example of TLC plates loaded with phospholipids extracted from membranes and purified complexes is shown in **Fig. 4.9**. RC-LH1 and LH2 complexes were purified from the same chromatophore preparation from photosynthetically grown cells On the basis of standards, we identified four phospholipids in the ICM, *i.e.* PE, PG, PC and CL, in agreement with previous studies (Ermler *et al.*, 1994; Katona *et al.*, 2003) by staining the lipid extracts with Molibdenum Blue (see par. 3.6.3).
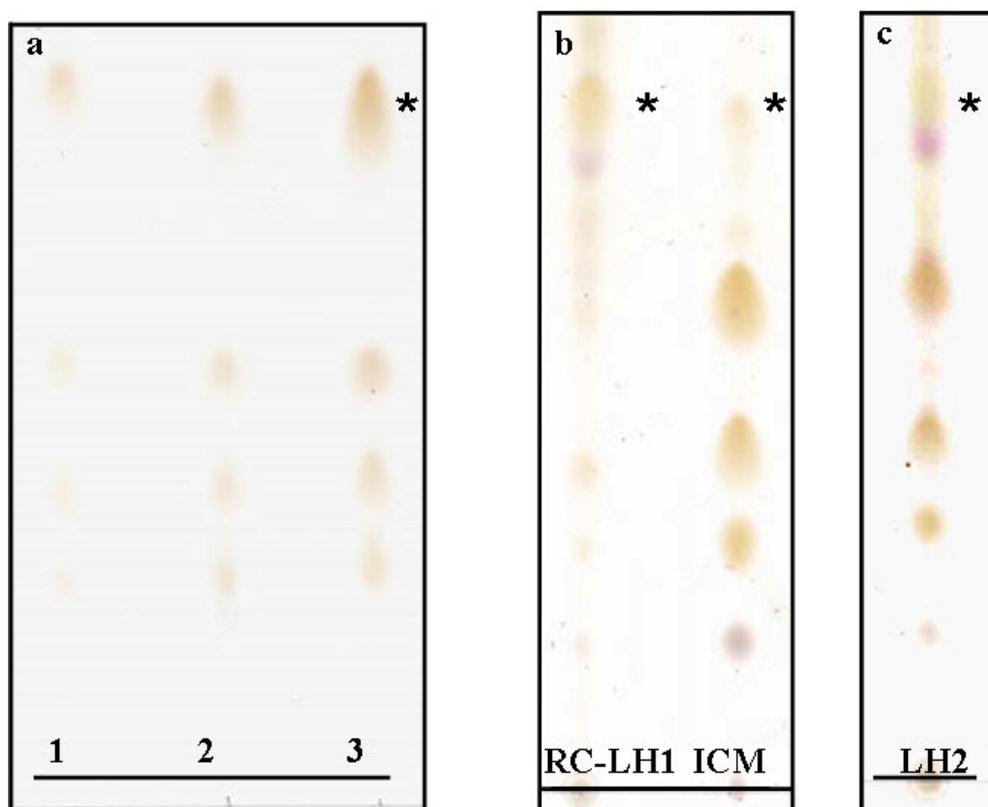
Fig. 4.9 TLC plates of standard phospholipid solutions (panel a) and lipid extracts from RC-LH1, chromatophores (ICM) (panel b) and LH2 complexes (panel c) stained by sulphuric acid. In panel a spots from the bottom correspond to PC, PG, PE and CL; in each line, from the left, each spot contains 1, 2, 4 μg of phospholipids respectively. In the plates shown in panel b and c, 100 μg of lipid extracts from RC-LH1 complex, ICM and LH2 were loaded. In panel b and c spots due to pigment contamination in the lipid extracts are present. The asterisk indicate the position of CL.

It is qualitatively evident that the contribution of PE, PG and PC largely exceeds that of CL in the chromatophore membranes (ICM) as well as in the LH2 antenna. The opposite is true in the RC-LH1 complex, where CL (labelled by the asterisk) becomes the dominant phospholipid. TLC analysis of lipid extracts provides clear evidence of a different lipid composition in the isolated core complexes as compared to the LH2 antennas and to chromatophores.
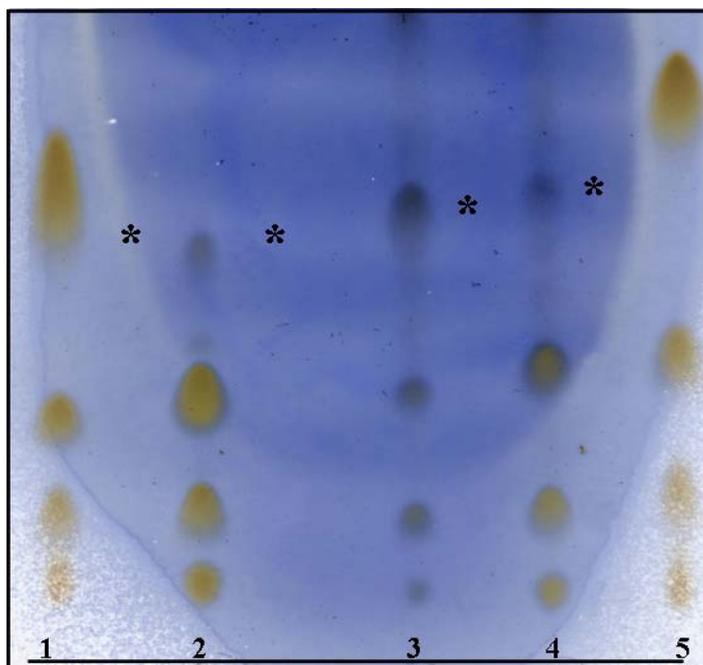
Fig. 4.10 TLC plates of standard phospholipid solutions (lane 1 and 5, 20 µg each spot) and lipid extracts from chromatophores (lane 2), RC-LH1 core complex (lane3) and LH2 complexes (lane 4) stained with Molibdenum Blue. In each lane spots from the bottom correspond to PC, PG, PE and CL. The position of the CL is indicated by the asterisks as the spots corresponding to the CL in the sample are not completely aligned to that in the standards lanes. This effect reflecting an inhomogeneous migration the solvent is common in the case of samples loaded in excess.

The results of the densitometric analysis of TLC plates are summarized in **Table 5**. In the chromatophore extract, PE, PG and PC are the dominant lipids, accounting for approximately 40%, 30 % and 20 % of the total weight respectively, in agreement with previous determinations (e.g. Onishi *et al.*, 1982; Donohue *et al.*, 1982). As already shown in the TLC, the composition of the LH2 antenna complex is similar, except for a moderate increase in the CL content at the expenses of PE. At variance, the fractional composition of the RC-LH1 complex is distinctly and drastically different from that of chromatophores as well as of the LH2 antenna. In the core complex, in fact, CL becomes the dominant lipid (accounting for about 50 % of the total). The CL increase is accompanied by a considerable decrease in PE and, to a lower extent, in PC.

sample	PG (%)	CL (%)	PE (%)	PC (%)
chromatophores	30.2 ± 1.3	8.8 ± 1.8	40.1 ± 0.6	20.9 ± 1.1
NaBr washed chromatophores	29.2 ± 1.4	9.0 ± 1.6	40.7 ± 0.8	21.1 ± 1.2
RC-LH1 dimer	24.0 ± 7.5	50.0 ± 9.4	12.1 ± 4.1	13.9 ± 4.5
LH2	29.4 ± 3.5	14.1 ± 5.8	36.6 ± 2.7	19.9 ± 2.4

Table 5 Relative composition of lipids extracted from chromatophore membranes, RC-LH1 and LH2 complexes determined from TLC densitometric analysis. The contribution of each lipid is expressed as percent of the total weight.

These effects are consistent with the results of ^{31}P-NMR analysis of lipids extracted from an independent set of chromatophores and purified complexes. Proton decoupled ^{31}P- NMR spectra of lipids extracted from membranes, RC-LH1 and LH2 complexes are shown in **Fig. 4.11**. The top and bottom spectra, corresponding to standard mixtures of PC, CL, PG and PE at high and low concentration, show that PC, CL and PG give rise to three distinct resonances (at 0.0, 0.77, and 1.25 ppm, respectively). As previously described in the literature (Murgia *et al.*, 2003), PE is detected at three frequencies (0.53, 0.47 and 0.18 ppm). The relative contribution of the corresponding peaks is concentration dependent. At high concentration of PE (see the top spectrum in **Fig. 4.11**), the peak at 0.53 ppm prevails, but dilution induces the development of the two high field NMR signals (at 0.47 ppm and 0.18 ppm), attributed to the formation of adducts between PE and guanidinium ions (see the bottom spectrum in **Fig. 4.11**).

Chromatophore extracts are rich in phospholipids and overnight averaging yielded well resolved spectra. On the contrary, when analyzing extracts from LH2 and RC-LH1 preparations one week averaging was required to obtain a reasonable statistics. In the spectra of chromatophore and LH2 extracts peaks corresponding to PG, PE, PC and CL could be detected. Each spectrum was deconvoluted in terms of a minimum number of Voightian functions and the relative phosphorous molar contribution was determined by integrating the peaks corresponding to PG, PC, CL and PE.
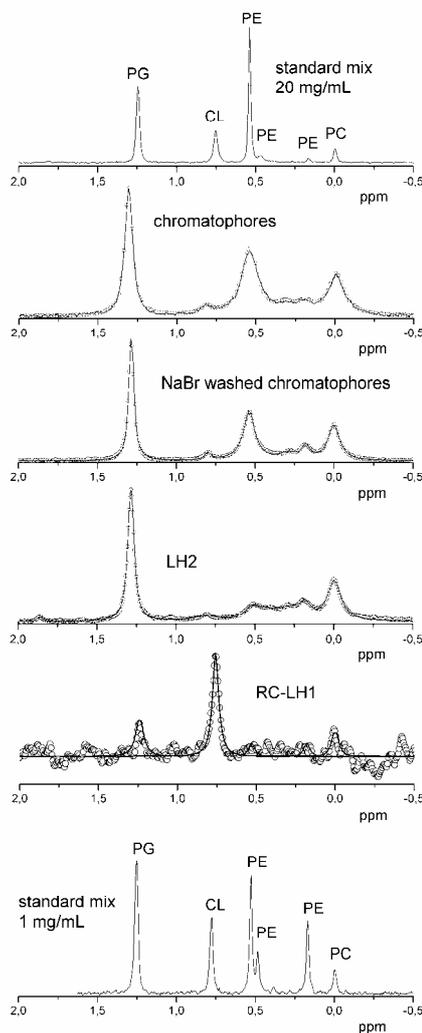
Fig. 4.11 Proton decoupled ^{31}P-NMR spectra of phospholipids extracted from different preparations and of mixtures of standards; the composition (*wt%*) of the standard mixture is PC=5.3%, PE=42.1%, PG=31.6%, CL=21.0%. From top to bottom: standard mixture, 20 mg overall lipids per mL; extract from chromatophores (overnight averaging), extract from chromatophores whased with NaBr (overnight averaging); extract from LH2 complexes (7 days averaging); extract from RC-LH1 complexes (7 days averaging); standard mixture, 1 mg overall lipids per mL. In the case of chromatophores and LH2 complexes continuous lines are fits to Voightian resonances; the peaks positions and the corresponding peak areas are listed in **Table 6** (see text for details). In the case of RC-LH1 the continuous line is a simulation based on the relative phospholipids composition determined by TLC. The following resonances have been considered: PG at 1.25 ppm, CL at 0.76 ppm, PC at 0.00 ppm, PE at 0.53 ppm and at 0.18 ppm. Peak widths were set to 0.05 ppm for all lipids and the areas have been fixed according to the ratios of Table 5 (PG=24%, CL= 50%, PC=14%, PE =12%, equally distributed over the two peaks considered).

In the case of PE (see above) the contribution of the peaks at 0.53 ppm, 0.47 ppm and 0.18 ppm were summed up. In LH2 extracts two additional Voightian functions had to be included, peaking at 1.8 ppm (unidentified phospholipid X1) and at 0.28 ppm

(unidentified phospholipid X2). Only this last additional peak was detectable in the case of the chromatophore membranes.The results of these deconvolution procedure are summarized in **Table 6**. The molar fractions of PE, PG and PC in the chromatophore extracts are in good agreement with TLC determinations, when similar molecular weights are assumed for these phospholipids. The cardiolipin content detected by NMR is systematically lower than that found by TLC if we assume that the CL molecular weight is twice that of other lipids. However, the relative changes of CL between samples is consistent: in both TLC and NMR determinations the CL content of LH2 complexes is about two times that found in membrane extracts. The quantitative disagreement could be due to the presence of the unidentified phospholipids probed by NMR but not by TLC. The presence of lipids other than PE, PC, PG and CL in the membranes of *Rb. sphaeroides* has been reported (see e.g. Onishi *et al.*, 1982; Donohue *et al.*, 1982).

sample	X1 1.80 ppm	PG 1.25 ppm	CL 0.77 ppm	PE 0.53, 0.43, 0.18 ppm	X2 0.28 ppm	PC 0.0 ppm
chromatophores	-	31.8	1.6	39.4	4.8	22.4
NaBr washed chromatophores	-	34.4	2.1	36.5	5.4	21.6
LH2	1.1	37.2	5.1	21.8	11.4	23.4

Table 6 Percentual lipid composition of chromatophores and LH2 antenna complexes determined by ^{31}P-NMR analysis of extracts. Data are from **Fig. 4.11**. The relative contribution of each lipid, calculated by integrating the Voightian functions fitted to the corresponding peak, is expressed as phosphorous mole percent of the total. Also listed are the average positions of the peaks; X1 and X2 indicate unidentified phospholipids. See text and legend of **Fig. 4.11** for further details.

We made no effort to identify such lipids detectable in our NMR spectra. Due to the long averaging time required by NMR analysis (see above) we cannot exclude that the unidentified lipids are degradation products. The increase in CL content of LH2 with respect to the average chromatophore composition is consistent with results obtained on spin-labelled chromatophores from *Rhodobacter sphaeroides* (Birrell *et al.*, 1978). This study provided evidence that the antenna proteins preferentially interact with negatively charged immobilized lipids. A specific composition, differing from that

of membranes, has been recently documented for the LH2 antenna of *Rhodopseudomonas acidophila* (Russel *et al.*, 2002).

In the spectrum of the lipid extract from the RC-LH1 complexes, due to the low signal to noise ratio, only the CL peak at 0.77 ppm is clearly detectable. Two peaks at the frequencies corresponding to PG and PC slightly exceed the level of noise. In agreement with TLC determinations, this indicates that the lipid complement of the RC-LH1 complex is largely dominated by cardiolipin. To further check for consistency, the ^{31}P-NMR spectrum of the RC-LH1 lipid extract was simulated assuming the lipid composition obtained from TLC (**Table 5**). The good agreement between the experimental spectrum and that simulated from TLC data (continuous line in **Fig. 4.11**) confirms that the massive increase in cardiolipin occurs mainly at the expenses of PE, whose contribution to the NMR spectrum is comparable to the noise level.

In summary, both TLC and NMR analyses concur to indicate that the fractional lipid composition of the core RC-LH1 complex differs substantially from the average composition of the cromatophore membrane, being strongly enriched in cardiolipin.

4.2 Discussion

4.2.1 *A ubiquinone pool copurifies with RC-LH1 core complexes*

In membranes from *Rb. sphaeroides* and *capsulatus* ubiquinone-10 is present in large stoichiometric excess over the RC. The size of this (thermodynamically homogeneous) pool varies from approximately 20 to 60 UQ_{10} molecules per RC depending on the growth conditions (see e.g. Venturoli *et al.*, 1986; Garcia *et al.*, 1987; Takamiya *et al.*, 1979). Its role in mediating the cyclic electron transfer catalyzed by the RC and the bc_1 complex is well established and explained by the current Q-cycle schemes (Crofts and Wraight, 1983). A number of studies performed in chromatophore vesicles and exploiting different approaches are consistent with the notion of a diffusional pathway for UQH_2/UQ between the RC and the bc_1 complex. These investigations indicate that oxidation of UQH_2 at the Q_o site of the bc_1 complex involves a collisional reaction; that the oxidizing site is in rapid equilibrium with a large ubiquinone pool and that ubiquinone, as well as soluble cyt c_2, diffuse between reaction

sites in a domain which includes several electron transfer chains and which seems to coincide with the chromatophore vesicle (Crofts and Wraight, 1983; Venturoli *et al.*, 1986; Crofts, 1986; Crofts *et al.*, 1983b; Fernandez-Velasco and Crofts, 1991). On the other hand studies with intact cells have led to propose that the enzymes of the photosynthetic electron transfer chain are organized in supercomplexes and that cofactor diffusion between reaction sites occurs *in vivo* in restricted domains limited to a small number of interacting complexes (Joliot *et al.*, 1989; Lavergne *et al.*, 1989; Lavergne *et al.*, 1991; Vermeglio *et al.*, 1993). Data interpreted as evidence for the existence of an heterogeneous spatial distribution of ubiquinone within the chromatophore membrane under oxidizing conditions have been put forward by Drachev *et al.* (1989). These different views are currently debated and several aspects of the *in vivo* interaction of quinone from the pool with its reaction partners remain open to investigation (see. e.g. Crofts *et al.*, 1998; Crofts, 2000a; Vermeglio and Joliot, 2000; Crofts, 2000b).

In the present thesis we show that, when relatively mild detergent extraction conditions are used to isolate RC-LH1 complexes, the purified core complex fractions contain a large complement of ubiquinone molecules. Analytical ubiquinone determinations yield UQ_{10}/RC ratios of approximately 10 in core complexes purified from photosynthetically grown *wt* cells. This stoichiometry corresponds to 40% of the total ubiquinone content of intact membrane vesicles (25 UQ_{10}/RC). A comparable, large stoichiometry is obtained when the quinone is evaluated by a functional assay based on the number of cyt c_2 molecules per RC rapidly oxidized under continuous illuminations. This demonstrates that all the ubiquinone molecules analytically detected in the purified RC-LH1 fractions are promptly available as electron acceptors at the Q_B site. More than 80% of the maximal cyt c_2 oxidation level is reached in the first 100 ms of continuous photoexcitation, giving a lower limit for the rate of quinone exchange at the Q_B site. Even higher UQ_{10}/RC ratios have been determined in core complexes purified from semiaerobically grown *wt* and X⁻ cells (see **Table 1**).

Several independent lines of evidence show that the high UQ_{10}/RC ratios detected in the purified RC-LH1 preparations are not due to quinone artefactually segregated into the detergent phase during extraction: (a) UQ_{10} containing detergent micelles are layered on top of the sucrose gradient over which RC-LH1 and LH2 complexes are

separated; (b) the UQ_{10}/P^+ ratio determined in the residual membrane pellet during the purification procedure is higher than that of the detergent extract (supernatant) suggesting that ubiquinone extraction by detergent is less efficient than RC-LH1extraction (see **Table 2**); (c) the ubiquinone concentration in the LH2 fraction (corresponding to 1.4 UQ_{10} molecule per LH2) is much lower than in the RC-LH1 fraction coming from the same detergent extract; (d) UQ_{10} is expected to exchange slowly between RC-LH1 micelles and pure detergent micelles (Shinkarev and Wraight, 1997) so that UQ_{10} molecules in pure detergent micelles disconnected from the RC-LH1 complex would not be available as electron acceptors at the Q_B site as required for the fast multiple oxidation of cytochrome c_2 observed under continuous illumination. We conclude therefore that the whole UQ_{10} complement detected in RC-LH1 fractions is strictly associated with the core complexes.

In the light of the limited information available on detergent-RC interaction (Roth *et al.*, 1989; Roth *et al.*, 1991; Gast *et al.*, 1994) it is conceivable that also in the case of the RC-LH1 and LH2 complexes, detergent molecules fill the available space around the membrane spanning helices, providing an hydrophobic phase for UQ_{10}. This phase is likely to include tightly-bound lipids, as recently evidenced for RC-only complexes (McAuley *et al.*, 1999; Fyfe *et al.*, 2001; Camara-Artigas *et al.*, 2002). Assuming that the UQ_{10} is aspecifically distributed in this hydrophobic belt both in RC-LH1 and LH2, in the absence of other interactions, the number of UQ_{10} molecules per RC-LH1 and LH2 is expected to be roughly proportional to the diameter of the respective ring structures. In this hypothesis, diameters of 90 (Walz *et al.*, 1998) to 110 (Scheuring *et al.*, 2004) for the RC-LH1(thought of as a monomer) and 70 (Walz *et al.*, 1998) Å for the LH2 would correspond to a ratio UQ_{10}/complex 1.3 to 1.6 times larger in RC-LH1 as compared to LH2. This is likely to be an upper limit, since the empty LH2 ring, although smaller, could locate in its inner space lipid and/or detergent molecules providing a more extended hydrophobic phase for quinone solubilization. At variance, from the data of **Table 1** it appears that the stoichiometry UQ_{10}/complex is always at least 6 times larger in RC-LH1 than in LH2. These considerations strongly suggest that the large ubiquinone pool copurifying with the RC-LH1 is the result of specific interactions of the cofactor with the core complex protein-lipid environment.

The structure of the core complex suggests the space between the RC and LH1 as a putative location for hydrophobic guest molecules. From the low-resolution projection map of the complex (Scheuring *et al.*, 2004) the area between the LH1 ring and the RC, roughly evaluated as the area between two concentric circles of diameter ≈ 75 and ≈ 50 Å, can be estimated as ≈ 2500 Å^2. When assuming a thickness of about 30 Å for the hydrophobic domain, this translates into a volume of about 7.5×10^4 Å^3. On the basis of a UQ$_{10}$ molar volume of approximately 1070 cm^3 mol^{-1} [estimated from the density of a UQ$_{10}$ solution in exane (Palazzo G., unpublished data)], a total complement of 10-15 UQ$_{10}$ molecules per RC-LH1 complex would correspond to a volume of $(1.8-2.7) \times 10^4$ Å^3. Although the conformation of the UQ$_{10}$ molecules copurifying with the complex (and consequently their actual volume) is not known, the above estimates suggest that the space between the antenna and the RC can well accommodate the ubiquinone complement.

Our analysis of the lipid and quinone complements of chromatophores and of the purified complexes indicates that a considerable fraction of the total ubiquinone pool present in the membrane, is retained by the purified RC-LH1 complexes in a lipid domain corresponding to about 80 tightly associated phospholipids (see **Table 4**). The resulting ubiquinone concentration in the core complex lipid phase is about 7-fold larger than the average ubiquinone concentration in the chromatophore membrane (**Table 4**). Such an enrichment in quinone is not found in the purified LH2 antenna complex, which is also characterized by a tightly associated lipid complement. These observations indicate that quinones tend to associate specifically with the RC-LH1 complex and support the idea of a strong *in vivo* heterogeneity in the spatial distribution of quinones within the chromatophore membrane. By exploiting an independent approach, Comayras *et al.* (2005a) have recently provided evidence for confinement of quinones within small domains. Our data support the view that quinone-rich patches in the membrane are promoted by interactions of quinones with the RC-LH1 protein subunits and/or with the specific lipid environment associated with the core complex. By studying the accumulation of Q$_A^-$ during the pool photoreduction, Comayras *et al.* (2005a) obtained information on the statistical distribution of the UQ$_{10}$/RC stoichiometry both in the purified RC-LH1 complexes and in the proposed quinone

domains of the chromatophore membranes. For both systems, data were consistent with a broad distribution. Since the effective quinone concentration in rapid equilibrium with the Q_B site affects the rate of $P^+Q_B^-$ recombination (Shinkarev and Wraight, 1993), a broadly distributed UQ_{10}/RC stoichiometry can well contribute to the broad distribution of the rate constant observed by us (**Fig. 4.5B**). Statistical fluctuations in the fractional composition of the lipids associated with the core complexes are also a possible source of kinetic heterogeneity, since the interaction of the RC with different lipids has been shown to affect differently the kinetics of charge recombination (see below). The kinetic heterogeneity observed in purified RC-only complexes could arise from the heterogeneity in the occupancy of one or more lipid binding sites that become exposed on the surface of the RC on detergent purification of this part of the RC-LH1 complex.

4.2.2 *Stabilization of the $P^+Q_AQ_B^-$ state in RC-LH1 complexes*

Despite the wide literature on the kinetics of charge recombination events measured in RC-only and the increasing structural knowledge of RC-LH1 complexes of photosynthetic bacteria, the effect of the antenna system on these intra-protein electron transfer processes has not yet been studied. We have compared the recombination kinetics of the light-induced $P^+Q_A^-Q_B$ and $P^+Q_AQ_B^-$ states in detergent suspensions of RC-LH1 core and RC-only complexes purified from *Rb. sphaeroides*. In the presence of o-phenanthroline, essentially the same $P^+Q_A^-Q_B$ recombination kinetics is observed following a light pulse in these two systems either varying the temperature or the pH (see **Fig. 4.2A** and **Fig. 4.4**). At variance, in the absence of the inhibitor, the recombination kinetics of the flash-generated $P^+Q_AQ_B^-$ state is strongly slowed down in the presence of the LH1 antenna in a wide range of temperature and pH values (see **Fig. 4.1**, **Fig. 4.2**, **Fig. 4.5** and **Table 1**).

At physiological pH, the average rate constant characterizing $P^+Q_AQ_B^-$ recombination decreases from approximately 1 s^{-1} in RC-only to 0.3 in RC-LH1 complexes isolated from photosynthetically grown *wt* cells; the slowing effect appears more pronounced ($<k>=0.2$ s^{-1}) in core complexes purified from semiaerobically grown *wt* cells, while a $<k>$ value close to 0.3 s^{-1} has been measured in RC-LH1 from the PufX deleted strain. Recombination appears therefore three-to-four times slowed down in all core complexes, being also possibly modulated by different structural organizations of

the RC-LH1 complex, as suggested by the different BChl/P$^+$ ratios measured in core complexes obtained from differently grown cells or X$^-$ strain (see **Table 1**). In fact, from the determination of the BChl content of purified core complexes it appears that deletion of PufX protein leads to an increase in the number of BChl molecules from 22 ± 2 to 33 ± 1 and, consequently, to a change in the number of (α,β) heterodimers forming the LH1 ring.

Susequently, we have compared the recombination kinetics of the light-induced P$^+$Q$_A^-$ and P$^+$Q$_B^-$ states in RC-LH1 core and RC-only complexes over a wide pH range (6.5-11.8). In these two systems essentially the same, pH independent, P$^+$Q$_A^-$ recombination kinetics are observed (see **Fig. 4.4**). Noteworthy, in order to block the electron transfer from Q$_A^-$ to Q$_B$ over the whole RC population, a higher o-phenanthroline concentration (10 mM) was needed in RC-LH1 complexes. Since o-phenanthroline competes with UQ$_{10}$ at the Q$_B$ site (Wraight, 1981), this observation is consistent with the presence of a large, functional ubiquinone pool in the core complexes. P$^+$Q$_A^-$ recombination kinetics were reasonably described by a single exponential decay. The average of the values shown in **Fig. 4.4** yields a rate constant $k_{AP} = 9.6$ s^{-1} in good agreement with a number of previous determinations in RC-only complexes (see e.g. Kleinfeld *et al.*, 1984b). By contrast, recombination of the P$^+$Q$_B^-$ state was strongly decelerated in the presence of the LH1 antenna at 6.5<pH<9.5 (see **Fig. 4.5**). At higher pH values this effect is progressively reduced, vanishing around pH 11; at pH>11.0 the average rate constant measured in the RC-LH1 complexes exceeds slightly that observed in RC-only complexes. Over the whole pH range examined no significant difference was found between the kinetics recorded in the dimeric and monomeric forms of the RC-LH1 complex purified from photosynthetically or semiarobically grown cells, as well as in the monomeric PufX$^-$ complex. At variance with this latter finding, Comayras *et al*. (2005b) have observed in PufX$^-$ RC-LH1 monomers a P$^+$Q$_B^-$ recombination markedly slower than in wild type core complexes. In PufX$^-$ monomers, at pH 8.0, they measured an half-time consistent with <k> values determined by us in all forms of core complexes, but observed a faster recombination in wild type RC-LH1 complexes. We have no explanation for this discrepancy. Both in RC-only and in RC-LH1 complexes P$^+$Q$_B^-$ recombination kinetics are characterized by a

continuous spectrum of rate constants. The variance of the rate distribution increases steeply above pH 10, giving rise to kinetics which are more strongly dispersed in the core complexes.

The pH dependence measured by us in OG suspensions of RC-only complexes is similar to that measured in LDAO suspensions of RCs (Kleinfeld *et al.*, 1984b). The values of the rate constant <k> measured in OG at 6.5<pH<9.5 are approximately two times larger than the rate constant values determined by Kleinfeld *et al.* (1984b) in LDAO suspensions. We confirmed that this difference is systematic and related to the detergent, by comparing the charge recombination kinetics in the same RC-only preparation, before and after replacement of LDAO by OG. A comparison of the structure of the detergent phase in crystals of *Rb. sphaeroides* grown in the presence of OG (Roth *et al.*, 1991) and in crystals of *Rhodopseudomonas viridis* in the presence of LDAO (Roth *et al.*, 1989) show a similar shape and position in the OG and LDAO rings around the transmembrane helices of the RC. These studies reveal however different interactions between the H subunits of the RC molecules and the OG and LDAO phase, which could be responsible for the different charge recombination kinetics observed in the presence of the two detergents.

The deceleration of the $P^+Q_B^-$ recombination observed in RC-LH1 complexes as compared to the RC-only at 6.5<pH<9.5 is consistent with measurements performed at pH≈8 by Comayras *et al.* (2005b). As outlined in the Introduction (par. 1.2.2), the kinetics of $P^+Q_B^-$ recombination can be analyzed in the frame of a general scheme, which takes into account the effects of a rapid exchange of quinone at the Q_B site of the RC. This scheme, developed by Shinkarev and Wraight (1993), illustrated in detail in the Introduction (scheme 1 in par. 1.2.2), is reported in the following for greater convenience:
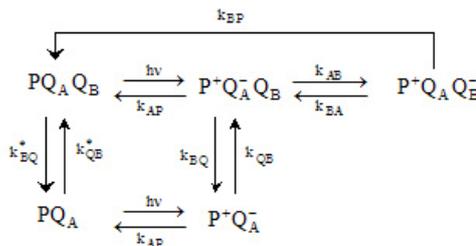
Both a direct (rate constant k_{BP}) and an indirect recombination route (by thermal repopulation of $P^+Q_A^-Q_B$) are considered. The rate constant k_{AP}, k_{AB}, k_{BA}, k_{BQ} and k_{BQ}^* are true first-order rate constant, while k_{QB} and k_{QB}^* are the pseudo-first-order binding rate constants of pool quinones to the Q_B site, $i.e.$ $k_{QB}=k_{QB}'$ [Q], $k_{QB}^* = k_{QB}^*{}'$ [Q], being [Q] the ubiquinone concentration. Kleinfeld et $al.$ (1984b) have demonstrated that in RC-only complexes recombination of the $P^+Q_AQ_B^-$ proceeds essentially via $P^+Q_A^-Q_B$, being the contribution of the direct route negligible. The direct pathway has been characterized in RC-only complexes in which the primary acceptor, Q_A, has been replaced with low potential quinone, raising the energy level of the state $P^+Q_A^-Q_B$ relative to $P^+Q_AQ_B^-$ and thus unfavouring the indirect pathway. Schmid and Labahn (2000) have determined a k_{BP} value of 0.12 s^{-1} at T=293K, 6<pH<8, in the presence of 60% glycerol. In the absence of cryosolvents $k_{BP}\approx 0.19$ s^{-1} has been evaluated under similar conditions (Allen et $al.$, 1998). In view of these values, the direct recombination route cannot be disregarded a $priori$ when analyzing $P^+Q_AQ_B^-$ recombination in core complexes; in the presence of the LH1 antenna, in fact, the recombination kinetics is characterized by an observable average rate constant ($<k>\approx 0.2$-0.3 s^{-1}) of the same order of magnitude of k_{BP} in RC-only complexes. Shinkarev and Wraight (1993) have shown that the kinetic scheme reported above can be analytically solved under two assumptions, which appear quite reasonable both in the case of RC-only and of RC-LH1 complexes, $i.e.$: (a) electron transfer between Q_A and Q_B is much faster than all other reactions, so that quasi-equilibrium can be assumed between states $P^+Q_AQ_B^-$ and $P^+Q_A^-Q_B$ (Crofts et $al.$, 1983b; Kleinfeld et $al.$, 1984b; Okamura et $al.$, 2000); (b) quinone molecules from the pool exchange rapidly at the Q_B site, so that one can assume quasi-equilibrium between states $P^+Q_A^-Q_B$ and $P^+Q_A^-$ (Shinkarev and Wraight, 1997; Mallardi et $al.$, 1997; Palazzo et $al.$, 2000). Under these conditions the observed rate constant of charge recombination is given by:

$$k \cong \left(k_{AP} + k_{BP}L_{AB}\frac{K}{1+K} \right) \Bigg/ \left(1 + L_{AB}\frac{K}{1+K} \right) \qquad (4.4)$$

where $L_{AB}=k_{AB}/k_{BA}$ is the equilibrium constant for electron transfer from Q_A to Q_B and $K=k_{QB}'$ [Q]/k_{BQ} is the dimensionless equilibrium constant of quinone binding to the Q_B site in the $P^+Q_A^-$ state (see Introduction, par. 1.2.2).

We have found that a large, functional ubiquinone pool copurify with RC-LH1 complexes, resulting in UQ_{10}/P^+ ratios at least 5 times larger than in RC-only. A first question we can address by using eq. 4.4 is whether and to which extent a higher quinone concentration can account for the slower recombination kinetics observed in core complexes. By considering dk/dK it is easily seen that eq. 4.4 predicts indeed a decrease in the rate constant k upon increasing [Q] (*i.e.* K), when $k_{BP}<k_{AP}$. The rate constant k_{AP} is close to $10 s^{-1}$ both in RC-only and in RC-LH1 complexes and $k_{BP}<0.2 s^{-1}$ (Allen *et al.*, 1998; Schmid and Laban, 2000) in RC-only. In RC-LH1 k_{BP} cannot be larger than the observed $<k>$ (ranging form 0.2 to 0.3 s^{-1}) so that the inequality $k_{BP}<k_{AP}$ will certainly hold also in core complexes. It appears therefore that according to eq. 4.4 an increase in the quinone concentration associated with the RC could in principle slow down $P^+Q_AQ_B^-$ recombination. However the strong slowing down of charge recombination observed in core complexes cannot be solely due to a quinone effect, as will be shown in the following on the basis of eq. 4.4 and of kinetic data available for RC-only complexes.

As pointed out in the Introduction (par. 1.2.2), under saturating quinone concentration, *i.e.* for $[Q] \rightarrow \infty$, the observed rate k will approach a minimal value, k_{min}, given by:

$$k_{min} = (k_{AP} + k_{BP}L_{AB})/(1 + L_{AB})$$ (4.5)

The equilibrium constant L_{AB} has been measured by a number of laboratories obtaining at room temperature values wich range from 14 to 22 in LDAO suspensions of RCs (Kleinfeld *et al.*, 1984b; Mancino *et al.*, 1984; Shinkarev and Wraight, 1997). A value of 22 has been obtained for RC incorporated in artificial phospholipid vesicles (Palazzo *et al.*, 2000) and in reverse micelles of phospholipids in n-exane (Mallardi *et al.*, 1997). Since $k_{AP}\cong10 s^{-1}$ in RC-only and in RC-LH1, and k_{BP} values range between 0.12 s^{-1} and 0.19 s^{-1}, eq. 4.5 yields k_{min} values between 0.84 s^{-1} and 0.55 s^{-1}. It appears therefore that an increase in the quinone concentration can at most decrease the observed rate constant k by less than a factor of 2, being unable to account for the stronger slowing down of the recombination kinetics observed in core complexes ($<k>=0.2 s^{-1}$). We note that, of course, the value of k_{min} given by eq. 4.5 represents the minimum value of k attainable also when maximizing the quinone occupancy of the Q_B site (*i.e.*, K) by changing the

rate constants k_{BQ} and k_{QB}'. Inspection of eq. 4.5 shows therefore that, in order to decrease k_{min}, we are left with only two possibilities, *i.e.* an increase of L_{AB} and/or a decrease of k_{BP}. Indeed these two effects are clearly related from an energetic point of view. In fact, since k_{AP} assumes the same value in RC-only and RC-LH1 complexes, the energy level of the state $P^+Q_A^-Q_B$ relative to the ground state is not expected to change in the two systems, and an increase of L_{AB} implies a stabilization of the state $P^+Q_AQ_B^-$, *i.e.* a decrease of its energy level relative to the ground state. This in turn corresponds to a decrease in the free-energy drop which drives the direct charge recombination process, so that a decrease in k_{BP} is also expected (assuming that the reorganization energy of this process in not altered). We conclude therefore that, independently of the actual relative contribution of the direct and of the indirect recombination pathways to <k>, the slowing down of charge recombination observed in the presence of the LH1 antenna implies necessarily a stabilization of the $P^+Q_AQ_B^-$ state.

From the analysis of charge recombination kinetics over a wide pH range we observed values of <k> at 6.5<pH<9.5 in the RC-LH1 complexes fluctuating between 0.1 and 0.4 s^{-1} (see **Fig. 4.5A**). As previously observed, they cannot be explained solely by a quinone concentration effect, although the high ubiquinone concentration in the associated lipid phase (see **Table 3** and **Table 4**) is likely to approach saturation. Under this condition, assuming that charge recombination proceeds essentially by thermal repopulation of the $P^+Q_A^-$ state (see below), the free energy difference ΔG^0 between the states $P^+Q_A^-Q_B$ and $P^+Q_AQ_B^-$ can be simply related to the rate constant for $P^+Q_B^-$ (<k>) and $P^+Q_A^-$ (k_{AP}) recombination, *i.e.*

$$\Delta G^0 = -k_B T \ln\left(k_{AP}/<k> -1\right) \qquad (4.6)$$

where k_B is the Boltzmann constant and T the absolute temperature (Kleinfeld *et al.*, 1984b; Schinkarev and Wraight, 1993).

Fig. 4.12 shows the pH dependence of ΔG^0 calculated from the data of **Fig. 4.5** by using eqn. 4.6 and setting k_{AP}=9.5 s^{-1} over the whole pH range (see **Fig. 4.4**). The pH dependence of electron transfer from Q_A^- to Q_B has been extensively studied in RC complexes (for a review see Schinkarev and Wraight, 1993). At pH>6.5 this dependence is basically explained by a simple thermodynamic model, which considers

the coupling between electron transfer and the protonation equilibrium of a single aminoacid residue near the Q_B site (Kleinfeld *et al.*, 1984b).
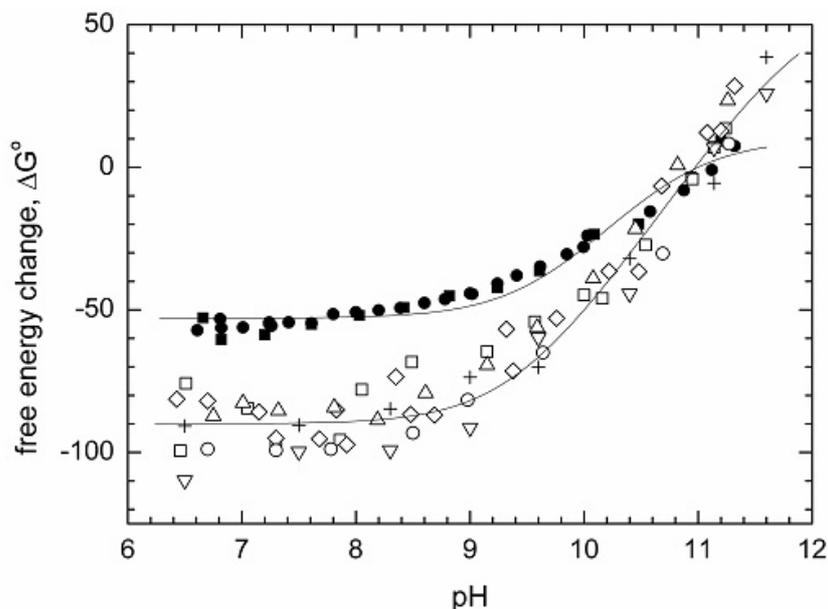

Fig. 4.12 The free energy difference ΔG^0 between $Q_A^-Q_B$ and $Q_AQ_B^-$ as a function of pH. ΔG^0 values were calculated according to eqn.4.6. The values of the average rate constant $\langle k \rangle$ are taken from **Fig. 4.5**; k_{AP} has been fixed to 9.5 s^{-1} on the basis of the data of **Fig. 4.4**. Continuous lines are best fit to eqn.4.7 corresponding to the following values of the fitting parameters. For RC-only: $\Delta G^0_{H^+}$ = - 53 meV, pK_A=9.6, pK_B=10.7. For RC-LH1 core complexes: $\Delta G^0_{H^+}$ = - 90 meV, pK_A=9.4, pK_B=11.9.

Detailed kinetic analyses in mutated RCs (reviewed in Schinkarev and Wraight, 1993) support the idea that the pH dependence of the free energy difference ΔG^0 is determined by protonation of GluL212, as originally proposed by Paddock *et al.* (1989). According to the model, the measured free energy difference ΔG^0 is given by (Kleinfeld *et al.*, 1984b):

$$\Delta G^0 = \Delta G^0_{H^+} - kT \ln \frac{1+10^{(pH-pK_B)}}{1+10^{(pH-pK_A)}} \qquad (4.7)$$

where $\Delta G^0_{H^+}$ is the free energy difference for Q_A^--to-Q_B electron transfer when the residue is protonated and pK_A and pK_B are the acid dissociation constants of the residue when the RC is in the $Q_A^-Q_B$ and $Q_AQ_B^-$ states, respectively. Eq. 4.7 describes an S-

shaped curve with turning points at pK_A and pK_B, being $\Delta G^0_{H^+}$ and $\Delta G^0_0 = \Delta G^0_{H^+} - kT \cdot \ln 10 \cdot \left(pK_A - pK_B \right)$ the limiting free energies at low and high pH values, respectively (Kleinfeld *et al.*, 1984b). When fitting eqn. 4.7 to the pH dependence measured in RC-only complexes we obtain $\Delta G^0_{H^+}$ = - 53 meV, pK_A=9.6, pK_B=10.7. These values are comparable to those obtained by Kleinfeld *et al.* (1984b) in LDAO suspensions of RCs ($\Delta G^0_{H^+}$ = - 67 meV, pK_A=9.8, pK_B=11.3), except that the presence of OG as detergent slightly destabilizes the $Q_A Q_B^-$ state when the coupled residue is protonated and the $Q_A^- Q_B$ state in the deprotonated form. Fitting to the pH dependence measured in the RC-LH1 complexes yields $\Delta G^0_{H^+}$ = - 90 meV, pK$_A$=9.4, pK$_B$=11.9. As it is evident from **Fig. 4.12**, over the physiological pH range (when the ionisable residue coupled to the electron transfer is protonated) the $Q_A Q_B^-$ state is markedly stabilized (by 37 meV) in the core complexes as compared to the RC-only complex. Moreover pK$_B$ is apparently shifted by about one pH unit, *i.e.*, at extremely alkaline pH values, the $Q_A Q_B^-$ state is more destabilized in RC-LH1 complexes (ΔG^0_0 =59.3 meV for the core complexes, as compared to ΔG^0_0 =8.0 meV in RC-only).

The value of ΔG^0 measured in RC-LH1 complexes under physiological conditions ($\Delta G^0_{H^+}$) agrees with estimates of the free energy difference in chromatophores (Arata, 1985), showing that the integrity of the core complex accounts quantitatively for the stabilization of the $Q_A Q_B^-$ observed in the native membranes. The lipid complement associated with the purified RC-LH1 complexes exhibits a specific composition (**Table 5** and **Fig. 4.11**) and is likely to play a role in this stabilization of the charge separated $P^+ Q_B^-$ state (see below).

The comparison of the temperature dependence of <k> in RC-only and in in RC-LH1 complexes at pH 7.8 (**Fig. 4.2A**) allows a rough estimate of the enthalpy and entropy changes coupled to Q_A^- to Q_B electron transfer in the two systems. Panel B of **Fig. 4.2** shows the temperature dependence of ΔG_{AB} in RC-only and in RC-LH1 obtained by eq.4.6 from the respective <k> values (circles in **Fig. 4.2A**) and by

interpolation of the temperature dependence of k_{AP} measured in the presence of the inhibitor o-phenanthroline (squares in **Fig. 4.2A**). Values of the enthalpy (ΔH_{AB}) and entropy (ΔS_{AB}) changes obtained from **Fig. 4.2B** are summarized in **Table 7**. For the sake of comparison, **Table 7** also collects previous estimates of the thermodynamic parameters characterizing the electron transfer equilibrium between Q_A and Q_B in different environments of the RC. In the case of RC-only ΔH_{AB}= -(167±12) meV and ΔS_{AB}= -(0.38±0.04) meV K^{-1}, in good agreement with previous determinations in LDAO suspensions of RCs (Mancino *et al.*, 1984). Comparable values have been reported for RCs in reverse micelles (Mallardi *et al.*, 1997) and in lipid vesicles (Palazzo *et al.*, 2000). This results in ΔG_{AB}= - 56 meV at T=293K, in good agreement with Kleinfeld *et al.* (1984b). In core complexes at T=293K, -ΔG_{AB} increases to 92 meV. The temperature dependence indicates that this considerable stabilization of the state $P^+Q_AQ_B^-$ (36 meV at 293K) is driven by an almost doubled enthalpic contribution (opposed by an entropy term that is almost twice that measured in RC-only).

To assess the limits of the estimates of ΔG_{AB} (see also **Fig. 4.12**, in which we neglected the contribution of the direct recombination route) we can now calculate the corresponding value for k_{BP} expected for ΔG_{AB}= -92 meV at 293K. Since a decrease in the energy level of the state $P^+Q_AQ_B^-$ relative to the ground state by 36 meV implies the same decrease in the free energy drop (-ΔG_{BP}) driving the direct charge recombination, on the basis of the free-energy dependence of k_{BP} determined by Schmid and Labahn (2000) in RC-only complexes a decreased rate constant, $k_{BP}\cong0.07$ s^{-1} can be calculated for core complexes. The maximal relative contibution of the direct route to the observed $<k>$ ($k_{BP}/<k>\cong0.07/0.2$) does not exceed 35%. Therefore, although the direct recombination pathway is likely to contribute to $<k>$, the indirect route will still dominate and the values of **Fig. 4.2B** should yield a reasonable estimate of the minimal extent of $P^+Q_AQ_B^-$ stabilization in RC-LH1.

Quite interestingly in intact chromatophores of *Rb. sphaeroides* the standard free energy decrease accompanying the electron transfer from Q_A to Q_B has been estimated 100 meV and 120 meV on the basis of the decay rate constant of P^+ and of the intensity of delayed fluorescence respectively (Overfield *et al.*, 1979). These values are in full

agreement with a lower limit of 92 meV, estimated by us in RC-LH1 (see **Table 7**). It appears therefore that the presence of the protein-lipid environment constituted by the LH1 antenna, increases the stability of the $P^+Q_AQ_B^-$ state in the native membrane, relative to isolated RC-only complexes.

system	ΔG_{AB} (meV)	ΔH_{AB} (meV)	ΔS_{AB} (meV K^{-1})	ref
RC in OG/cholate	-(56 ± 2)	-(167 ± 12)	-(0.38 ± 0.04)	this work
RC-LH1 in OG/cholate	-(91 ± 3)	-(281 ± 23)	-(0.65 ± 0.08)	this work
RC in LDAO	-(71.4 ± 1.4)	-(150 ± 11)	-(0.27 ± 0.03)	Mancino *et al.*, 1994
RC in LDAO	-69	-230	-0.55	Kleinfeld *et al.*, 1984
RC in LDAO	-78.5[b]			Shinkarev and Wraight, 1997
RC in reverse micelles	-(81 ± 3)	-(140 ± 7)	-(0.20 ± 0.03)	Maliardi *et al.*, 1997
RC in lipid vesicles	-(81 ± 0.5)	-(157 ± 12)	-(0.26 ± 0.04)	Palazzo *et al.*, 2000
chromatophores	-120[c]			Arata *et al.*, 1985

[a] Unless otherwise stated, values of the free energy changes (ΔG_{AB}) are given at 293 K. [b] Evaluated at 295 K. [c] Evaluated at 309 K.

Table 7 Thermodynamic Parameters for the Electron Transfer between Q_A and Q_B Evaluated for Different Environments of the RC

Our analysis of P^+ decay shows that the kinetics of $P^+Q_B^-$ recombination, which are moderately distributed below pH 9, becomes strongly non exponential at increasing pH values (see **Fig. 4.3** and **Fig. 4.5B**). This behaviour, which is more pronounced in core complexes (but is also observed in RC-only complexes) has not been reported previously for RCs purified from *Rb. spaheroides* (Kleinfeld *et al.*, 1984b). In RC-only complexes, the width, σ, of the rate distribution function is always considerably smaller (about one third) than the average rate constant, <k> (see **Fig. 4.5A** and **B**). At variance, in RC-LH1 complexes, it is systematically comparable to <k>, indicating a substantial kinetic heterogeneity. In view of the pH dependence of the recombination rate, the observed distribution of the kinetics may result from an ensemble of conformations differing in the protonation state of the residue(s) thermodynamically coupled to the electron transfer between Q_A and Q_B. We note that in general the existence of an

ensemble of conformations, each characterized by a different rate constant, will give rise to an observable kinetic heterogeneity only when the interconversion between conformations is slower than the electron transfer process observed (in our case the recombination of the $P^+Q_B^-$ state). A faster interconversion will average the kinetic heterogeneity, resulting in the observation of monoexponential (or scarsely distributed) kinetics. This could explain the increase of the distribution width at alkaline pH values (**Fig. 4.5B**), when assuming that the relevant conformations interconvert at a rate which is comparable to the rate of charge recombination at pH <9. In fact, at higher pH values, the rate of interconversion would become progressively lower than the rate of recombination of the $P^+Q_B^-$ state, and the conformational heterogeneity would become progressively observable.

Interestingly at alkaline pH values the variance of the rate distribution is considerably larger in RC-LH1 than in RC-only complexes, suggesting that the conformational heterogeneity of the system increases when its structural complexity and integrity increase. A recent AFM investigation has revealed large molecule-to-molecule variations for the LH1 ring, in terms of both shape and size (Bahatyrova *et al.*, 2004). The large kinetic heterogeneity we observed in RC-LH1 complexes is consistent with results obtained in chromatophores of *Rhodobacter capsulatus* FJ2 (Lavergne *et al.*, 1999), a c_2- and c_y-minus strain, in which the kinetics of $P^+Q_B^-$ recombination can be accurately studied by avoiding any interference due to exogenous electron donors/acceptors. In this system charge recombination kinetics were fitted to the sum of two exponential decays at pH ≤ 8.5, but at pH 10 a third exponential phase had to be added to account for the kinetics (Lavergne *et al.*, 1999), indicating that also in chromatophores recombination kinetics becomes progressively non exponential (distributed) at alkaline pH values.

4.2.3 *The role of the lipid environment*

The effects of a lipid environment on the thermodynamics and kinetics of electron transfer processes within the RC have been studied mainly by comparing the behaviour of RCs in detergent suspensions and when incorporated into liposomes of different phospholipid composition. A systematic analysis (Nagy *et al.*, 2004) showed that in RCs embedded in PC vesicles the rate constant for $P^+Q_B^-$ recombination decreases from

0.77 s^{-1}, measured in LDAO detergent suspension, to 0.39 s^{-1} at pH 7. Incorporation into PG liposomes induces a further decrease of the rate constant to 0.13 s^{-1}. Correspondingly, the calculated free energy differences for Q_A^- to Q_B electron transfer, ΔG^0, equal to -61.8 meV in detergent, decreased in PC and PG to -79.6 meV and to -88.5 meV, respectively (Nagy *et al.*, 2004). The values obtained in the presence of PG are close to our estimate in RC-LH1 complexes. The authors attribute the changes observed in ΔG^0 to a modification of the Q_A/Q_A^- redox potential, measured by delayed fluorescence (Nagy *et al.*, 2004). Addition of PG and CL to RC in detergent suspension also caused a significant slowing of $P^+Q_B^-$ recombination (Rinyu *et al.*, 2004), which was more pronounced (approximately 3-fold) in the case of CL. The effect was attributed to a 30 meV decrease of the redox potential of Q_A/Q_A^- as probed by delayed fluorescence emission. Giustini *et al.* (2005) found that recombination of the primary charge separated state was accelerated in Q_B-deprived RCs incorporated into cardiolipin/lecithin liposomes or suspended in detergent micelles doped with cardiolipin, suggesting a destabilization of the $P^+Q_A^-$ state induced by cardiolipin and the occurrence of several CL binding sites on the RC. The effect was consistent with the occurrence of a high-affinity binding site and an additional cooperative binding to the RC involving about four cardiolipin molecules. The extent of $P^+Q_B^-$ deceleration induced by the addition of CL (Rinyu *et al.*, 2004) is comparable to the slowing down observed by us in RC-LH1 with respect to RC-only complexes. In the case of RC-LH1 complexes, however, we have proposed that the stabilization of the charge separated $P^+Q_B^-$ state is due to a change in the energy level of the Q_B^- state, rather than in the redox potential of the primary quinone acceptor. Such a change would affect the rate k_{AP} of $P^+Q_A^-$ recombination, which, on the contrary has been found to coincide in RC-only and in core complexes. The k_{AP} values we measured (**Fig. 4.4**) are fully consistent with the kinetics reported by Comayras *et al.* (2005b) for *wt* dimeric RC-LH1 complex and for monomeric complexes isolated from the PufX-deleted strain. The rate constant of $P^+Q_A^-$ recombination has been shown to be quite sensitive to variations in the associated free energy change, obeying at room temperature a classical Marcus relation (Lin *et al.*, 1994). According to the data of Lin *et al.* (1994) an increase of 30 meV in the free energy change is expected to increase the value of k_{AP} from 9.4 s^{-1} to approximately

11.5 s^{-1}, an effect which is not seen in the RC-LH1 complex (**Fig. 4.4** and Comayras *et al.*, 2005b).

Taken together, the results obtained in proteoliposomes (Nagy *et al.*, 2004; Giustini *et al.*, 2005) and cardiolipin-doped detergent suspensions (Rinyu *et al.*, 2004; Giustini *et al.*, 2005) indicate that the PG and CL can significantly perturb the electron transfer equilibrium between Q$_A$ and Q$_B$. This suggests that the deceleration of charge recombination observed by us in RC-LH1 complexes is mainly due to the interaction of the RC with the native lipid environment which is preserved in the purified core complexes. Remarkably, the contributions of PG and CL, which appear more effective in perturbing the thermodynamics of interquinone electron transfer, account for about 75% of the total weight of the lipid complement associated with the RC-LH1 complexes (**Table 5**). The lipid composition of the RC-LH1 complex appears to be quite specific, differing markedly from that of the purified LH2 antenna, which is more similar to the average chromatophore composition and is characterized by a much lower content of cardiolipin (see **Table 5**, **Table 6** and **Fig. 4.11**). The presence of negatively charged lipids, tightly bound to the RC-LH1 complex, is likely to perturb the local electrostatics as well as the extended hydrogen-bond network in the region of the Q$_B$ pocket of the RC as discussed by Nagy *et al.* (2004), resulting in the increased stability of the P$^+$Q$_B^-$ state at 6.5<pH<9.5 and in the alteration of the pH dependence of the free energy ΔG^0 for interquinone electron transfer (**Fig. 4.12**). The Q$_A$Q$_B$ acceptor complex constitutes a finely tunable structural and functional unit, responding to long distance interactions (Sebban *et al.*, 1995). It is conceivable that in systems (RC-only and RC-LH1 complexes) characterized by specific protein-lipid and protein-protein contacts the lipid environment affects the quinone acceptor complex differently, altering the thermodynamic properties either of Q$_A$ or of Q$_B$.

A significant fraction of the X-ray crystal structures of the *Rb. spaheroides* RC contains a molecule of CL tightly bound to the intra-membrane surface of the M subunit (for a recent review see Jones, 2007). In a recent x-ray diffraction study two lipid binding sites have been identified unequivocally in RCs cocrystallized with added brominated phospholipids (Roszak *et al.*, 2007). Since the elucidation of the structural details of CL-RC interactions (McAuley *et al.*, 1999), molecules of CL have been

modelled in a variety of membrane protein complexes, including the cytochrome bc_1 complex and the bovine cytochrome c oxidase (for a review see Palsdottir *et al.*, 2004). Interestingly in these structures, cardiolipin molecules were bound frequently at monomer interfaces of oligomeric assemblies or at subunit interfaces of multisubunit complexes, suggesting a role in the stabilization of supermolecular assemblies (Palsdottir *et al.*, 2004). In view of this, it is not surprising that the lipid complement tightly bound to the RC-LH1 complex showed a specific composition, characterized by a marked enrichment in the CL content as compared to the LH2 antenna and to the average chromatophore composition. Noteworthy, when cardiolipin binding was destabilized by site-directed mutagenesis, the preparation of highly pure mutated RCs could be more easily achieved, omitting a final ion exchange purification step (Fyfe *et al.*, 2004). This has been taken as evidence that, in the absence of the CL molecule, the tendency of the RC to associate with other proteins is lessened. An additional observation which points to a role of cardiolipin in mediating protein-protein interactions is that, in the lipidic cubic phase crystal structure of *Rb. sphaeroides* RC, the head group phosphatides of cardiolipin interacts electrostatically not only with three positively charged residues of the M subunit (Lys144, His145 and Arg267) but also with Lys202 of the L subunit of a symmetry related reaction center. In this way, strong crystal contacts are formed between two symmetry-related RCs at the membrane surface, resulting in a quasi-dimeric structure (Katona *et al.*, 2003).

Phospholipids are expected to interact with the RC-LH1 complex at the protein surfaces, forming annular shells, as well as in cavities and clefts located more deeply and frequently observed in multisubunit complexes and multimeric assemblies. On the basis of the calculation made in par. 4.2.1, we can roughly estimate the number of lipid molecules necessary to build a complete annular shell at the outer membrane spanning surface of the complex. By assuming an area of 60 Å^2 for an average phospholipid head (McLaughlin, 1977) approximately 50-60 molecules per RC-LH1 monomer can be accommodate to form an external annular shell. An hydrophobic volume of about 7.5 x 10^4 Å^3 has been previously estimated for the interstice between the inner surface of the LH1 antenna ring and the outer RC surface. After subtracting the volume estimated for a pool of 10 UQ_{10} molecules (of approximately 1.8 x 10^4 Å^3, see above), filling of the

remaining space would require approximately 30-35 additional phospholipid heads, so that a total of 80-95 phospholipid molecules per RC-LH1 monomer could be placed in close interaction with the core complex. Although this estimate is based on extremely crude assumptions, it compares well with a phosphorous/RC ratio ~ 80, determined after detergent washing both in dimeric and monomeric RC-LH1 complexes. A pictorial representation of this arrangment of the lipid-quinone complement in the RC-LH1 complex is shown in **Fig. 4.13**. By examining a structural model of the RC-LH1 complex built by Fotiadis *et al.* (2004) it has been pointed out that a large cavity exists between the surface of the RC (in the region of the Q_B site) and the inner surface of the surrounding LH1 antenna (Jones, 2007). As already suggested (Jones, 2007), this large cavity provides additional space for lipid molecules, forming a suitably flexible environment for quinone molecules waiting in proximity of the Q_B site.

Based on the increasing number of membrane protein structures with tightly bound lipids, some features of lipid-binding sites have been tentatively identified (Palsdottir *et al.*, 2004). Basic residues, including in the order of occurrence Arg, Lys, Tyr, His, have been observed as primary ligands of phosphodiester groups. Aromatic residues are frequently involved in lipid stabilization. Tryptophan residues, located in the hydrophobic/hydrophilic transition zone, interact by hydrogen bonds between the indole nitrogen and the phosphodisester group and by a lamellar orientation of their indole rings between adjacent phospholipids chains. This pattern is thought to provide an interlocking system for the annular lipid shell (Palsdottir *et al.*, 2004). A ring of surface exposed arginine and histidine side chains is located at the boundary between the transmembrane and the extrinsic portions of the RC on the cytoplasmic side (Deisenhofer *et al.*, 1989). Moreover rings of lipid-exposed tryptophan residues are present both in the LH1 and in the RC complexes (Hu and Schulten, 1997). These regular arrays of residues provide in principle a structural basis for the supermolecular organization of the antenna-RC complex by lipid-mediated protein-protein interactions. It may be of interest that two tryptofan residues are found close to the N-terminal end of the transmembrane α-helix of the PufX protein of *Rb. spaheroides* (Francia *et al.*, 1998; Tunnicliffe *et al.*, 2006; Wang *et al.*, 2007) and that, among all second-site mutations that suppress the PufX$^-$ phenotype, most are non-sense mutations of the LH1 lipid-

exposed tryptophans which prevent the assembly of the LH1 subunits (Barz *et al.*, 1994).
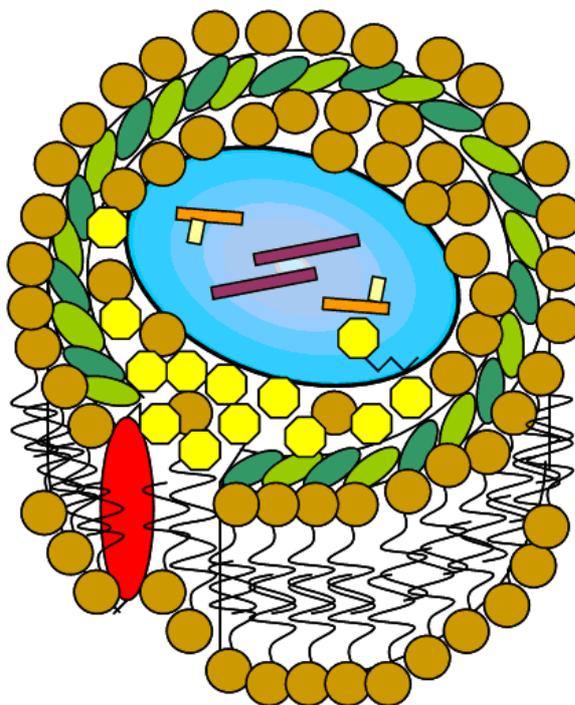
Fig. 4.13 Cartoon model of the RC-LH1 core complex with the associated phospholipid and quinone molecules. The α and β subunits of the LH1 structure surrounding the RC are shown as elliptical shapes (light- and dark-green) in cross-sections. The pufX protein is schematized as a red vertical elongated ellipse, while quinone molecules are represented by yellow hexagons. Phospholipids (brown spheres) fill in the interstice between the RC and the LH1 antenna and also make an annular shell at the hydrophobic external surface of the complex.

As a whole, our data suggest that the confinement of cardiolipin in the RC-antenna complex play a role in the structural organization of the complex as well as in the stabilization of the charge separated state of the RC. The quinone enrichment of the lipid domain tightly associated with the complex further promotes the stability of the $P^+Q_B^-$ state. Whether the high quinone concentration in the complex is in turn determined or assisted by the cardiolipin-rich lipid environment of the core complex needs to be investigated. It seems in any case that protein-lipid-quinone interactions interconnect closely at the level of the core complex and cooperate in optimizing the yield and the turnover rate of charge separation by the RC.

5   ELECTRON TRANSFER IN PHOTOSYNTHETIC REACTION CENTERS EMBEDDED IN SACCHARIDIC AMORPHOUS MATRICES

As described in Introduction (par. 1.5.2), the incorporation of proteins into saccharide-water glassy matrices is a powerful tool in the study of solvent effects on protein internal dynamics. In particular, this approach has been shown to provide useful information on the coupling between electron transfer and protein motions (see Introduction, par. 1.5.2).

The RC complex is becoming a paradigmatic system for the analysis of these relations. It has already been shown that a progressive dehydration of RC-trehalose-water matrices first affects Q_A^- to Q_B electron transfer (Francia *et al.*, 2003). When the amount of water is further reduced, kinetic analysis of flash induced $P^+Q_A^-$ recombination reveals that RC relaxation from the *dark-* to the *light- adapted* conformation as well as interconversion between conformational substates are dramatically hindered at room temperature (Palazzo *et al.*, 2002).

From the literature it clearly appears that, among sugars, trehalose is the most effective in preserving proteins and membranes against stressing conditions. In order to clarify the mechanism of such a strong bioprotectant effect, we made a comparative analysis of the electron transfer processes described above in RC incorporated into water-trehalose, water-sucrose and water-glucose matrices, as a function of the hydration level. We have choosen to examine matrices formed by two homologous disaccharides, *i.e.* sucrose and trehalose, in order to investigate the specificity of sugar effects. We also studied glucose, the costitutive component of trehalose, to explore the possible role of structural complexity of the sugar. The bioprotecting efficacy of trehalose and sucrose has been also compared by studying the RC thermal stability in dehydrated glassy matrices of the two disaccharides. In spite of their structural similarity, we have obtained evidences that the structural and dynamical coupling between the RC and the sugar matrix is extremely weaker in sucrose as compared to trehalose, even under extreme dehydration. Interestingly, glucose is a better bioprotectant than sucrose, even though it does not reach the efficacy of trehalose. The results described in this chapter conrtibute to understand the nanoscopic mechanisms by which such matrices condition the conformational protein dynamics and exert a biopretective effect. Both the interaction of

the matrix molecules with protein surface groups, via direct or water mediated hydrogen bond networks, and the glassy nature of the surrounding environment seem to be imortant for bioprotection.

5.1   Results

5.1.1   *Kinetics of $P^+Q_A^-$ recombination in trehalose and sucrose glasses*

In **Fig. 5.1** a comparison of the kinetics of $P^+Q_A^-$ recombination following a laser flash recorded in o-phenanthroline-inhibited RCs embedded into sucrose (panel A) and trehalose (panel B) amorphous matrices at different contents of residual water is presented. As previously shown for dehydrated trehalose matrices (Palazzo *et al.*, 2002), also in the case of dehydrated sucrose-coated RCs, kinetics are non-exponential and their description requires a continuous distribution p of rate constants k, *i.e.*, the survival probability of the $P^+Q_A^-$ state is given by:

$$\frac{P^+Q_A^-(t)}{P^+Q_A^-(0)} = \frac{\Delta A_{422}(t)}{\Delta A_{422}(0)} = \int_0^\infty p(k)e^{-kt}\,dk \qquad (5.1)$$

where $\Delta A_{422}(t)$ is the absorbance change measured at 422 nm at time t, being t=0 the time of the laser pulse. Both in the case of trehalose and sucrose matrices kinetics can be accounted for by assuming that *p(k)* is a gamma distribution function:

$$p(k) = \frac{k^{n-1}}{k_0^n}\frac{\exp(-k/k_0)}{\Gamma(n)} \qquad (5.2)$$

where $\Gamma(n)$ is the gamma function and k_0 and n are related to the average rate constant, $<k>$ and to the variance, σ^2, of the distribution by:

$$\langle k \rangle = nk_0 \qquad\qquad \sigma^2 = nk_0^2 \qquad (5.3)$$

By taking the Laplace transform of *p(k)* and using eq. 5.3, one obtains for the charge recombination kinetics a power law of the form:

$$\frac{\Delta A_{422}(t)}{\Delta A_{422}(0)} = \left(1 + \frac{\sigma^2}{<k>}\cdot t\right)^{-\frac{<k>^2}{\sigma^2}} \qquad (5.4)$$

to which the traces in **Fig. 5.1** have been fitted, being $<k>$ and the distribution width σ free parameters.
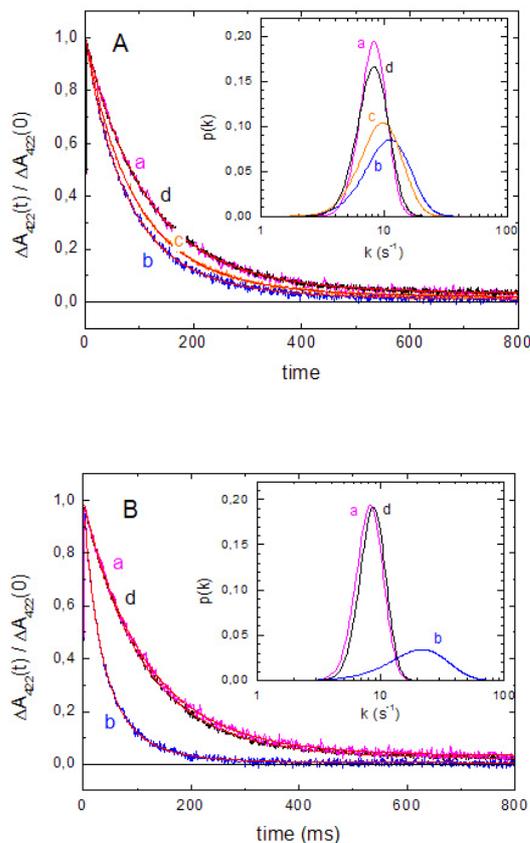
Fig. 5.1 Kinetic analysis of $P^+Q_A^-$ recombination following flash excitation of RC in sucrose (A) and trehalose (B) amorphous matrices. The decays of the absorbance change induced at 422 nm by a laser pulse have been normalized to the maximal absorbance change immediately after the photo-excitation (t=0). Best fit to eq. 5.4 are shown as continuous red curves. The inset of each panel shows the corresponding rate distribution functions $p(k)$, defined by eqns. (5.2) and (5.3). The uncertainties associated with best fitting $<k>$ and σ values are reported in brackets as the extremes of the calculated confidence interval within two standard deviations. Panel A: trace a (magenta), solution in the absence of disaccharides ($<k>$ = 8.78 (8.50, 9.07) s^{-1}, σ = 2.11 (1.11, 2.89) s^{-1}); trace b (blue), dehydrated sucrose matrix characterized by 5200 H_2O molecules per RC ($<k>$ = 13.03 (12.72, 13.36) s^{-1}, σ = 5.00 (4.43, 5.56) s^{-1}); trace c (orange) extensively dehydrated sucrose matrix characterized by 800 H_2O molecules per RC ($<k>$ = 11.22 (11.08, 11.35) s^{-1}, σ = 4.07 (3.80, 4.34) s^{-1}); trace d (black), sucrose solution obtained by re-dissolving the extensively dehydrated matrix ($<k>$ = 8.94 (8.82, 9.07) s^{-1}, σ = 2.48 (1.94, 2.91) s^{-1}). Panel B: trace a (magenta), same as trace a of Panel A; trace b (blue), dehydrated trehalose matrix characterized by 5600 H_2O molecules per RC ($<k>$ = 27.56 (26.88, 28.26) s^{-1}, σ = 12.90 (11.68, 14.15) s^{-1}); trace d (black), trehalose solution obtained following re-solubilization of the dehydrated glass, in which trace b had been measured ($<k>$ = 9.23 (9.11, 9.35) s^{-1}, σ = 2.13 (1.83, 2.40) s^{-1}).

In agreement with previous observations (Palazzo *et al.*, 2002), dehydration of the trehalose matrix results in a strong acceleration of the recombination kinetics (**Fig. 5.1B**) and a marked broadening of the rate distribution (**Fig. 5.1B** inset). On the contrary, these effects are very limited in the sucrose matrix (**Fig. 5.1A**). In trehalose and sucrose matrices characterized by a comparable content of residual water (5200 and

5600 H_2O molecules per RC) an average rate constant, $<k>$, equal to 28 s^{-1} and 13 s^{-1} is obtained, respectively, as compared to $<k>=9$ s^{-1} in solution. The corresponding values of the distribution width are 13 s^{-1} and 5 s^{-1} in trehalose and sucrose, respectively. Further dehydration does not enhance the weak effects observed in the sucrose matrix, but rather reduces their extent. Upon re-dissolving both saccharidic matrices, the recombination kinetics measured in solution are essentially restored, demonstrating the reversibility of the observed effects.

The radically different behaviour of the $P^+Q_A^-$ recombination kinetics in the sucrose and trehalose glassy samples is fully appreciated when the dependence of $<k>$ and σ upon the water content of the matrix is examined systematically (**Fig. 5.2**). In relatively wet trehalose and sucrose glassy matrices, the average rate constant and the distribution width assume essentially coincident values, which increase slightly when the content of residual water is reduced from ~20 x 10^3 to ~8 x 10^3 H_2O molecules per RC. Below this hydration level, in the trehalose matrix, both $<k>$ and σ undergo a sudden, dramatic increase, reaching values close to 35 s^{-1} and 20s^{-1} respectively (Palazzo *et al.*, 2002; Francia *et al.*, 2004c). On the contrary, in the sucrose matrices, $<k>$ and σ values remains essentially unchanged (close to 12 s^{-1} and 5 s^{-1} respectively) upon decreasing the water content over this range. In the trehalose samples the water content could not be decreased below a minimum value of $\sim$ 4 x 10^3 H_2O/RC (corresponding to 0.4 water per trehalose molecule), even by incubating the sample under vacuum at 37°C for several days. At variance, in the sucrose glasses the residual water was easily decreased at room temperature down to the NIR detection limit, *i.e.* $\sim$ 800 H_2O/RC (*i.e.* 0.08 water per sucrose molecules). When reducing the water content from 0.4 to 0.08 H_2O per sucrose molecule the kinetics of $P^+Q_A^-$ recombination does not change substantially, exhibiting $<k>$ and σ values which seem to decrease slightly when approaching an extreme dehydration (**Fig. 5.2**).

It is noteworthy that, in such hard glassy matrices $P^+Q_A^-$ recombination kinetics are scarcely affected as compared to solution and strongly resemble those measured in weakly interacting polymeric matrices (poly vinyl alcohol films) (Francia *et al.*, 2004b)

or in extensively dehydrated RC films in the absence of any saccharide (Palazzo *et al.*, 2002).
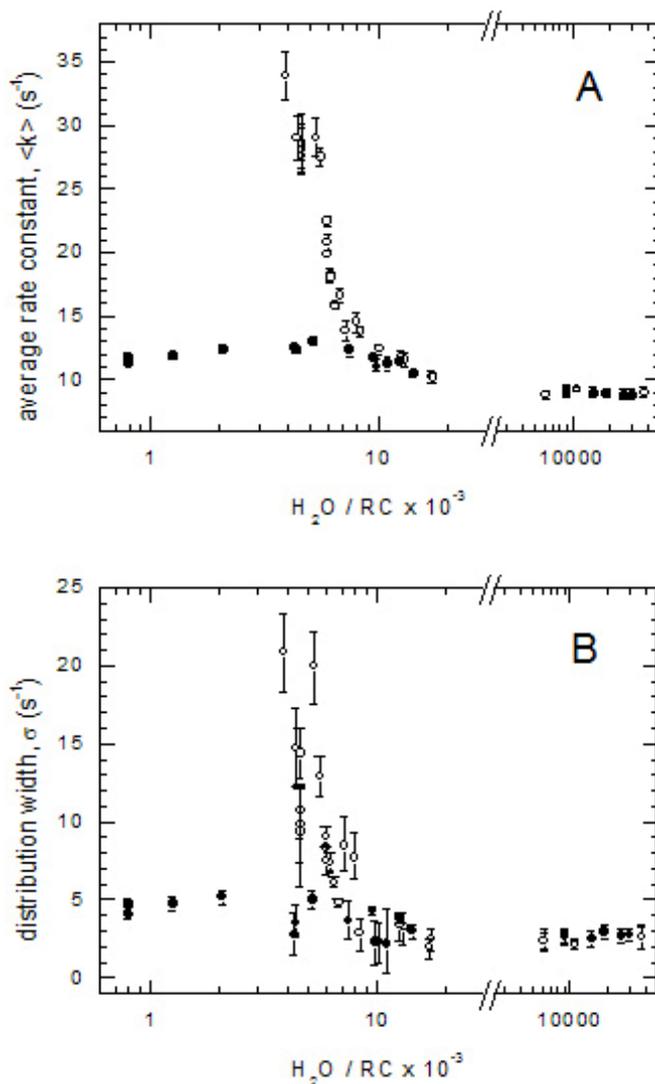

Fig. 5.2 Dependence of the kinetics of $P^+Q_A^-$ recombination upon the H_2O/RC ratio in sucrose (closed circles) and trehalose (open circles) solutions and amorphous matrices. Kinetic analysis was performed as illustrated in **Fig. 5.1.** Panel A and B show the values of the average rate constant, $<k>$, and of the rate distribution width, σ, respectively. For both disaccharides, the experimental points on the right of the break in the abscissa scale were obtained in solutions, while those on the left in glassy matrices. Vertical bars indicate confidence intervals within two standard deviations.

From this behaviour we infer that the incorporation of the RC into dehydrated sucrose samples, at variance with trehalose matrices, affects marginally the ability of the

protein to relax from the *dark-adapted* to the *light-adapted* state over the time scale of charge recombination. In fact, as explained in detail in the introduction, low temperature experiments have shown that the inhibition of protein relaxation from the *dark-adapted* to the *light-adapted* conformation gives rise to an accelerated recombination of the $P^+Q_A^-$ state (see Fig. 1.5 in par. 1.3 of Introduction). Low temeperature experiments have also shown that freezing of the interconversion between conformationmal substates makes apparent the static heterogeneity of the RC, resulting in broadening of the spectrum of rate constants. Since no substantial broadening of the rate distribution is observed in sucrose, even at extremely low water contents, we deduce that the static structural heterogeneity of the RC is averaged effectively by thermal fluctuations between conformational substates. This contrasts the behaviour observed in trehalose matrices, where a large, continuous spectrum of conformational substates appears to be frozen over the same time scale in spite of the larger content of residual water in the matrix.

5.1.2 *Effects of trehalose and sucrose matrices on electron transfer from Q_A^- to Q_B*

When a secondary quinone acceptor is available at the Q_B site of the RC, the formation of the primary flash-induced $P^+Q_A^-$ state is followed by fast electron transfer to Q_B. This reaction occurs in hundreds of microseconds and competes successfully with $P^+Q_A^-$ recombination ($\tau \sim 0.1$ s). Accordingly, the $P^+Q_B^-$ state is formed with an extremely high quantum efficiency and recombines slowly ($\tau \sim 1$ s), *via* thermal repopulation of the $P^+Q_A^-$ state (Kelinfeld *et al.*, 1984b). A drastic rate reduction (or block) of electron transfer from Q_A^- to Q_B in a fraction of the RC population will result therefore in clearly biphasic kinetics of charge recombination (P^+ decay after photoexcitation), where the fast ($\tau \sim 0.1$ s) and slow ($\tau \sim 1$ s) components will monitor recombination occurring from the $P^+Q_A^-$ and $P^+Q_B^-$ states, respectively. As a consequence, under conditions affecting Q_A^- to Q_B electron transfer, the relative amplitude of the slow recombination kinetics measures the fraction of the residual RC subpopulation in which interquinone electron transfer still occurs at a rate large enough to compete efficiently with recombination of the primary ($P^+Q_A^-$) charge separated state.

It has been previously shown that in Q_B-reconstituted RCs, incorporated into trehalose amorphous matrices, the kinetics of P^+ decay include in general two kinetic

components, each describable by a power law:

$$\frac{\Delta A_{422}(t)}{\Delta A_{422}(0)} = (1 - A_s) \left(1 + \frac{\sigma_f^2}{<k_f>} \cdot t\right)^{-\frac{<k_f>^2}{\sigma_f^2}} + A_s \left(1 + \frac{\sigma_s^2}{<k_s>} \cdot t\right)^{-\frac{<k_s>^2}{\sigma_s^2}} \quad (5.5)$$

where the indexes f and s refer to the fast and slow phase, respectively (Francia et $al.$, 2003). At high water contents, in wet, plasticized trehalose matrices (H_2O/RC > 2 x 10^4), the amplitude A_s of the slow component dominates (A_s>0.8), $i.e.$ $P^+Q_B^-$ recombination occurs in the majority of the RC population. Progressive dehydration of the sample leads to a progressive decrease of A_s (Francia et $al.$, 2003). The effect occurs over a narrow range of hydration levels, and the residual amplitude of the slow kinetic component vanishes at H_2O/RC ratios close to 10^4, $i.e.$ at approximately one water molecule per trehalose (see **Fig. 5.3**, open symbols). The values found for k_f and σ_f are consistent with those determined for the $P^+Q_A^-$ recombination kinetics in the absence of Q_B, at the corresponding H_2O/RC ratios (see **Fig. 5.2**). Such a behaviour has been taken as evidence of an $inhomogeneous$ inhibition of Q_A^- to Q_B electron transfer, involving two subpopulations of RCs, a "Q_B-active" and a "Q_B-inactive" one, the size of the latter increasing upon dehydration of the glassy matrix. This view has been confirmed by monitoring the kinetics of electrochromic spectral changes of bacteriopheophytin associated with flash-induced Q_A^- to Q_B electron transfer. Upon decreasing the water content of the amorphous trehalose matrix, also the amplitude of the electrochromic signal decreases, in agreement with the decrease observed in the amplitude of the slow component of charge recombination. However, the kinetics of the residual electrochromic signal was not drastically decelerated, showing that in the residual "Q_B-active" subpopulation, interquinone electron transfer could still successfully compete with $P^+Q_A^-$ recombination (Francia et $al.$, 2003). The $inhomogeneity$ of the inhibition in response to dehydration was further corroborated by a double flash experiment (see Francia et $al.$, 2003, for a detailed analysis). These findings are fully consistent with the notion that Q_A^- to Q_B electron transfer is a conformationally gated process (Graige et $al.$, 1998), and suggest that the conformational RC dynamics governing the reaction is $inhomogeneously$ hindered in an increasing fraction of the RC population when the content of residual water in the trehalose matrix is decreased.
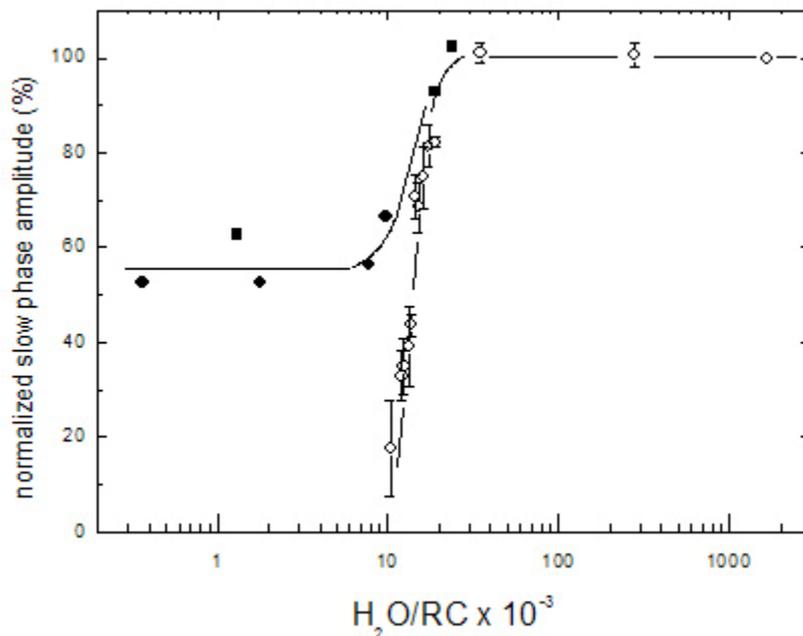
Fig. 5.3 Normalized amplitude of the slow kinetic component of charge recombination in Q_B-reconstituted RCs incorporated into trehalose (open circles) and into sucrose (closed circles) matrices as a function of the H_2O/RC ratio. The plot includes experimental points obtained in solution, at $H_2O/RC > 30$. Lower H_2O/RC values correspond to glassy matrices. Data in trehalose are from reference (Francia *et al.*, 2003). Continuous lines are drawn simply to guide the eye. Each experimental point obtained in glassy matrices correspond to an independent sample. Following each kinetic measurement the dehydrated matrix was redissolved and recombination kinetics measured and analyzed. The reported amplitude of the slow phase has been normalized to the relative slow phase amplitude measured after re-dissolving the sample. The procedure, which is described and discussed in detail in Francia *et al.* (2003), was made necessary by the incomplete recovery of the slow phase amplitude after solubilization of the glassy matrix. This has been shown to be due to irreversible reduction of Q_B to QH_2 in a fraction of the RC population, induced by prolonged exposition to N_2 during desiccation of the samples (Francia *et al.*, 2003).

When Q_B-reconstituted RCs are embedded into a sucrose matrix, the response of Q_A^- to Q_B electron transfer to dehydration of the sample is distinctly different. Kinetics of P^+ decay are still accurately described by eq. 5.5, with kinetic parameters of the fast and slow phases characteristic of recombination of $P^+Q_A^-$ and $P^+Q_B^-$, respectively. A decrease of the water content below approximately 2×10^4 H_2O/RC (*i.e.* about 2 water molecules per sucrose) results in a sizeable reduction of the slow phase amplitude A_s, as observed in the trehalose matrix, but the effect is smaller in sucrose (**Fig. 5.3**, closed symbols). Most importantly, at about one water molecule per sucrose, the relative amplitude of the slow kinetic components levels at 50-60% of the total, and does not decrease further upon reducing the water content. Under these conditions, the slow

kinetic phase ($P^+Q_B^-$ recombination) is moderately slowed down ($<k_s> \sim 0.4$ s^{-1}) and distributed ($\sigma_s \sim 0.2$ s^{-1}) as compared to solution. Similar values have been observed in the dehydrated trehalose matrices (Francia *et al.*, 2003). The average rate constant ($<k_f>$) and distribution width (σ_f) of the residual fast phase remain close to 10 s^{-1} and 3 s^{-1}, respectively, *i.e.* to the values measured for $P^+Q_A^-$ recombination in Q_B-deprived RCs, incorporated into the sucrose matrices (see **Fig. 5.2A** and **B**). It is clear that in sucrose slow recombination of the $P^+Q_B^-$ state still occurs in more than 50% of the RC population, even at extremely low contents of residual water (~ 0.03 water molecules per sucrose). This behaviour shows that partial *inhomogeneous* inhibition of interquinone electron transfer occurs also in the sucrose matrix, but, at variance with what observed in trehalose, an efficient Q_A^- to Q_B electron transfer survives in half of the RC population, even under extreme dehydration. The behaviour observed in sucrose glassy matrices strongly resembles the one observed in RC films dehydrated in the absence of saccharides (Francia *et al.*, 2003). Also in this case inhibition of Q_A^- to Q_B electron transfer can be achieved only in a fraction ($\sim 50\%$) of the RC population, despite extremely low water contents. It appears therefore that, in the dehydrated matrix, sucrose plays a marginal (or negligible) role in hindering the RC conformational dynamics which regulates the interquinone electron transfer.

5.1.3 *Thermal stability of the reaction center in dehydrated trehalose and sucrose matrices*

The observations described in the previous sections concur to indicate that the dynamical coupling between the RC protein and the hosting matrix is much weaker in sucrose than in trehalose. The drastic hindering of conformational dynamics induced at room temperature by incorporation into trehalose glasses has been put in relation with the effectiveness of this disaccharide in preserving structure and functionality of biomolecules under extreme environmental conditions. To test this hypothesis we have compared the thermal stability of the RC when hosted into trehalose and sucrose glasses. RCs embedded into a trehalose and a sucrose glassy matrix, characterized by a comparable amount of residual water (~ 5000 H$_2$O/RC), have been incubated at 37°C under a nitrogen atmosphere for a period of six days.
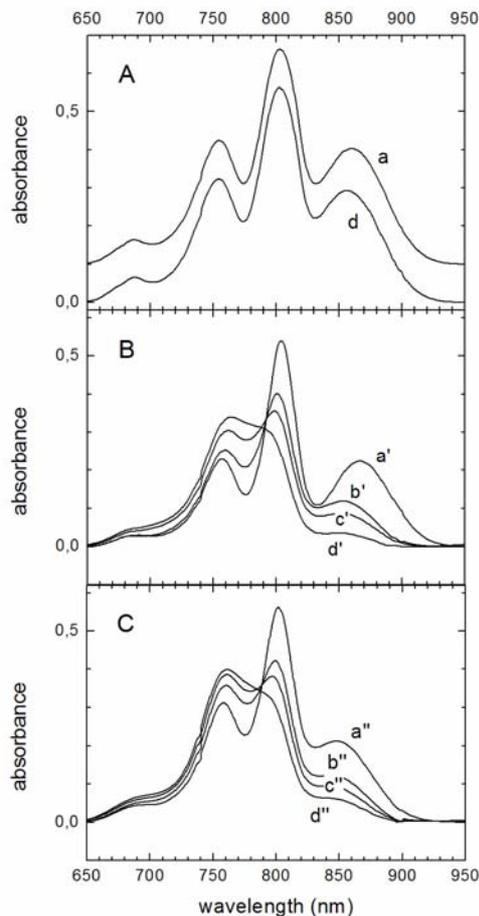
Fig. 5.4 Near infrared absorbance spectra of RC-trehalose (A), RC-sucrose (B) matrixes, and of a RC film dehydrated in the absence of sugar (C), following incubation at 37°C over a period of 6 days. Both the sucrose and the trehalose systems were dried at room temperature to a final content of residual water corresponding to about 5 x 10^3 H$_2$O/RC. The RC film was dehydrated in the absence of sugars to NIR undetectable water contents. All samples were then thermostated under a dry N$_2$ atmosphere at 37°C (t=0 h); spectra were recorded at selected times. Panel A: spectra of RC in trehalose, recorded at t=0 h (spectrum *a*, offset at 0.1 absorbance for visual clarity) and following incubation for 6 days, *i.e.* at t= 144 h (spectrum *d*). Panel B: spectra *a'*, *b'*, *c'* and *d'* were measured in the sucrose matrix at t=0 h, t= 20.5 h, t= 45.5 h and t= 147 h, respectively. Panel C: spectra *a''*, *b''*, *c''* and *d''* were measured in the RC film at t=0 h, t= 21 h, t= 49 h and t= 109 h, respectively. All spectra were corrected for background scattering between 640 nm and 950 nm.

Thermal stability has been examined by recording at selected time intervals the optical-NIR spectrum between 690 and 950 nm (Hughes *et al.*, 2006). This spectral region is characterized by four absorption bands (**Fig. 5.4**).

The band centered around 760 nm, 800 nm and 860 nm are principally assigned to the Q$_y$ transitions of the two bacteriopheophytins, of the two monomeric accessory

bacterichlorophyls and to the low energy exciton component of the Q_y transition of the special-pair bacteriochlorophyls (P), respectively. The assignment of the fourth small band, centered at 670 nm, is uncertain (Hughes *et al.*, 2006). The exact position of the bands, particularly of the special-pair absorbtion peak (at ~ 860 nm), varied somewhat in response to changes in detergent type and concentration (Wang *et al.*, 1994; Gast *et al.*, 1996), dehydration both in the presence and in the absence of trehalose (Palazzo *et al.*, 2002), phase segregation of RCs (Piazza *et al.*, 2003).

The spectrum of the RC incorporated into the trehalose matrix did not change appreciably even after six days of incubation (see spectum *a'* and *d'* in **Fig. 5.4**). When the trehalose glass was subsequently re-dissolved the amount of primary donor photoxidized by a laser pulse was found unaffected as compared to that measured in solution before dehydration and glass formation (not shown). On the contrary, the spectrum of the RC embedded into the sucrose matrix underwent drastic changes, as shown by the temporal sequence (*a-d*) in **Fig. 5.4**. A progressive decrease in the amplitude of the bands at 860 nm and 800 nm (already pronounced after 20 hours incubation) was accompanied by a concomitant increase of the band at 760 nm. Because both bacteriochlorophyll and bacteriopheophytin exhibit in organic solvent an absorption maximum in the 750-770 nm spectral range (Van der Rest and Gringas, 1974), it is clear that BChl (and possibly BPheo) molecules of the RC have lost progressively their native protein environment. As expected this process is paralleled by a decrease in the extent of flash-induced P photoxidation (**Fig. 5.5**), and primary photochemistry is essentially and irreversibly lost after about six days of incubation at 37°C. The kinetics of loss of the native state was examined according to the following procedure. Spectra have been fitted to the sum of four Gaussian peaks (an example is shown in the inset of **Fig. 5.5**). At any sampled time during incubation the areas of the obtained Gaussian bands, centered at ~ 760 nm (band1), at ~ 800 nm (band 2) and at ~ 860 nm (band 3) have been normalized to their sum. Each normalized area has been further normalized to the full extent of its variation during the incubation time. The results (**Fig. 5.5**) indicate that, during incubation, the decrease observed in the spectral contributions of bands 2 and 3 roughly matches the increase of band 1. Notably the

progressive inactivation of primary RC photochemistry parallels these kinetics, which are reasonably accounted for by a single exponential decay.
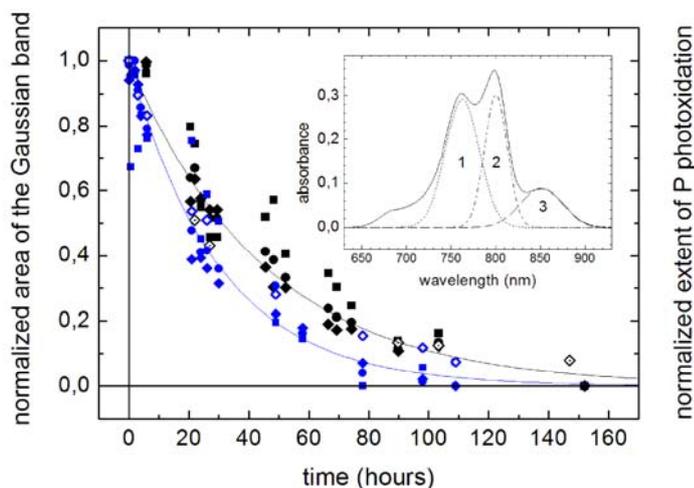

Fig. 5.5 Time dependence of the NIR RC absorbance observed in sucrose (black symbols) and in a film dehydrated in the absence of sugar (blue symbols), during incubation at 37°C. Each absorbance spectrum was fitted to the sum of four Gaussian bands, centred at 680 nm, 750 nm, 800 nm and 850 nm. The spectrum recorded in the sucrose after 45.5 h is shown in the inset as an example; the individual Gaussian bands at 750 nm (band 1), 800 nm (band 2) and 850 nm (band 3) are plotted as dotted lines. The area of each band, normalized to the sum of the areas of band 1, 2 and 3, has been plotted as a function of the incubation time (after further normalization to the full extent of variation observed between t=0 and the maximum sampled time). In the case of band 1, the amplitude of which increases with time, the complement to one has been plotted (closed circles). Closed squares and diamonds correspond to band 2 and band 3, respectively. The extent of P photoxidized by a single laser pulse, normalized to that measured at t=0, is also shown (open diamonds). The continuous curves represent exponential decays with a characteristic time $\tau = 45$ h (sucrose matrix, black line) and $\tau = 30$ h (RC film, blue line).

To assess the (limited) extent to which sucrose could protect against thermal denaturation, we performed the same set of measurements on a RC film extensively dried in the absence of any sugar. The results (see **Fig. 5.4C** and **Fig. 5.5**, blue symbols) show that the extent and the rate of thermal denaturation are essentially comparable for RCs dried in the absence and in the presence of sucrose. The loss of photochemical activity and of the native structure appears to be only slightly faster in the absence of sugar (see denaturation kinetics of **Fig. 5.5**).

In summary, under conditions in which the trehalose matrix fully preserves the RC structural and functional integrity, the RC in the sucrose matrix looses irreversibly its native state and photoactivity. It appears that the RC motional freedom which allows

thermal denaturation is barely affected in the sucrose matrix, being on the contrary drastically reduced at 37°C in the trehalose matrix.

5.1.4   The reaction center-matrix coupling in glucose

To further examine the specificity of the matrix-protein coupling with respect to the sugar composition, we have extended the analysis of $P^+Q_A^-$ charge recombination to RCs incorporated into glucose-water matrices. To keep constant the number of glycosidic rings per RC as compared to the disaccharide matrices, the glucose/RC ratio was fixed to 2 x 10^4, *i.e.* to a value doubled with respect to that in the trehalose and sucrose glasses. A shown in **Fig. 5.6A** the hardening of RC-containing sglucose matrix induced by dehydration determines a moderately strong acceleration of the $P^+Q_A^-$ charge recombination and, in parallel, an increase of the rate distribution width, as compared to RC in solution. Though in the glucose glass the drastic effects induced by the trehalose are not reached, at the maximal dehydration attainable, *i.e* 100 H_2O molecules per RC, we determined a <k> value of 18.0 s^{-1}, which is markedly larger than the maximal <k> values measured in sucrose. The response of the $P^+Q_A^-$ recombination kinetics to incorporation into a dehydrated glucose matrix is more evident in **Fig. 5.6B**, where kinetics measured in RC embedded in glucose, trehalose and sucrose are directly compared.

Although very low levels of hydration could be reached also in glucose, the loss of water in this sugar was extremely slow and the matrix, even at very low water contents, had the character of a plasticized glass, rather than of a solid. In order to reach the minimal contents of residual water in the glucose glasses, in fact, we left the sample in a hoven at 35°C for more than 25 days, washing it routinely under nitrogen flux. A totally different dehydration behaviour was observed for the sucrose matrices, which reached an extreme dehydration following conditioning in N_2 at room temperature in about 2-3 days. This shows that, in the case of sucrose, water is more weakly bound to the sugar, while trehalose, and even more glucose, have a stronger propensity to retain water.

Interestingly, in the glucose matrix, the long incubation at high temperature did not damaged the RC, because a normal photoactivity and recombination kinetics were observed following resuspension of the protein at the end of the experiment.

Consistently, also the spectral features typical of an undamaged RC complex were retained.
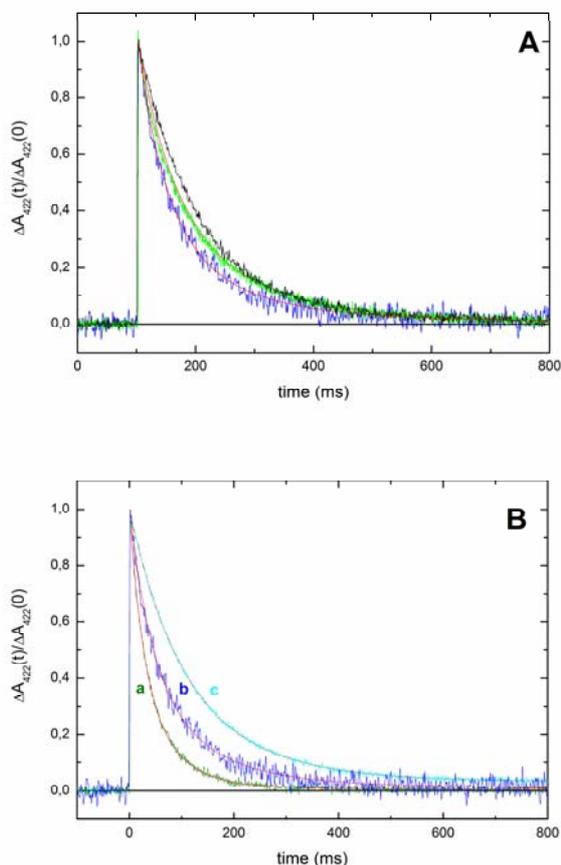

Fig. 5.6 Kinetic analysis of $P^+Q_A^-$ charge recombination of RC embedded in glucose matrix (panel A). In panel B the kinetics measured in trehalose, sucrose and glucose matrices are compared. As in trehalose and sucrose matrices, the electron transfer from Q_A^- to Q_B was inhibited by o-phenantroline. The experimental traces were normalized to the maximal absorbance change following the laser pulse and the red lines are the best fit to eq. 5.4. Panel A: black trace, solution in the absence of glucose ($<k> = 9.86$ s^{-1} and $\sigma = 1.63$ s^{-1}); green trace, dehydrated matrix in which we calculated 5230 H$_2$O / RC ($<k> = 12.61$ s^{-1}, $\sigma = 6.71$ s^{-1}); blue trace, extremely dehydrated glucose matrix characterized by a 100 H$_2$O/RC ratio ($<k> = 17.96$ s^{-1}, $\sigma = 11.12$ s^{-1}). Panel B: trace a (olive green), dehydrated trehalose matrix characterized by 5600 H$_2$O molecules per RC ($<k> = 27.6$ s^{-1}, $\sigma = 12.9$ s^{-1}; trace b (blue), same of trace blue in panel A; trace c (cyan), strongly dehydrated sucrose matrix ($<k> = 11.2$ s^{-1}, $\sigma = 4.1$ s^{-1}).

Fig. 5.7 shows the results of the analysis of $P^+Q_A^-$ charge recombination performed on a glucose matrix during its dehydration. Analysis was performed as shown in **Fig. 5.6A**. Both $<k>$ (**Fig. 5.7A**) and σ (**Fig. 5.7B**) values (red symbols) are reported as a function of the content of residual water of the matrix. For the sake of

comparison, the trehalose and sucrose data of **Fig. 5.2** are also plotted (black symbols). As observed in the trehalose matrix, also in glucose the average rate constant and the distribution width increase following dehydration below a threshold of about 800 H_2O molecules per RC, but the dependence upon hydration is, in glucose, systematically shifted to lower values of residual water. Moreover, even at the maximal dehydration attained in glucose, the effect is lower (about one half) than the one detectable in the extremely dehydrated trehalose matrix.
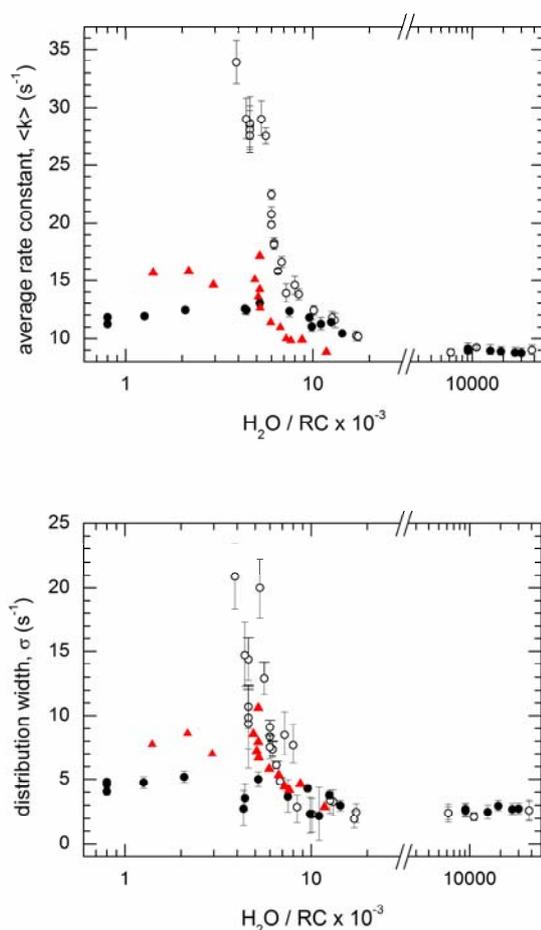

Fig. 5.7 Kinetics of $P^+Q_A^-$ charge recombination as a function of the H_2O/RC ratio in glucose (red symbols) compared to that in trehalose (open circles) and sucrose (closet circles) solution and dehydrated matrices are shown. For a detailed description see **Fig. 5.2** capture.

Data in **Fig. 5.7** enable us to infer that the incorporation of RCs into dehydrated glucose samples, affect the RC relaxation from the *dark-adapted* to the *light-adapted* to a lower extent. A moderate, comaparable increase in <k> values is observed in the two matrices at different hydration levels, being that of glucose systematically lower. This

suggests that to obtain a comparable inhibition of RC dynamics, the glucose matrix has to be appreciably more dry than the trehalose one. However, if we compare the effect of glucose to that of sucrose it appears that in glucose matrices a network of hydrogen bonds is formed upon dehydration, which locks the matrix to the protein surface via water molecules. This is consistent with the fact that, at variance with sucrose, glucose seems to resemble trehalose in its ability to protect the native structure of the RC, at least over a period of about one months at 35°C.

5.2   Discussion

5.2.1   *The role of protein matrix coupling in controlling electron transfer*

Protein dynamics play a central role in determining protein function (Frauenfelder & McMahon, 1998). The understanding of the salient interactions with the environment which affect and control protein dynamics is therefore a biologically relevant problem. In this chapter we focussed on the structural/dynamical coupling between sugar glassy matrices and a large integral protein-complex. By examining the kinetics of electron transfer processes within bacterial reaction centers incorporated into sucrose, glucose and trehalose matrices, we have provided evidence that the tightness of the protein-matrix coupling is strongly matrix-specific, differing substantially in matrices of comparable hydration, rigidity and viscosity, formed by structurally related saccharides.

The kinetics of $P^+Q_A^-$ recombination is a sensitive probe of the ability of the RC protein-solvent system to thermally fluctuate between conformational substates and to relax from the *dark-adapted* to the *light-adapted* state, in which primary charge separation is energetically stabilized (Kleinfeld *et al.*, 1984a; McMahon *et al.*, 1998). When these kinetics are examined in trehalose- and sucrose-matrices, a substantially different response to dehydration is observed. Upon decreasing the content of residual water below a threshold corresponding to ~ 0.8 water molecules per sugar, both the average rate constant and the rate distribution width undergo a steep increase in the trehalose matrix, indicating that substate interconversion and RC relaxation coupled to formation of the charge separated state are drastically hindered. Since these room temperature effects are similar to those observable in water-glycerol at cryogenic

temperatures (McMahon *et al.*, 1998), we infer that in the extensively dehydrated trehalose matrix the RC conformational energy landscape is drastically changed so that the conformational dynamics "seen" by $P^+Q_A^-$ recombination kinetics result totally frozen. Such a behaviour is not observed in sucrose. In fact, dehydration of the sucrose matrix results in a marginal increase of $<k>$ and σ, which parallels the one observed in the trehloase matrices, when the hydration level is reduced from $\sim$1.5 to $\sim$0.8 H$_2$O/sugar molecules. Below this threshold, however, the behaviour observed in the trehalose and in the sucrose matrices diverges strongly: in the latter matrix $<k>$ and σ values remain essentially unaffected by further drying, even under extreme drought. Notably, the kinetic parameters measured in the sucrose matrix are comparable to those determined in RC films dehydrated in the absence of any sugar, and characterized by extremely low contents of residual water, undetectable by NIR spectroscopy (Palazzo *et al.*, 2002). These observations make clear that in the sucrose matrix, the conformational RC dynamics probed by the $P^+Q_A^-$ recombination kinetics is marginally affected as compared to solution, in spite of the extreme viscosity and hardness of the embedding matrix.

Molecular dynamic (MD) simulations performed in simple trehalose- and sucrose-water systems have evidenced some significant differences between the two systems. Due to formation of intramolecular hydrogen bonds, sucrose was found more rigid and less hydrated than trehalose (Conrad and de Pablo, 1999; Ekdawi-Sever *et al.*, 2001). The larger number of sites available in a trehalose matrix to hydrogen bond with water is most likely responsible for the structural and dynamical differences enlighted by MD simulations of trehalose- and sucrose-water-matrices containing MbCO (Cottone *et al.*, 2001; Cottone *et al.*, 2005). These studies showed in fact that, in both systems, hydrogen-bond networks are formed in which residual water molecules bridge sugar molecules with Mb surface groups. The fraction of water molecules simultaneously interacting with the protein and the sugar appeared to be lower in sucrose than in trehalose, suggesting a tighter matrix-protein coupling in trehalose. Correspondingly, some regions of the protein were found more flexible in sucrose than in trehalose.

MD simulations are consistent with the results of FTIR measurements, performed in non-liquid ware-sugar-MbCO matrices (Giuffrida *et al.*, 2003, 2004, 2006), in which

the thermal evolution of the stretching band of the bound CO and that of the water association band were followed in parallel between 300 and 20 K. Analysis showed that the amplitude of protein internal motions is regulated by the water content of the matrix in a way which is sugar specific. In particular, sucrose (as well as maltose, raffinose and glucose) exhibited a looser protein-solvent coupling than trehalose. On these bases it has been proposed that the formation (and modulation) of hydrogen-bond networks involving residual water molecules, and anchoring the protein surface to the matrix, is the main interaction regulating the structural/dynamical coupling in water-sugar-matrices, which, in turn, determines the efficacy of bioprotection. This view can well explain our observation that the RC dynamics coupled to $P^+Q_A^-$ recombination is radically different in dehydrated sucrose and trehalose matrices. The response of $<k>$ and σ to dehydration suggests that in the trehalose matrix, when the number of residual water molecules decreases below a threshold value, a network of hydrogen-bonds develops which locks the protein surface to the matrix, impairing dramatically the RC relaxation and conformational dynamics coupled to electron transfer. On the contrary, the behaviour observed in sucrose matrices suggests that, upon dehydration, the sucrose competes successfully with the RC protein for hydrogen bond formation, resulting in "phase separation" between the RC protein and the matrix. As a consequence the motional freedom of the RC surface is essentially unrestricted, in spite of the rigidity of the embedding matrix, and the RC protein undergoes a fast relaxation to the *light-adapted* conformation as it does in dehydrated films in the absence of any sugar. In line with our data and interpretation, a recent NMR study of protein mobility in lysozyme-sugar systems has shown that "phase separation" between the protein and the sugar matrix occurs in lactose *but not* in trehalose (Lam *et al.*, 2002). We suggest that "phase separation" is determined essentially by a mismatch between the water-sugar structures of the matrix and the protein surface. It is not surprising that the protein-solvent coupling in trehalose and sucrose matrices differs so markedly in the case of a large, integral protein complex, surrounded by detergent molecules. For such a complex system the occurrence of a tight structural/dynamical matching at the protein-water-matrix interface is expected to be particularly demanding and, correspondingly, more sugar specific.

The response of the $P^+Q_A^-$ charge recombination kinetics to incorporation of the RC into a glucose dehydrated matrix is somewhat intermediate between that observed in trehalose and in sucrose glasses. This behaviour can be qualitatively rationalized in the frame of the model described above (sugar-protein-water structures) when considering that the larger trehalose molecule, when involved in the water-mediated H-bond network, can more easily stiffen the RC surface, coupling more efficiently the matrix and protein dynamics. In the case of glucose, *i.e.* of a single glucopyranose unit, it is conceivable that, at comparable water content of the matrix, the locking of the protein surface is weaker than in trehalose, even in the presence of an H-bond network. Due to the weaker coupling, a comparable inhibition of the RC dynamics requires in glucose a more drastic hardening of the embedding matrix, *i.e.* a more dehydrated glass.

The different response of interquinone electron transfer to dehydration of trehalose- and sucrose-coated RCs is fully consistent with the notions outlined above. Electron transfer from Q_A^- to Q_B is rate-limited by a conformational change (Graige *et al.*, 1998), although the precise mechanism of the conformational gating is still debated. In the crystal structure of the RC cooled to cryogenic temperatures under illumination, *i.e.* trapped in an active state, Q_B has been found 2.7 Å closer to Q_A than in the protein frozen in the dark, and twisted by 180° around the isoprenoid chain (Stowell *et al.*, 1997). The observation of two different positions of Q_B, *distal* and *proximal* in the neutral and charge-separated state respectively, has been recently confirmed by x-ray diffraction data of improved quality (Koepke *et al.*, 2007). In this work a new orientation of Q_B in its distal position was observed, which shows no ring-flip compared to the orientation in the proximal position. It seems that in the new conformation, no rotation of the head-group of Q_B is needed for the movement from distal to proximal position. Howevere, in addition or in alternative to the Q_B movement, a number of different reorganizations have been proposed to play a role in gating the reaction. They include dielectric responses of RC residues, displacements and reorientations of water molecules within the RC region connecting Q_B with the RC surface as well as rearrangements of intra-protein hydrogen bond networks (e.g. Graige *et al.*, 1998; Cherepanov *et al.*, 2001; Xu *et al.*, 2002a). Whatever the gating mechanism(s), the associated conformational changes appear to be very sensitive to the

structural/dynamical alterations of the environment. When the RC is embedded into a non liquid trehalose-water matrix, dehydration causes *inhomogeneous* inhibition of Q_A^- to Q_B electron transfer, involving two subpopulation of RCs. In one of them ("active"), electron transfer to Q_B is still observable, competing successfully with $P^+Q_A^-$ recombination; in the other one ("inactive") the interquinone electron transfer is drastically inhibited, because only recombination of the $P^+Q_A^-$ is observed. A limited residual water variation (from ~2 to ~0.8 H_2O per trehalose molecule) suppress totally the active population (Francia *et al.*, 2003). We have ascribed the full inhibition of the reaction in the trehalose matrix to a block, over the whole RC population, of the conformational transitions which gate the electron transfer process. Again the different behaviour observed in the sucrose matrix reveals a much looser protein-matrix coupling. In sucrose, in fact, a smaller decrease of the "active" subpopulation is found when decreasing the water content over the same range and an "active" subpopulation accounting for more than 50% of the total survives even under extreme dehydration. Such an effect (inhibition of Q_A^- to Q_B electron transfer in about half of the RC population) has been observed in RC films, dehydrated in the absence of any sugar (Francia *et al.*, 2003). This suggests that sucrose plays essentially no role, consistently with the idea that the RC and the sucrose matrix "phase separate" following dehydration. The partial inhibition detected in the RC-sucrose matrix, as well as in the RC film in the absence of sugars, suggests that water-protein interactions are involved in the gating process. At variance, the total inhibition of the reaction, attained in the trehalose matrix at relatively high H_2O/sugar ratios, puts forward the relevance of hydrogen bond networks in blocking protein conformations.

The highly *inhomogeneous* kinetic behaviour of the system, both in the absence and in the presence of sugars, most likely reflects the structural conformational heterogeneity of the RC protein as well as the local, spatial heterogeneous dynamics which characterizes nonsolid glasses (Roberts and Debenedetti, 1999; Ediger, 2000 and references therein). By studying single green fluorescent protein molecules embedded into trehalose-water matrices, the simultaneous presence of different, interconverting protein-trehalose-water nanostructures has been recently evidenced (D'Alfonso *et al.*, 2007).

5.2.2   *Protrein-matrix coupling and thermal stability*

It has been suggested that non liquid carbohydrate matrices prevent damages of biological structures by constraining their conformational dynamics and precluding the structural changes which lead to denaturation. If this is correct, a tighter protein-matrix coupling in trehalose with respect to sucrose implies a better efficiency of the former disaccharide as bioprotectant. A remarkable superiority of trehalose in preserving the structural and functional activity at low water content and elevated temperatures has been indeed demonstrated for a number of soluble proteins, including DNA restriction and modifying enzymes (Roser, 1991; Colaço *et al.*, 1992; Uritani *et al.*, 1995), glucose-6-phosphate dehydrogenase (Sun and Davidson, 1998) and trypsin (López-Díez and Bone, 2004). In the case of the RC, by examining the kinetics of two specific electron transfer processes, we argued that the structural/dynamical protein-matrix coupling is extremely weak in sucrose as compared to trehalose. This led us to test in parallel the RC thermal stability when the protein is embedded in sucrose and trehalose matrices. As expected, we have found that is sucrose the structural and functional integrity of the RC is lost progressively and irreversibly following storage at 37° over a period of a few days. The decrease of the photochemically active RC population in the sucrose matrix parallels in time the loss of the native state of the protein, as evaluated from the changes observed in the bacteriochlorin Q_y bands. On the contrary, when embedded into a trehalose matrix, the RC fully retains its primary photochemical activity and no spectral change in the near IR bands of its bacteriochlorophyll and bacteriopheophytin cofactors is observable even after six days of incubation under the same conditions. This behaviour is fully consistent with the conclusion that the RC and the sucrose matrix "phase separate" at low water activity. At variance with what occurs in the trehalose matrix, in sucrose no large energy barrier prevents the RC protein to explore at moderately high temperatures non-native conformations along the route to denaturation. In agreement with these observations, the kinetics of thermal denaturation measured in the sucrose matrix and in a RC film dehydrated in the absence of any sugar barely differ (see **Fig. 5.5**), demonstrating the negligible role of sucrose.

In the case of glucose, a sizeable inhibition of the RC dynamics coupled to $P^+Q_A^-$ recombination was paralleled by a relevant bioprotective effect. Therefore, the results

obtained in matrices formed by three different sugars are consistent with the notion that protein dynamics anf thermal denaturation are closely related.

6 FUNCTIONALITY OF PHOTOSYNTHETIC REACTION CENTERS IN POLYELECTROLYTE MULTILAYERS

The development of protein-friendly materials that can house enzymes or other proteins with retention of their functionality is receiving a growing attention by researchers in the fields of chemistry, biology, physics and material science. The efficient immobilization of proteins on suitable matrices and their integration on precisely engineered nanoscale architectures is often a key step for their use in novel technical applications (Gill *et al.*, 2000a and b; Lebedev *et al.*, 2006). Therefore the study of protein functionality within non-natural, non-liquid environments plays an important role in the development of devices for sensing, energy storage/conversion and bioelectronic applications (Hampp, 2000; Stuart *et al.*, 2002; Das *et al.*, 2004; Holden *et al.*, 2005; O'Neill *et al.*, 2005). At the same time, as discussed in the previous chapter, the functional charcaterization of proteins within non-native environments can yield new insight into their mechanism of action, sheding light particularly on the relation between function and internal dynamics of the protein (see also Cordone *et al.*, 2005). Of course these two aims of the research (application- and protein-oriented) are fully interconnected. In the present thesis we have extended our previous studies on photosynthetic bacterial reaction center (RC) incorporated into amorphous matrices (see chapter 5) to the assembly of this membrane protein and a cationic polymer, poly(dimethyldiallylammonium chloride) (PDDA), in ordinate multilayers. The alternate deposition of polyanions and polycations on a solid surface leads to the formation of films called polyelectrolyte multilayers (PEM). Such films are readily prepared by layer-by-layer assembly, a simple process based on the sequential adsorption, driven by electrostatic interactions, of cationic and anionic species on a charged substrate (for reviews see Decher *et al.*, 2003; Schonhoff, 2003). This technique has been used to prepare ordered protein films by alternating polyion layers with a number of different positively and negatively charged soluble proteins (Lvov *et al.*, 1995). The incorporation into PEM multilayers of an integral membrane protein has been also achieved, using as a guest model system the photosynthetic reaction center purified from purple bacteria (Kong *et al.*, 1998; Zhao *et al.*, 2002).

A striking functional homology exists between the electron quinone acceptors of the bacterial RC and of photosystem II (PSII) in plants (Draber *et al.*, 1991). In both systems, the two acceptor quinones (Q_A and Q_B), act in series and function as a two electron gate which passes reducing equivalents out of the RC only in pairs, *i.e.* when QH_2 is formed at the Q_B site (Shinkarev and Wraight, 1993). This homology is reflected by similar inhibitor sensitivities: many economically important herbicides, largely used in agriculture, known to act at PS II, are effective in the bacterial RC, where they compete with quinone for binding at the Q_B site. In view of these properties and of the crystallographic information available, the bacterial RC has become over the last decades the reference model in studying several features of the more complex PS II system (Deisenhofer *et al.*, 1985; Allen *et al.*, 1987a).

In this chapter we show that bacterial RCs can be incorporated into PDDA multilayers, preserveing the functionality of the Q_B site as an electron acceptor. Kinetics of charge recombination following a single turnover photoexcitation have been found to be affected by the hydration state of the PDDA-RC multilayers. This sensitivity has been put in relation with similar effects observed on RCs embedded in different non-liquid matrices of low water content. PDDA-RC multilayer turn out to provide unique advantages in investigating the thermodynamics and kinetics of herbicide binding. An assay for herbicides, based on the response of PDDA-RC multilayer to continuous illumination, has been extensively tested and modeled quantitatively. Based on these results, the properties of the system are discussed in view of its use in the design of a simple optical biosensor for herbicides.

6.1 Results and Discussion

6.1.1 *Preparation of PDDA-RC multilayers*

The main driving forces for layer-by-layer assembly are electrostatic interactions. Immersion of a negatively charged surface (glass) into a solution of cationic polyelectrolyte (*i.e.* PDDA) results in the coverage of the surface by a positively charged polymer layer. Of course, immersion of this new cationic surface in a solution of negatively charged protein results in the protein adsorption and in re-establishing of a negative charge density. Basically, the process can be repeated indefinitely as long as

the charge of the cationic and anionic adsorbed polyelectrolytes remains unaffected by the immersion in the three relevant solutions, viz. cationic and anionic polymer solutions and water (in passing between the two adsorbing baths the specimen must be rinsed with water, otherwise free polyelectrolytes will interact in solution forming neutral complexes).

In the case of membrane proteins what is relevant is the charge of the protein-detergent complex. RC is extracted from the bacterial intracytoplasmic membrane by using N,N,-dimethyldodecylamine-N-oxide (LDAO), a neutral detergent. However, the amine-N-oxide moiety of LDAO can be protonated at acidic pH leading to the formation of the cationic detergent N,N,-dimethyldodecylammonium-N-hydroxide. The presence of negative charges on the RC surface shifts the pK_a of protein-bound LDAO to physiological values so that for pH< 7.5 the protein detergent complex is neutral (Piazza *et al.*, 2003; Palazzo *et al.*, 2004). In preliminary attempts to form polycation-RC multilayers using LDAO-RC complex we found a low adsorption efficiency, probably because the polycation adsorption and the rinsing steps were performed in unbuffered water characterized by slightly acidic pH. We have therefore exchanged LDAO with octylglucoside (a pH insensitive detergent) on a DEAE column (1-2 mL volume). The column was loaded with with ourified RC in 0.025% w/v LDAO, and then, washed with buffer without detergent in order to eliminate LDAO. Subsequently it was washed with 100 volumes of buffer contating 0.8% w/v OG. The detailed procedure of PDDA-RC multilayer formation is described under Materials and methods (3.10.3).

It should be noted that the assembly of PDDA-RC PEM on gold substrates was previously achieved by Kong *et al.* (1998) using as detergent Triton X100 (another pH-insensitive surfactant). Using OG-solubilized RCs, the alternate deposition of PDDA and RC layers is very effective as shown by the absorption spectra of **Fig. 6.1**. PDDA does not absorb in the spectral region considered, while the RC bacteriochlorins give rise to three intense absorbance bands in the region between 700 and 950 nm (Steffen *et al.*, 1994; Cherepy *et al.*, 1997). The band at 760 nm is ascribable to the Q_y transition of bacteriopheophytin molecules. The band at 802 nm is due to the Q_y transitions of the monomeric bacteriochlorophyls, together with a contribution from the high energy

exciton component of the Q_y transition of the bacteriochlorophyll molecules forming the special pair P. The long-wavelength band (at 865 nm in solution) is identified as the low energy exciton component of the Q_y transition of P.
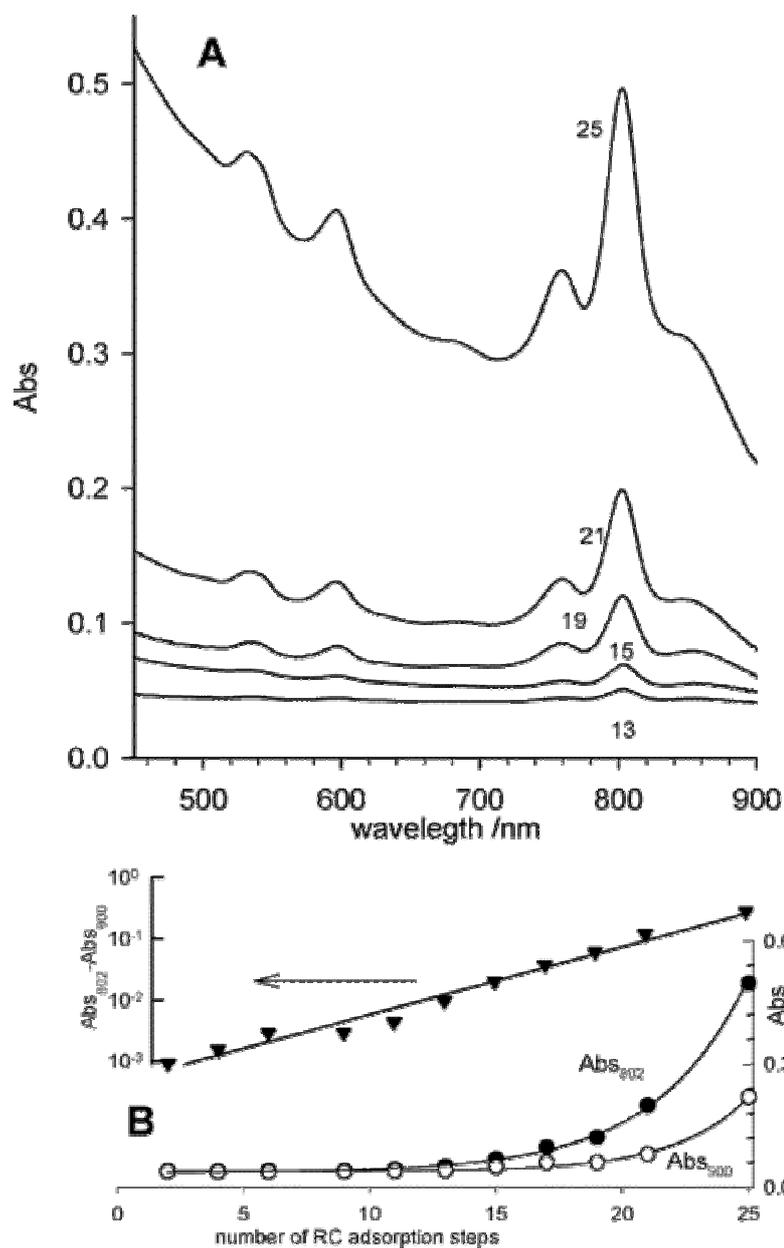

Fig. 6.1 A) Visible-NIR absorption spectra of PDDA-RC multilayers obtained following a different number of RC adsorption cycles (indicated in the labels). B) Lower plot: absorbance (right linear ordinate) at 802 nm (closed dots) and 900 nm (open dots) as a function of the number of RC adsorption cycles. Upper plot (close triangles): difference between absorbance measured at 802 and 900 nm (left logarithmic ordinate) as a function of the number of adsorption cycles. Solid lines represent exponential fits.

As shown in **Fig. 6.1**, absorption spectra of PDDA-RC multilayers retain all these features superimposed to a background scattering which is a strongly decreasing function of the wavelength. The position of absorption maxima can be safely determined from the first derivative of the absorption spectrum. Applying this procedure we have found in the near IR region maxima at 760 nm and 802 nm, independently from the number of adsorbed RC-layers. At variance, the position of the long-wavelength maximum appeared to depend on the number of layers, ranging from 853 nm (15 and 19 RC deposition steps) to 843 nm (25 RC deposition steps). Therefore, the only difference between RC spectra measured in PDDA-RC PEM and in solution is a 12-22 nm blue shift of the special pair (P) long-wavelength absorption band. The addition of cationic and zwitterionic (betaines) detergents has been shown to induce a moderate (10 nm) blue-shift in the position of the Q_y-band of P (Palazzo *et al.*, 2004; Müh *et al.*, 1998). ENDOR/TRIPLE studies have correlated this effect with a change in the spin density distribution within the P special pair (Müh *et al.*, 1998). A blue shift (to ~850 nm) has also been observed at very high local concentrations of RC, as in various dry RC films (Clayton, 1978; Palazzo *et al.*, 2002; Francia *et al.*, 2004) or RC aggregates in solution (Gast *et al.*, 1996; Palazzo *et al.*, 2004). In the present case the protein film is characterized by a large RC density and by strong electrostatic interactions with the cationic moiety of PDDA. Both these factors are likely to concur in determining the large blue shift observed in PDDA-RC PEM.

The adsorption of RC during the PEM assembly can be probed from the absorbance of the band at 802 nm. Kong *et al.* (1998) reported a linear dependence of RC absorbance on the number of PDDA-RC multilayers (Zhao *et al.*, 2002). In our system, the optical density grows exponentially with the number of adsorption steps over the whole spectral range investigated (see **Fig. 6.1**). To probe the growth of protein layers we have subtracted the absorption at 900 nm (were the RC absorbance is very small) from the absorbance at 802 nm (a maximum in the RC absorbance spectrum). According to the result shown in **Fig. 6.1B**, the RC absorbance increases exponentially over three decades with the number of adsorption cycles. The different adsorption behaviors found by us and by Kong's group are probably due to the use of different detergents (OG in our system, instead of Triton X100).

The PDDA-RC PEMs prepared with the above described procedure, and stored in distilled water at 4°C in the dark, display a striking stability, maintaining their spectral features as well as RC photoactivity over a period of several months. It turned out that, although the amount of RC adsorbed decreased to some extent over a period of a few months, the absorption spectra and the photoactivity (described in the following) retained the features of the native, functional protein. While most of the work was done within three-four months from the multilayer preparation, selected specimen where assayed and found to be functional after seven months.

6.1.2 *Kinetic of charge recombination in PDDA-RC multilayers*

The functional integrity of the RC when it acts as a constituent of PEM has been tested by studying light-induced charge separation and recombination reactions in single-turnover experiments. As already explained (see par. 1.2.2 and 4.2.2), following a flash of light and in the absence of electron donors to P^+, the electron on Q_B (or Q_A) can recombine with the hole on the primary donor. The decay of P^+ following a short photoexcitation includes in general two kinetic components, a fast and a slow one, ascribed to RC subpopulations which undergo $P^+Q_A^-$ and $P^+Q_B^-$ recombination respectively (see par. 1.2.2 and 4.2.2). The relative contributions of the two components depend on the fraction of RCs in which the final electron transfer from Q_A^- to Q_B cannot take place. In principle, therefore, kinetic analysis of charge recombination yields information on $P^+Q_A^-$ recombination as well as on electron transfer from Q_A^- to Q_B.

Since the reduced and oxidized forms of P have different extinction coefficients in the visible spectral range, the transient flash-induced formation of P^+ and its subsequent decay by charge recombination can be monitored spectrophotometrically at the appropriate wavelengths and time resolution. Kinetic and spectral features of absorbance changes induced by single turnover excitation in PDDA-RC multilayers are shown in **Fig. 6.2**. Absorbance changes detected immediately after photoexcitation over the 540-640 spectral range yield a light-dark differential spectrum (**Fig. 6.2B**, inset) which coincides with that reported for RC in solution, confirming the capability of the RC in PDDA multilayers to perform charge separation. **Fig. 6.2A** shows the kinetics of flash-induced absorbance changes (ΔAbs) recorded at three different wavelengths for PDDA-RC multilayers allowed to dry in air for 10 min.

The absorbance changes at 600 and 550 nm are due to the photoxidation and subsequent re-reduction of the primary donor P (Feher *et al.*, 1978). The change recorded at 422 nm includes contributions from both P^+ and from the semiquinone formed on the acceptor complex. The time course of absorption changes is essentially the same at the three wavelengths as shown in **Fig. 6.2B,** where traces are normalized in amplitude.
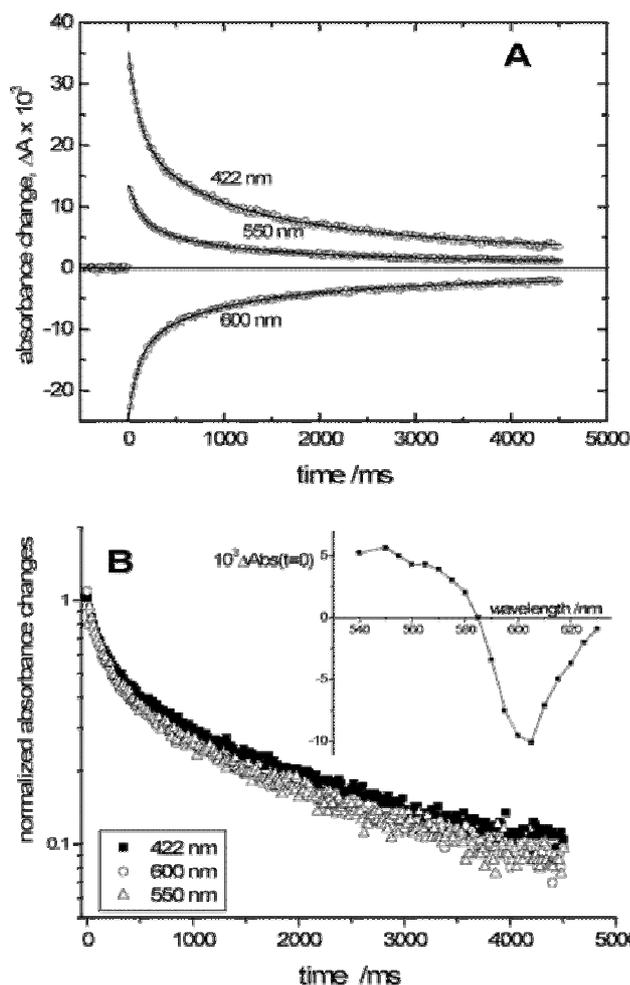

Fig. 6.2 Single-turnover experiments in dry PDDA-RC multilayers (25 cycles of RC adsorption). For each kinetic trace, 5000 data points were used in the fit; to increase readability, only 250 points are shown in the figures. (A) Charge recombination kinetics measured at three wavelengths in PDDA-RC PEM after a laser pulse fired at time $t = 0$; dots represent experimental data and lines the fits according to eq 6.1. Best fit parameters are as follows: at 422 nm, $A_f = 0.34$, $k_f = 9.3$ s^{-1}, $\lambda = 1.2$ s^{-1}, $\sigma = 1.3$ s^{-1}; at 600 nm, $A_f = 0.39$, $k_f = 10.1$ s^{-1}, $\lambda = 1.4$ s^{-1}, $\sigma = 1.4$ s^{-1}; at 550 nm, $A_f = 0.34$, $k_f = 9.3$ s^{-1}, $\lambda = 1.6$ s^{-1}, $\sigma = 1.6$ s^{-1}. (B) The same data of panel A normalized to the maximal absorbance change recorded immediately after the photoexcitation pulse and reported in a semilog plot. Inset: light-dark spectrum; each point at a given wavelength represents the absorbance change extrapolated at the time of the flash ($t = 0$) by fitting the kinetic trace to eq 6.1.

This implies that the decays of P^+ and semiquinone are concomitant and that, therefore, recovery kinetics recorded at these wavelengths are due to charge recombination processes only, without any interference from side reactions re-reducing P^+ or re-oxidizing the semiquinone. Charge recombination is clearly biphasic. Moreover, attempts to fit the data to the sum of two exponential decays, reveal that the slow phase deviates significantly from an exponential behavior. Incorporation of the RC into dehydrated amorphous matrices (*i.e.* sugar glasses (Palazzo *et al.*, 2002; Cordone *et al.*, 2005) and polyvinyl alcohol (PVA) films (Francia *et al.*, 2004b)) has been previously found to result in non-exponential, distributed kinetics of charge recombination (see also chapter 5). In the case of $P^+Q_B^-$ recombination, this effect, which depends on the chemical nature and on the hydration state of the embedding matrix, occurs even in weakly interacting matrices (PVA) and relatively hydrated states (Francia *et al.*, 2003; Francia *et al.*, 2004b; Cordone *et al.*, 2005). It has been interpreted as reflecting a matrix-induced inhibition of the RC dynamics, leading to a decreased rate of interconversion between different conformational substates of the RC, each characterized by its individual electron transfer rate constant. When inter-conversions become slower than the electron transfer process examined, kinetics of electron transfer is expected to exhibit a non-exponential character, describable by a continuous rate distribution. It has been shown that distributed kinetic phases of charge recombination can be adequately accounted for by a power law (Kleinfeld *et al.*, 1984a; Palazzo *et al.*, 2002). Such a function accounts well for the distributed kinetics of the slow component of P^+ decay also in RC multylayers, so that an adequate and physically meaningful function fitting charge recombination kinetics shown in **Fig. 6.2** is:

$$\frac{P^+(t)}{P^+(0)} = \frac{\Delta Abs(t)}{\Delta Abs(0)} = A_f e^{-k_f t} + \left(1 - A_f\right) \Big/ \left(1 + \frac{\sigma^2}{\lambda} \cdot t\right)^{\frac{\lambda^2}{\sigma^2}} \qquad (6.1)$$

where the A_f is the fraction of fast phase; λ is the average rate constant and σ the width of the rate distribution function characterizing the slow phase. The values obtained by this procedure for the kinetic parameters (listed in the caption of **Fig. 6.2**) deserve some comments. First, very close values are obtained for A_f, k_f, λ, and σ at the three wavelengths considered, confirming quantitatively the essential coincidence of the

kinetics, as inferred by visual inspection of normalized traces (**Fig. 6.2B**). The rate constant of the fast exponential phase, k_f, assumes, within the experimental uncertainty, the same values found in solution ($\approx$10 s^{-1}) for the charge recombination from P$^+$Q$_A^-$ so that we can safely attribute this phase to RCs in which the final electron transfer from Q$_A^-$ to Q$_B$ cannot take place, either because the protein lacks the quinone at the Q$_B$ site or because this electron transfer step is inhibited. On the other hand, the average rate constant characteristic of the slow phase (λ=1.2 s^{-1}) is slightly larger than the λ value observed for Q$_B$-reconstituted RC in solution (λ=1.0 s^{-1}) (see par. 4.2.2) suggesting a destabilization of the P$^+$Q$_A$Q$_B^-$ with respect to the P$^+$Q$_A^-$Q$_B$ state. Interestingly the width of the correspondent rate distribution is very high. The σ-value is actually larger than 1.2 s^{-1} in PDDA-RC multilayers, *i.e.* much higher than the values found for RC in solution (σ=0.19 s^{-1}) (Francia *et al.*, 2003) and when incorporated in amorphous sugar matrices (σ=0.25 s^{-1}) (Francia *et al.*, 2003) and polyvinylalcohol films (σ=0.20 s^{-1}) (Francia *et al.*, 2004). Most likely such a huge polydispersity in charge recombination rates reflects some local heterogeneity in the electric charge distribution within the PEM matrix.

The last parameter, characterizing the charge recombination kinetics in PDDA-RC, is the relative weight of the fast phase (A_f). In dry PDDA-RC multilayers prepared from RCs with the Q$_B$ site fully reconstituted, about 62% of the RC population undergoes slow charge recombination from P$^+$Q$_B^-$ (A_f=0.36-0.39, see legend of **Fig. 6.2**). In the remaining RC population, recombination occurs from the P$^+$Q$_A^-$ state. It is quite unlikely that this is due to quinone extraction during the multilayer assembly as demonstrated by the fact that a substantial recovery in the relative amplitude of the slow phase, (1-A$_f$), is observed upon re-hydration of multilayers (**Fig. 6.3A**). When the hydration state of PDDA-RC multilayers was examined by NIR spectroscopy, it turned out that during exposition to air, after rinsing in water, the multilayer retains a substantial amount of water during the first three minutes. However, in the subsequent 6-8 minutes, the content of residual water decreases dramatically, becoming practically undetectable after 10 minutes, and leading to what we call *dry* multilayer (see **Fig. 6.3B**). In this state, the PDDA-RC multilayer is characterized, as stated above, by a consistent fraction of RCs undergoing fast P$^+$Q$_A^-$ recombination.

At variance, when charge recombination kinetics are measured in "wet" PDDA-RC multilayers (within about three minutes after rinsing), P^+ decay is dominated by the slow component as shown in **Fig. 6.3A**. It appears that in "wet" PEMs at least 80% of RCs are fully functional at the Q_B site, indicating that the amount of water strongly affects the yield of Q_A^- to Q_B electron transfer in PDDA-RC multilayers.
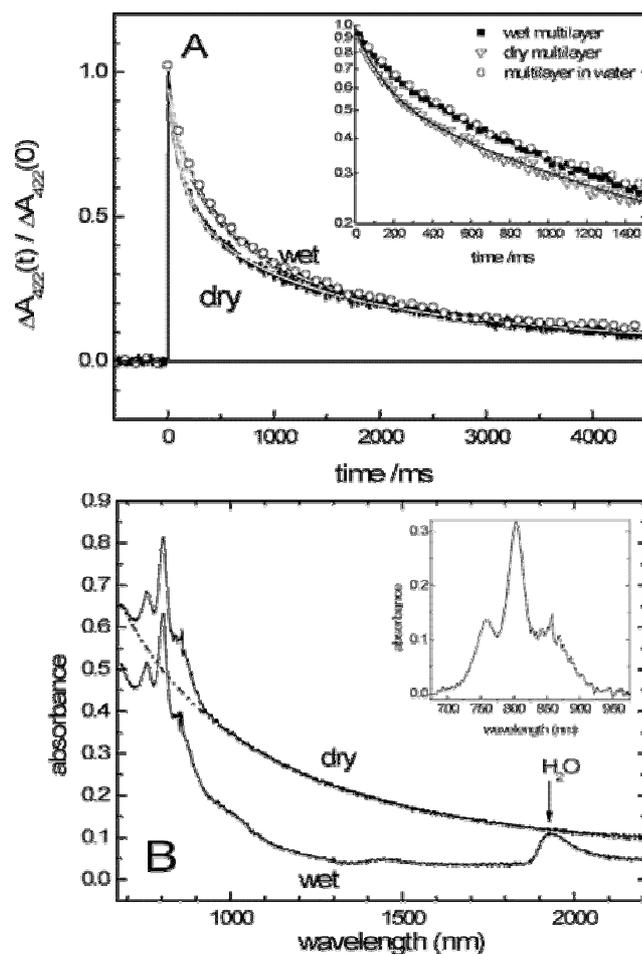

Fig. 6.3 (A) Charge recombination kinetics measured on the same PDDA-RC PEM at different degrees of hydration. "Dry" and "wet" refers to PEM allowed to desiccate for 10 and 3 min, respectively (black traces). The inset shows enlarged the first part of the decays in a semilog plot (closed squares and inverted triangles are data sampled in the "wet" and "dry" state, respectively). In both plots, open circles refer to measurements performed on the same PEM immersed in water. Because this last kinetics essentially coincide with that measured in the "wet" PEM, only a selected number of points is reported. Fits of kinetics according to eq 6.1 for wet and dry PEM are shown as gray lines. Best fit parameters are as follows: $A_s = 0.80$, $k_f = 10.4$ s^{-1}, $\lambda = 1.2$ s^{-1}, $\sigma = 1.1$ s^{-1} for the wet state; $A_s = 0.62$, $k_f = 8.2$ s^{-1}, $\lambda = 0.91$ s^{-1}, $\sigma = 0.8$ s^{-1} for the dry state. (B) NIR spectra of dry and wet PEM. The dashed curve shows the power-law dependence used to describe the background scattering in dry PEM. Inset: the RC spectrum obtained after correction for the background; the spike at 860 nm is an artifact due to the change in light source of the measuring beam.

As shown in **Fig. 6.3A** charge recombination kinetics of RC in wet multilayers are quite similar to those observed in PEM directly dipped in water (immersion in water results only in a further 5% increase in the relative amplitude of the slow kinetic component).

The absorption spectra in the visible-NIR region allow the quantification of the RCs involved in the building of multilayers and of the residual water present in wet specimens. As shown in **Fig. 6.3B**, dry PEMs lack any absorption band in the region 1000-2200 nm. In both dry and wet PEMs, absorbance increases continuously at decreasing wavelengths. By subtracting this background, which can be fitted to a power-law, a corrected absorption spectrum is obtained (see the inset of **Fig. 6.3B**) quite similar to that of the RC in solution (except for the blue shift of the long-wavelength band, discussed in previous paragraph). From the absorbance at 800 nm, assuming that the extinction coefficient determined for RC in solution holds also for RC in PDDA-RC, a surface density of 1.1 nmoles RC/cm^2 (for 25 RC layers on each side of the glass substrate) can be estimated. In wet PEMs a water/RC molar ratio of about 7×10^4 can be evaluated from the area of the water absorption band centered at 1930**,** following the procedure described in par. 3.11.2 of Materials and methods. Since, as described above, further hydration of the RC multilayer causes only a limited (5%) increase in the fraction of slow charge recombination, it appears that such a water/RC ratio is sufficient to retrieve the function of Q_B as secondary electron acceptor in most of the RC population.

6.1.3 Functional integrity of reaction center and the effects of dehydration

The sensitivity of Q_A^- to Q_B electron transfer to the hydration level of RC multilayers is reminiscent of a similar behaviour, previously observed by us in RC embedded in different non-liquid matrices. In particular, by studying the kinetics of charge recombination in trehalose coated RCs as a function of the content of residual water (see par. 5.1.2 and relative references), we have shown that a progressive dehydration of the matrix blocks Q_A^- to Q_B electron transfer in a progressively increasing fraction of the RC population, leading to complete inhibition in relatively wet matrices. A further reduction in the amount of residual water affects the kinetics of $P^+Q_A^-$ recombination, which, in extensively dried matrices, is strongly accelerated and

becomes distributed over a spectrum of rate constants. These effects have been taken to indicate a strong coupling between dynamics of the RC protein and of the trehalose matrix, the latter being progressively hampered upon dehydration. More specifically, the severe hardening of the trehalose matrix occurring at extremely low hydration levels, suppresses the transition from a *dark-adapted* to a *light-adapted* conformation, which stabilizes the primary charge separated state $P^+Q_A^-$ (Francia *et al.*, 2004c). As a consequence, $P^+Q_A^-$ charge recombination occurs from an unstabilized, unrelaxed RC conformation, with a rate (k_{AP}) larger than that measured in solution. In more soft (wet) matrices, stabilization of the $P^+Q_A^-$ state can take place, but the trehalose matrix heavily hinders the conformational changes coupled to Q_A^- to Q_B electron transfer. This process has been shown indeed to be conformationally gated (Graige *et al.*, 1998).

When the RC is incorporated in a weakly interacting matrix, *i.e.* in a PVA film, k_{AP} is affected to a much lower extent, even when the content of residual water is below the detection limit of NIR spectroscopy (Francia *et al.*, 2004b). Also in PVA, dehydration primarily affects the functionality of the secondary quinone acceptor, but a complete inhibition of Q_A^- to Q_B electron transfer over the whole RC population is never attained, even under extreme dehydration (Francia *et al.*, 2004b). Taken together, these observations can help in interpreting the behavior observed in RC multilayers. In PEM the rate constant k_f of the fast phase is unchanged with respect to RC in solution, suggesting that in PDDA-RC multilayers the relaxation of the RC protein from the *dark-adapted* to the *light-adapted* conformation is still faster than $P^+Q_A^-$ recombination. At variance, incorporation in PEMs and their dehydration appears to block Q_A^- to Q_B electron transfer in a significant fraction of the RC population. The effect is qualitatively similar to that observed in trehalose matrices and PVA films, but it is much weaker in RC-multilayers. Even after extensive drying (dry PDDA-RC multilayers) more than 60% of RC displays $P^+Q_B^-$ recombination, while in "wet" trehalose matrices only $P^+Q_A^-$ recombination is observed. Full hindering of interquinone electron transfer appears to require, in addition to dehydration, a structural and dynamical protein-matrix coupling, which is peculiar of trehalose glasses but not of PVA films and PDDA-RC PEM.

In summary, analysis of charge recombination in PDDA-RC multilayers indicates that hydration has a non-negligible, but minor effect on the intraprotein electron transfer within RCs. From a practical point of view, layer-by-layer assemblies have an additional advantage over the other non liquid systems discussed above: they can be dipped repeatedly in water without destroying the matrix. This allowed to test extensively the reversibility of hydration/dehydration processes. Hydration/dehydration effects on the charge recombination kinetics can be observed reproducibly after a number of dehydration cycles and immersions in water, performed over a period of several months on the same multilayer. In view of their stability, RC-multilayers provide a powerful tool in studying the interaction of herbicides with the Q_B site.

6.1.4 Effects of herbicides

A wide variety of agents are found to be specific inhibitors of the electron transfer between the quinone electron acceptors of the photosystem II complex (PSII) in higher plants and of bacterial RCs. Due to their use for the control of weeds these agents are termed PSII-herbicides. PSII-herbicides bind, *in vivo*, to the D1 protein of the PSII complex and displace the secondary electron acceptor (a plastoquinone in higher plants). Due to the structural and functional analogies of the quinone acceptor complex in bacterial RCs and plant PSII, this class of herbicides includes components which act efficiently as competitive inhibitors also at the Q_B site of bacterial RCs. The binding of herbicides to bacterial RCs has been studied in solution by analyzing the kinetics of charge recombination following a short flash of light (Stein *et al.*, 1984). In fact, the relative amplitude of the fast phase of recombination kinetics can be taken as a measure of the fraction of the RC population in which the herbicide is bound at the Q_B site and inhibits electron transfer to the secondary acceptor.(Shinkarev and Wraight, 1993).

As shown in **Fig. 6.4**, dipping of PDDA-RC PEM into a concentrated (0.8 mM) solution of o-phenantroline, a classical competitive inhibitor of the Q_B site in bacterial RCs, has a dramatic effect on the charge recombination kinetics. Following exposure of PDDA-RC PEM to o-phenantroline, the flash-generated P^+ decays in a few hundreds of milliseconds instead of several seconds. In PDDA-RC multilayers exposed to o-phenantroline, most of P^+ decay occurs exponentially with a rate constant which

essentially coincides with k_{AP} found in solution, indicating that this herbicide successfully competes for the Q_B site of the protein in PDDA-RC PEM as well.
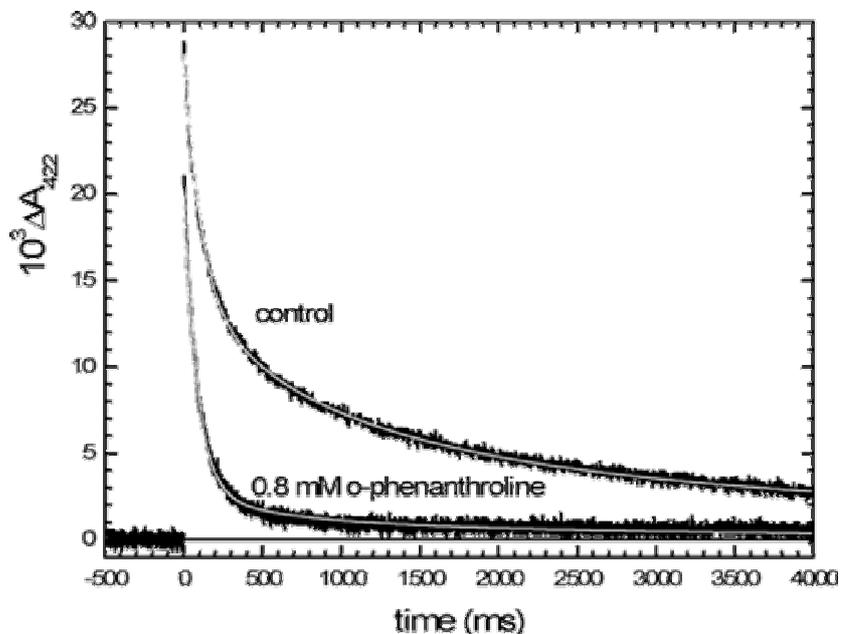

Fig. 6.4 Charge recombination kinetics measured in dry PDDA-RC PEM after immersion in water (control) and 0.8 mM *o*-phenanthroline solution.

The decrease in the maximal absorbance change reached immediately after the flash indicates that exposure to o-phenantroline at very high concentration displaces also the quinone at the Q_A site (as reported for RC in liposomes (Wraight, 1981)). Quite surprisingly, the inhibitory effects described above are caused by exposure to the herbicide for a relatively short time: few seconds of dipping in the herbicide solution are sufficient to affect the kinetics as illustrated in **Fig. 6.4**. The acquisition of charge recombination kinetics characterized by a good signal-to-noise ratio requires the averaging of several transients separated by a one minute time interval during which the sample is *dark adapted* to allow full relaxation of photo-generated species. Because of these constraints the kinetics of herbicide binding and release were probed on *dry* PDDA-RC films. The procedure was the following. PDDA-RC PEM previously stored in pure water was dipped in 6 mL of herbicide solution for a given time. Then the specimen was removed from the solution, placed vertically on absorbing paper and dried for 10 minutes in air. Finally the charge recombination kinetics was recorded. The

same sample was then dipped again in the herbicide solution for a longer time and the procedure was repeated until the relative amplitude of the fast phase in the measured P^+ decay reached a maximum, constant value.

To study the kinetics of herbicide de-binding, the same fully-inhibited sample was rinsed with pure water. The procedure was analogous to that used for the binding kinetics; the specimen was dipped in 100 mL water for different times and the charge recombination kinetics were measured subsequently in the dry PEM. The results obtained in a consecutive binding and de-binding experiment are shown in **Fig. 6.5**, were the fraction of fast phase of the P^+ decay is reported as a function of the immersion time. Both processes of binding and release are accomplished in few seconds and are reasonably described by first-order kinetics. Binding appears to be faster, with a characteristic time of 2.5 ± 0.5 s, as compared to a time of 13 ± 2 s for de-binding. As to the decrease in the absorbance change measured immediately after the flash ($\Delta Abs(0)$), we note that it is also fully reversible by rinsing the PEM with water; difficulties in the exact repositioning of the specimen preclude a detailed kinetic analysis of the decrease and recovery observed in $\Delta Abs(0)$; however the o-phenantroline-induced drop in $\Delta Abs(0)$ reaches a steady state within 100 s of incubation in the herbicide solution, while 50 s of rinsing with water are enough to revert this effect.

Following the determination of binding and de-binding kinetics, we have built an equilibrium binding isotherm by measuring the charge recombination kinetics after a 5 minutes equilibration of the RC-multilayer with o-phenantroline solutions at increasing herbicide concentration. Rather than using dried RC-multilayers, measurements were performed directly on PDDA-RC PEM immersed into the o-phenantroline solution. This procedure minimizes the scattering artifacts and maximizes the effect of the herbicide because in fully hydrated PDDA-RC PEM the $Q_A^-Q_B \rightarrow Q_A Q_B^-$ electron transfer works efficiently over a larger RC population (see previous paragraph).
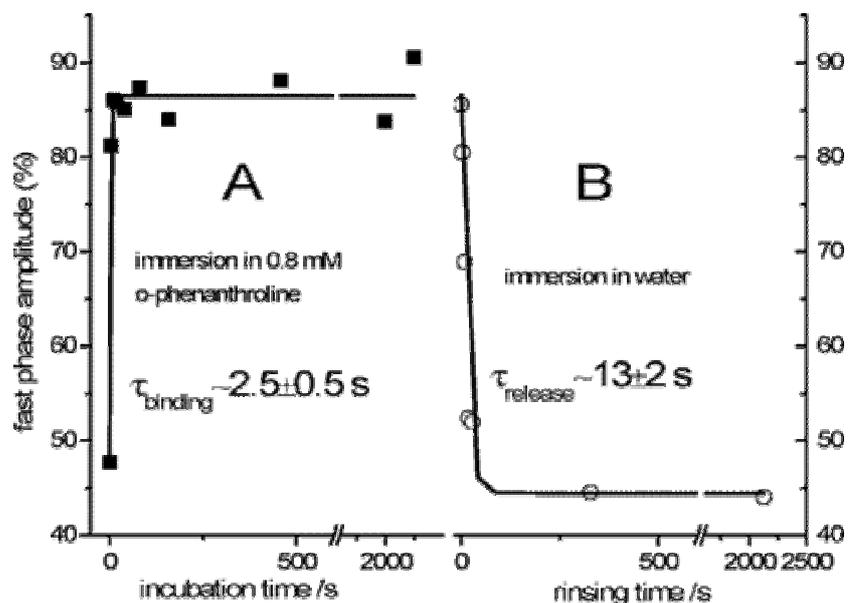
Fig. 6.5 Inhibitor binding and release kinetics (see text for details). (A) Relative fast phase amplitude of charge recombination kinetics measured on PDDA-RC PEM as a function of the incubation time in a 0.8 mM *o*-phenanthroline solution. (B) Relative fast phase amplitude of charge recombination kinetics for fully inhibited PDDA-RC PEM (last point of panel A) after rinsing with water for different times. Lines are fitting according to first-order kinetics.

The data, shown in **Fig. 6.6**, indicate that the fraction of RCs in which the electron transfer to Q_B is inhibited (because the site is occupied by o-phenantroline) increases when the herbicide concentration of the solution in equilibrium with the PDDA-RC PEM is increased and it finally reaches a plateau for o-phenantroline concentrations higher than 400 μM.

It is not clear, *a priori*, whether the interaction of a ligand with proteins assembled to form a film should be treated as a classical binding process or as the adsorption to a surface. In any case, both processes are expected to obey formally the same equation

$$X = \frac{K[I]}{1+K[I]}$$ (6.2)

where [*I*] is the concentration of the ligand/adsorbate *I*. *X* represents the fraction of protein bound to *I* and K is the binding constant (the reciprocal of the dissociation constant). In the case of adsorption to a surface, eq. 6.2 identifies with the Langmuir's isotherm, where *X* denotes the fraction of adsorption sites occupied and K is the Langmuir constant (the ratio between the adsorption and desorption rate constants).
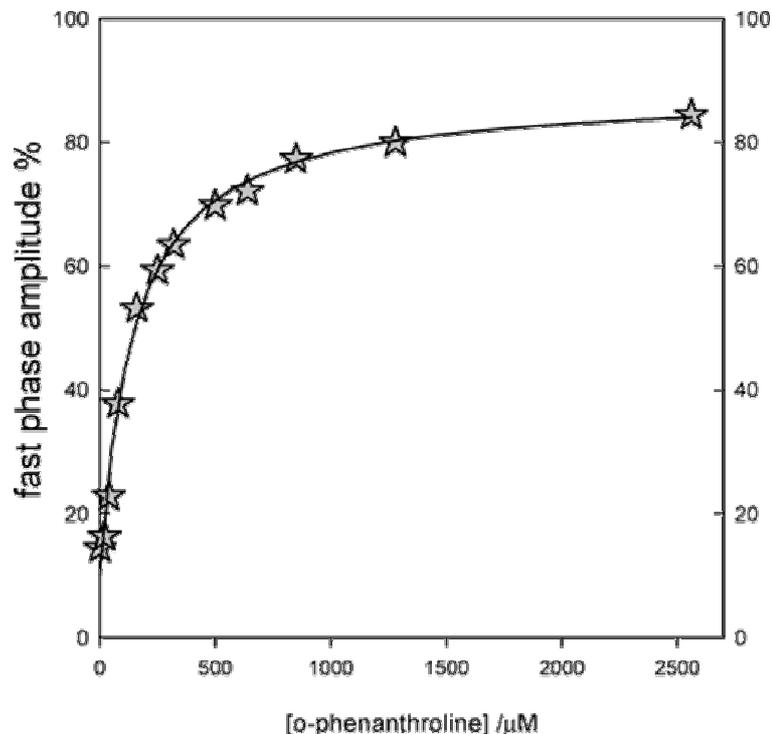
Fig. 6.6 Relative amplitude of the fast phase of charge recombination kinetics measured on a PDDA-RC PEM as a function of *o*-phenanthroline concentration. The data (stars) were fitted to eq 6.2 (continuous line) under the assumption that the herbicide concentration in solution is unaffected by the binding process (*o*-phenanthroline is always in large excess compared to RC). The best fitting binding constant is $K = 6.9 \pm 0.7$ mM

Whichever of the processes is considered, in our case X can be taken as the fraction of the RC population undergoing $P^+Q_A^-$ recombination (*i.e.* the relative amplitude A_f of the fast phase in the decay of the absorbance change after a light pulse). From the data of **Fig. 6.6** it is clear that in absence of o-phenantroline a fast phase of non negligible relative amplitude is already present in the recombination kinetics and that, even at high herbicide loading, A_f does not reach unity (the latter feature is observed also in solution and is generally attributed to the competition between herbicide and quinone) (Stein *et al.*, 1984). Accordingly, we have modified eq. 6.2 in the form below by adding two adjustable parameters representing the values X assumes when $[I]=0$ and $[I]=\infty$ (X_{min} and X_{max}, respectively).

$$X = X_{min} + \left(X_{max} - X_{min}\right)\frac{K[I]}{1 + K[I]} \qquad (6.3)$$

As illustrated in **Fig. 6.6**, eq. 6.3 nicely fits the experimental data for K=6.9±0.7 mM^{-1}. This value corresponds to a dissociation constant (145±15 μM) of the same order of magnitude of the one reported for RCs in solution (Stein *et al.*, 1984). Extensive rinsing with water allows the recovery of the Q_B activity so that the same specimen can be used repeatedly; the effect of the inhibitor is reproducible within the uncertainty associated with fitting of the charge recombination kinetics. These features are promising for the use of PDDA-RC PEM as biomediator in herbicide bioassays.

6.1.5   *PDDA-RC multilayers as potential herbicide biosensors*

Herbicides are widely used on a variety of crops for the control of broadleaf weeds but can be highly toxic for human and animal health. Their wide use in agriculture has resulted often in the herbicide pollution of water and the level of herbicides allowed in drinking water is subject to regulation, at least in the industrialized countries. Different attempts have been made to introduce biological detection systems in order to overcome the high cost of time consuming HPLC analysis. Several immunoassays have been proposed, mainly ELISA (Schneider *et al.*, 1994; Piletskaya *et al.*, 1999; Banks *et al.*, 2003) and immunosensors (Bier *et al.*, 1994; Brecht *et al.*, 1995; Harris *et al.*, 1999; Skl'adal, 1999). However, antibodies can detect only one or few cross-reacting substances. To overcome this limit, the analytical use of PSII as a receptor protein in bioassays has been investigated (Giardi *et al.*, 2005). The practical application of herbicide biosensors based on PSII preparations is seriously hampered by their instability (in particular when illuminated) (Giardi *et al.*, 2005). At variance, the bacterial RC is remarkably stable against denaturation. Its use in optical bioassays was proposed already in 1993 by exploiting phenomenologically the response to herbicides of the extent of primary donor P photoxidized under continuous illumination (Jockers *et al.*, 1993).

The steady-state attained by RCs under continuous light is different in the presence and in the absence of an inhibitor of Q_A^--to-Q_B electron transfer. Intuitively (see scheme 1 in par. 1.2.2), the level of photoxidation reached by P under continuous photoexcitation will be determined by the competition between charge separating processes and charge recombination reactions. The latter are faster when occurring from

the $P^+Q_A^-$ state (*i.e.* in the presence of inhibitor) than from the $P^+Q_B^-$ state (in the uninhibited RC); a progressively lower level of P oxidation is therefore expected in steady state at increasing herbicide concentrations.

Before describing the experimental results obtained on PDDA-RCs in continuous light experiments, a quantitative analysis of the processes mentioned above may be useful. Steady state behavior under continuous illumination can be described with the aid of a simple kinetic scheme:

$$
\begin{array}{ccc}
& k_L & \\
PQ_AQ_B & \rightleftharpoons & P^+(Q_AQ_B)^- \\
& \lambda & \\
+I \quad k_I \Big\updownarrow k_{-I} & & \\
& k_L & \\
PQ_AI & \rightleftharpoons & P^+Q_A^-I \\
& k_{AP} &
\end{array}
$$
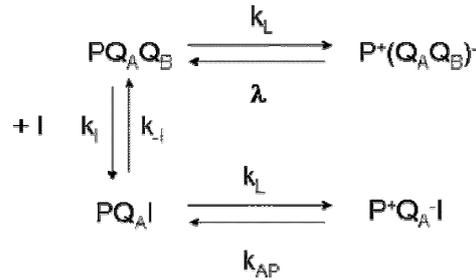
Acceptors prior to Q_A are incorporated into the light-dependent rate constant k_L, which is actually the product of an absorption cross-section and photon flux. Equilibration of the electron between Q_A and Q_B has been assumed much faster than the other considered processes (Shinkarev and Wraight, 1993); under this condition, recombination from the $P^+(Q_AQ_B)^-$ state in the uninhibited complex can be described by a single rate constant $\lambda = k_{AP}/(1+L_{AB})$, where $L_{AB}=k_{AB}/k_{BA}$ is the equilibrium constant for interquinone electron transfer (see scheme 1.2.1 in 1.2.2 and Shinkarev and Wraight, 1993).

The rate equations describing the electron transfer kinetics and binding equilibrium summarized in the above kinetic scheme are given by:

$$
\frac{d}{dt}\begin{pmatrix} [PQ_AQ_B] \\ [P^+(Q_AQ_B)^-] \\ [PQ_AI] \\ [P^+Q_A^-I] \end{pmatrix} = \begin{pmatrix} -(k_L+k_I[I]) & \lambda & k_{-I} & 0 \\ k_L & -\lambda & 0 & 0 \\ k_I[I] & 0 & -(k_L+k_{-I}) & k_{AP} \\ 0 & 0 & k_L & -k_{AP} \end{pmatrix} \cdot \begin{pmatrix} [PQ_AQ_B] \\ [P^+(Q_AQ_B)^-] \\ [PQ_AI] \\ [P^+Q_A^-I] \end{pmatrix} \quad (6.4)
$$

The steady state solutions of eq.6.4 are:

$$\begin{pmatrix} [PQ_AQ_B] \\ [P^+(Q_AQ_B)^-] \\ [PQ_AI] \\ [P^+Q_A^-I] \end{pmatrix}_{t\to\infty} = \frac{N}{k_{AP}k_{-I}(\lambda+k_L)+\lambda k_I[I](k_{AP}+k_L)} \cdot \begin{pmatrix} \lambda k_{AP}k_{-I} \\ k_{AP}k_{-I}k_L \\ \lambda k_{AP}k_I[I] \\ \lambda k_Lk_I[I] \end{pmatrix} \tag{6.5}$$

Where $N = [PQ_AQ_B]_t + [P^+(Q_AQ_B)^-]_t + [PQ_AI]_t + [P^+Q_A^-I]_t$ is the total concentration of reaction centers.

Eq.6.5 yields the following relation for the fraction, F_O, of photoxidized RC, as a function of the inhibitor concentration [I]:

$$F_O = \frac{[P^+(Q_AQ_B)^-]+[P^+Q_A^-]}{[N]} = \frac{k_L(k_{AP}+\lambda K[I])}{k_{AP}(\lambda+k_L)+\lambda(k_{AP}+k_L)K[I]} \tag{6.6}$$

where [N] is the total concentration of RCs and $K=k_I/k_{-I}$ is the binding equilibrium for the herbicide. From eq. 6.6, by considering that $k_{AP}\!\gg\!\lambda$ ($k_{AP}\!\approx\!10$ s^{-1}, $\lambda\!\approx\!0.5$ s^{-1}) (Shinkarev and Wraight, 1993), it is clearly seen that the photoxidation level of P varies from a maximum, $F_{O,max} = k_L/(k_L+\lambda)$, for I=0, to a minimum value, $F_{O,min} = k_L/(k_L+k_{AP})$, for I→∞. Actually, as these relationships show, under extreme conditions the steady state level of P$^+$ is simply determined by the competition between charge separation (rate constant k_L) and recombination from P$^+$Q$_A^-$ (rate constant k_{AP}) and P$^+$(Q$_A$Q$_B$)$^-$ (rate constant λ), respectively. It appears therefore that F_O can be taken as a simple measure of herbicide inhibition.

We have tested the behavior predicted by eq. 6.6 in PDDA-RC PEM by measuring the time course of P photoxidation from the absorbance bleaching induced at 870 nm by continuous illumination. The measuring beam at 870 nm was sufficiently intense to act also as excitation (actinic) light source.
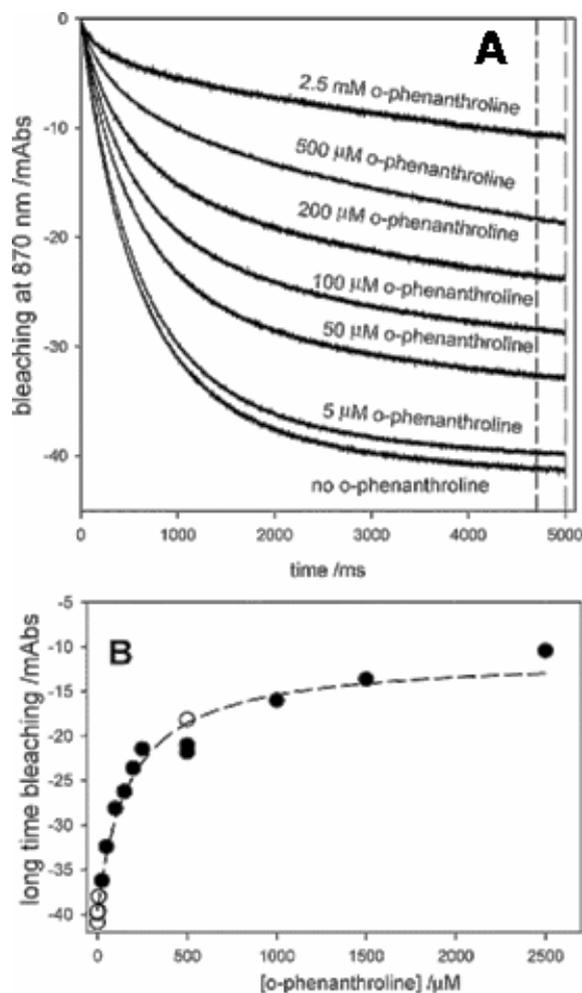
Fig. 6.7 (A) Time course of RC photobleaching induced by continuous illumination at 870 nm and measured on the same PDDA-RC PEM immersed in solutions of *o*-phenanthroline at different concentration (indicated in the labels). (B) Values of absorbance change after 5 s of illumination versus herbicide concentration (values of absorbance change are from the traces of panel A, averaged over the time interval bracketed by the dashed lines). Closed circles refer to measurements done by dipping the specimen in solutions of increasing *o*-phenanthroline concentration; the specimen was then extensively washed with water and selected solutions were assayed (open circles). Fitting the data to eq 6.7 (dashed line) yields $aK = 6 \pm 1$ mM^{-1}.

Fig. 6.7 shows the absorbance changes recorded over 5 s for a PDDA-RC PEM dipped in solutions of different o-phenantroline concentration. It is clear that the measuring beam is actinic enough to induce an evident bleaching at this wavelength (*i.e.* photoxidation of the primary donor P); moreover the steady maximal extent of this bleaching reached after prolonged illumination decreases upon increasing the inhibitor concentration in equilibrium with the multilayer, as expected from eq. 6.6 (see **Fig.**

6.7B). The fractional extent of P photoxidation (F_O) reached under continuous illumination can be compared with the fraction X of RC bound to the inhibitor, evaluated from the relative amplitude of fast $P^+Q_A^-$ recombination in single-turnover experiments as described in the previous section. Starting from equation. 6.6, a useful index of inhibition F_I, based on the measured bleaching data, can be defined as

$$F_I = \frac{F_{O,\max} - F_O}{F_{O,\max} - F_{O,\min}} = \frac{aK[I]}{1 + aK[I]} \tag{6.7}$$

where $a = \dfrac{\lambda(k_L + k_{AP})}{k_{AP}(k_L + \lambda)}$ and $0 \le F_I \le 1$. Eq. 6.5 has the form of a binding isotherm (see

equation 6.2), where the binding constant is replaced by (aK). Being $k_{AP} > \lambda$ (see above), it follows that $a \le 1$, *i.e.* F_I will titrate with an apparent binding constant lower or equal than the real one. According to eq. 6.3, the corresponding fractional inhibition based on X is $F'_i = (X - X_{\min})/(X_{\max} - X_{\min}) = K[I](1 + K[I])^{-1}$, and depends only on the true binding constant K. The inhibition index F_I obtained from continuous light measurements and the fractional inhibition F'_I of the Q_B-site evaluated from single turnover recombination kinetics are compared in **Fig. 6.8**. It is clear that the two approaches, probing on different time scales and illumination regimes the interaction between the herbicide and RC, yield very close binding isotherms. In fact, the dependence of F_I upon *[I]* fits eq. 6.7 for *(aK)*=6±1 mM^{-1}, *i.e. a*=0.9±0.2≈1. Being *a* so close to unity, under our experimental conditions, $k_L \ll \lambda \sim 1$ s^{-1}. This is somehow expected because photobleaching reaches a steady level only after a long illumination (several seconds, see. **Fig. 6.7A**). A remarkable implication of the results shown in **Fig. 6.8** is that photobleaching measurements performed on PDDA-RC with a low enough intensity of the measuring beam, successfully probe the inhibition of Q_B site within the RC protein. The main advantage of this approach is that it requires a simple instrumentation (single beam at fixed wavelength and very low time resolution) and it does not require any deconvolution of kinetic traces (only the steady state value F_O is required).
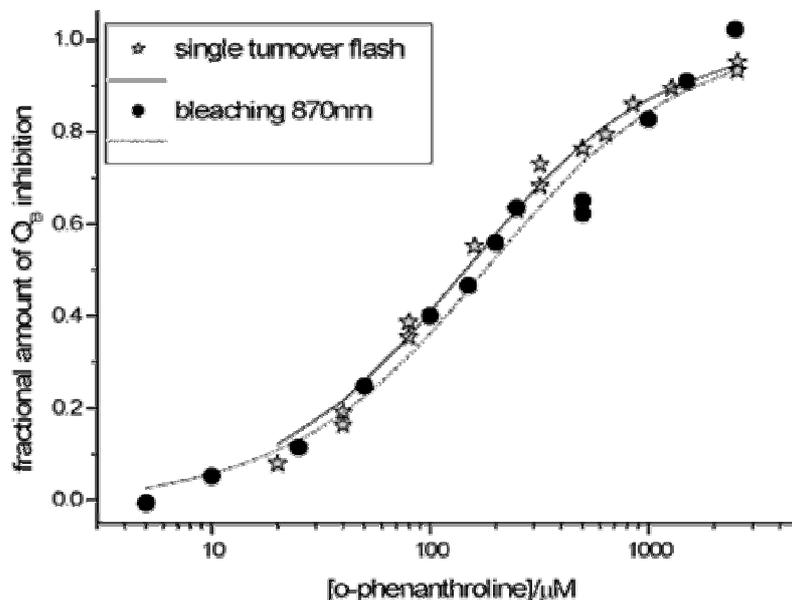
Fig. 6.8 A comparison between the fractional extent of Q_B inhibition determined from single-turnover flash (stars) and continuous illumination (closed circles) experiments. See text for details.

In agreement with our observations, previous studies had shown that titration-like curves could be obtained in *solutions* of RCs by plotting the extent of bleaching against the herbicide concentration (Jockers *et al.*, 1993; Baldini *et al.*, 2003). We note, however, that no attempt was made in these studies to quantitatively account for the obtained titrations in terms of the binding constant and of the kinetic parameters of the system. We have shown here that, under appropriate conditions, a true binding constant can be easily evaluated from photobleaching induced by continuous illumination.

Several limitations have precluded a practical use of bacterial RC solutions in herbicide bioassays. A first drawback is the low intrinsic affinity of most herbicides for the RCs from purple bacteria; this aspects, which is related to a specific feature of the protein and not to the bioassay design, limits considerably the sensitivity of any RC-based bioassay. Other limitations are related to the cost of the protein and to the repeatability and reproducibility of the bioassay test. Although the purification protocols for RC are well assessed, its purification suffers of all the problems common to membrane proteins: high cost and low yield (compared to hydrosoluble proteins). In addition, the inhibitor/quinone competition at Q_B site implies that the binding

equilibrium of quinone itself has to be considered. While the mechanisms of the herbicide/quinone competition are reasonably well understood (Shinkarev and Wraight, 1993), a practical strategy to control the quinone occupancy at the Q_B site is still lacking. Native ubiquinone is very hydrophobic and its loading requires the use of detergents or organic solvents. On the other hand, hydrophilic quinones are relatively labile in solution. In both cases a high controlled level of Q_B occupancy is not easily obtained and maintained upon storage in solution RCs. For analytical purposes this means that a relatively large amount of RCs (reconstituted at the Q_B site) must be used to determine the calibration curve (bleaching versus herbicide concentration) and to test in close sequence the unknown samples. Most importantly, the protein in solution cannot of course be reemployed in subsequent assays. All these aspects make quite unpractical the use of RC solutions for large scale herbicide screenings.

The incorporation of RC into layer-by-layer assemblies overcomes many of these weaknesses. Since the herbicides can be efficiently washed out, the PDDA-RC multilayers can be reused for several samples. This property, coupled with the exceptional stability of the RC when embedded into layer-by-layer assemblies (up to seven months when stored at 4°C), make possible to perform complete runs (calibration curve plus unknowns) with a small amount of protein (1-2 nmoles with our plates). As an example in **Fig. 6.9** we show titration curves obtained with the same specimen for two different herbicides (o-phenantroline and terbutrine). Also in the case of terbutrine, the dependence of steady state photobleaching upon the inhibitor concentration is well described by eq. 6.7, yielding a binding constant aK=0.39±0.06 mM^{-1}. It should be stressed that the two isotherms in **Fig. 6.9** have been obtained using the same PDDA-RC PEM (the time elapsed between the assays on different herbicide was one month). Moreover, experiments with a given herbicide were performed during several days and some measurements were carried out after extensive washing (see caption in **Fig. 6.9**) thus simulating the assay of an unknown sample. The consistent, reproducible results shown in **Fig. 6.9** denote that this approach allows to assay many samples by using a single PDDA-RC over an extended period of time.
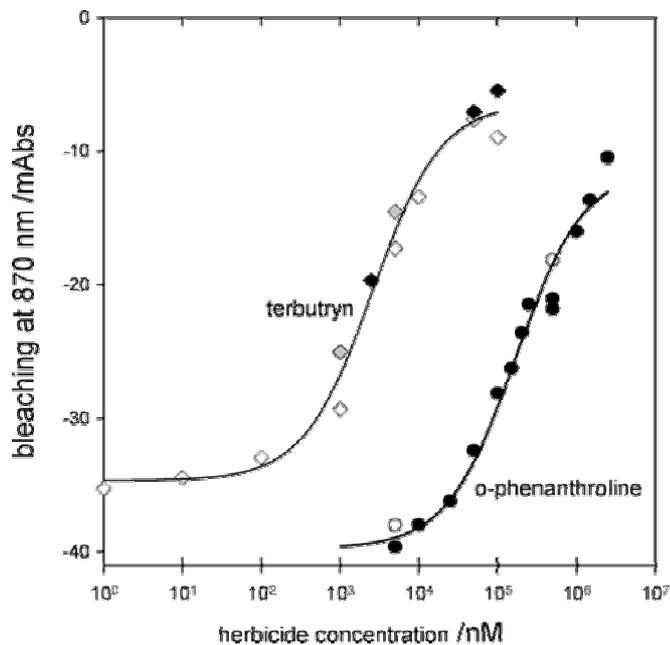
Fig. 6.9 Titration-like curves (extent of photobleaching vs herbicide concentration) obtained by continuous illumination of the same PDDA-RC PEM: Circles, o-phenanthroline; diamonds, terbutryn. In both cases open, closed, and shadowed symbols refer to different runs performed after extensive rinsing with water. Continuous curves are fit to the data according to eq 6.7 (o-phenanthroline, $aK = 6 \pm 1$ mM^{-1}; terbutryn, $aK = 0.39 \pm 0.06$ mM^{-1}).

7   CONCLUSIONS

The more relevant results obtained by examining the RC in its native environment, *i.e.* when associated with the inner antenna complex LH1, are:

i)   The light-induced charge separated state $P^+Q_B^-$ is markedly stabilized (by about 40 meV) in the core complex as compared to the RC-only system over a physiological pH range;

ii) The RC-LH1 complex copurifies with a tightly bound lipid complement of about 90 phospholipid molecules per RC, which is strongly enriched in cardiolipin as compared to the average composition of the membrane;

iii) A large fraction of the ubiquinone pool of the intracytoplasmic membranes is found associated with the RC-LH1 complex, giving rise to a quinone concentration about ten times larger than the average one in the membrane. This quinone pool is fully functional, *i.e.* it is promptly available at the Q_B site during multiple turnover excitation of the RC.

The latter two observations suggest important heterogeneities and anisotropies in the native membranes which can in principle account for the stabilization of the charge separated state in the core complex. The thermodynamic and kinetic parameters obtained in the RC-LH1 complex are very close to those measured in intact membranes, indicating that the electron transfer properties of the RC *in vivo* are essentially determined by its local environment.

The studies performed by incorporating the RC into saccharidic matrices evidenced the relevance of solvent-protein interactions and dynamical coupling in determining the kinetics of electron transfer processes. This analysis also showed that embedding the RC into trehalose glasses is a powerfull tool in probing the relationship between conformational dynamics and electron transfer. The usual approach when studying the interplay between internal motions and protein function consists in freezing the degrees of freedom of the protein at cryogenic temperature. The trehalose approach discussed in the present thesis offers distinct advantages with respect to this traditional methodology. We showed, in fact, that the RC conformational dynamics, coupled to specific electron transfer processes, can be modulated by varying the hydration level of the trehalose

matrix *at room temperature*, thus allowing to disentangle solvent from temperature effects.

The comparison between different saccharidic matrices has revealed that the structural and dynamical protein-matrix coupling depends strongly upon the sugar. In particular we found that two homologous disaccharides, trehalose and sucrose, determine a tight-coupling and a nano phase separation respectively. This conclusion was inferred independently from the kinetic analysis of charge recombination and from the time course of thermal denaturation in RC embedded in sucrose and trehalose glasses characterized by a comparable water content. The comparison between the behaviour in trehalose and sucrose can provide an explanation for the peculiar efficacy of trehalose in biopreservation. In agreement with experimental observations and molecular dynamics simulations performed on soluble proteins incorporated into sugar amorphous matrices, we propose that the protein-matrix coupling in these systems is essentially determined by a network of water-mediated hydrogen bonds which connects the protein surface to the matrix. In the case of trehalose, upon decreasing the hydration of the matrix, a progressively larger fraction of the residual water molecules is involved in such a hydrogen bond network. In this way the protein surface is locked to the matrix, which becomes more and more rigid upon dehydration. The tight structural and dynamical RC-matrix coupling hinders the protein conformational changes which are associated with electron transfer and also the large scale conformational dynamics involved in protein denaturation. As compared to trehalose, sucrose exhibit a low propensity to form such water-protein-sugar structures, most likely because in the case of sucrose the formation of intra-molecular H-bonds competes successfully with the formation of an hydrogen bond network connecting sugar molecules with protein surface groups via water molecules. As a result, at sufficiently low water contents, the dynamics of the RC becomes uncoupled from that of the rigid sucrose matrix (nano phase separation), and the electron transfer kinetics resembles that observed in solution. In line with this scenario the kinetics of thermal denaturation of the RC in an extensively dehydrated, solid sucrose matrix barely differs from that of a RC-film dehydrated in the absence of sugar.

The analyses performed in RCs embedded in polyelectrolyte multilayers (PEM) structures have shown that the electron transfer from Q_A^- to Q_B, a conformationally gated process extremely sensitive to the RC environment, can be strongly modulated by the hydration level of the matrix, confirming analogous results obtained for this electron transfer reaction in sugar matrices. We found that PEM-RCs are a very stable system, particularly suitable to study the thermodynamics and kinetics of herbicide binding to the Q_B site. These features make PEM-RC structures quite promising in the development of herbicide biosensors.

The studies discussed in the present thesis have shown that, although the effects on electron transfer induced by the native and artificial environments tested are markedly different, they can be described on the basis of a common kinetic model which takes into account the static conformational heterogeneity of the RC and the interconversion between conformational substates. Interestingly, the same distribution of rate constants (*i.e.* a Gamma distribution function) can describe charge recombination processes in solutions of purified RC, in RC-LH1 complexes, in wet and dry RC-PEM structures and in glassy saccharidic matrices over a wide range of hydration levels. In all systems the $P^+Q_A^-$ recombination kinetics was found to probe the RC conformational state and dynamics; the average rate constant and the variance of the rate distribution function gave valuable and consistent information on the ability of the RC to relax from the *dark-adapted* to the stabilized *light-adapted* state and on the rate of thermal interconversion over the essentially continuous ensemble of conformational substates. This kinetic model come out to be appropriate also when discussing charge recombination of the $P^+Q_B^-$ state in a highly organized system (LH1-RC core complex), in which it could account for the pH dependence of the rate constant distribution in terms of RC protonation states and of their interconversion rate relative to that of charge recombination.

In conclusion, the results obtained for RCs in different physico-chemical environments emphasize the relevance of the structure/dynamics solvent/protein coupling in determining the energetics and the kinetics of electron transfer processes in a membrane protein complex.

8 REFERENCES

Aklujkar M., Beatty J.T. (2006) *Photosynt. Res.* **88**: 159-171

Alexov E.G., Gunner M.R. (1999) *Biochemistry* **38**: 8253-8270

Allen J.P., Williams J.C., Graige M.S:, Paddock M.L., Feher G., Okamura M.Y. (1998) *Photosyn. Res.* **55**: 227-233

Allen J.P., Feher G., Yeates T.O., Komiya H., Rees D.C. (1987a) *Proc. Natl. Acad. Sci. USA* **84**: 5730-5734.

Allen J.P., Feher G., Yeates T.O., Komiya H., Rees D.C. (1987b) *Proc. Natl. Acad. Sci. USA* **84**: 6162-6166.

Arata H. (1985) *Biochim,. Biophys. Acta* **809**: 284-287

Arata H., Parson W.W. (1981) *a* **636**: 70-81

Baccarini-Melandri A., Melandri B.A. (1971) *Methods Enzymol.* **23**: 556-561

Bahatyrova S., Frese R.N., Siebert C.A., Olsen J.D., van der Werf K.O., van Grondelle R., Niederman R.A., Bullogh P.A., Otto C., Hunter C.N. (2004) *Nature* **430**: 1058-1061

Bahatyrova S., Frese R.N., van der Werf K.O., Otto C., hunter C.N., Olsen J.D. (2004b) *J. Biol. Chem.* **279**: 21327-21333

Baldini F., Domenici C., Giannetti A., Masci D., Mencaglia A. (2003) *Sens. Actuators* **90**: 198-203

Banks K.E., Hernandez S. (2003) *Talanta* **61**: 257-265

Barz W.P., Oesterhelt D. (1994) *Biochemistry* **33**: 9741-9752

Barzen C., Brecht A., Gauglitz G. (2002) *Biosens. Bioelectron.* **17**: 289-295

Belton P.S. and Gil A.M. (1984) *Biopolymers* **34**: 957-961

Benning C., (1998) in "Lipids in photosynthesis: Structure, Function and Genetics" eds. Siegenthaler P.A. & Murata N. (Kluwer, Dordrecht, The Netherlands) pp. 83-101

Bier F.F., Jockers R., Schmid R.D. (1994) *Analyst* **119**: 437-441

Birrell G.B., Sistrom W.R., Griffith O.H. (1978) *Biochemistry* **17**: 3768-3773

Bligh E.G., Dyer WJ. (1959) *Can. J. Biochem. Physiol.* **37**: 911-917

Bonner O.D., Choi Y.S. (1974) *J. Phys. Chem.* **78**: 1723-1731

Bosco M., Culeddu N., Toffanin R., Pollesello P. (1997) *Anal. Biochem.* **245**: 38-47

References

Bourgeois D., Vallone B., Schotte F., Arcovito A., Miele A.E., Sciara G., Wulff P., Anfinrud M., Brunori M. (2003) *Proc. Natl. Acad. Sci.* **100**: 8704-8709

Bowyer J.R., Meinhardt S.W:, Tierney G.V.,Crofts A.R. (1981) *Biochim. Biophys. Acta* **635**: 167-186

Bradford M.M. (1976) *Anal. Biochem.* **72**: 248-254

Braun P., Scherz A. (1991) *Biochemistry* **21**: 5177-5184

Brecht A., Piehler J., Lang G., Gauglitz G. (1995) *Anal. Chim. Acta* **311**: 289-299

Breton J. (2004) *Biochemistry* **43**: 3318-3326

Breton J., Boullais C., Mioskowsky C., Sebban P., Baciou L., Nabedryk E. (2002) *Biochemistry* **41**: 12921-12927

Brzezinski P., Andreasson L.E. (1995) *Biochemistry* **34**: 7498-7506

Busselez J., Cottevieille M., Coniasse P., Gubellini F., Boisset N. (2007) *Structure* **15**: 1674-1683

Byrne B., Iwata S. (2002) *Curr. Opin. Structural. Biol.* **12**: 239-243

Camara-Artigas A., Brune D., Allen J.P. (2002) *Proc. Natl. Acad. Sci.* **99**: 11055-11060

Carpenter J.F. and Crowe J.H. (1989) *Biochemistry* **28**,: 3916-3922

Casadio R., Melandri B.A., Piretti M.V., Serrazanetti G.P. (1979) *Ital. J. Biochem.* **28**: 183-193

Cherepanov D.A., Krishtalik L.I., Mulkidjanian A.Y. (2001) *Biophys. J.* **80**: 1033-1049

Cherepy N.J., Shreve A.P., Moore L.J., Boxer S.G., Mathies R.A. (1997) *J. Phys. Chem. B* **101**: 3250-3260

Chory J., Donohue T.J., Warga A.R., Staehelin L.A., Kaplan S. (1984) *J. Bacteriol.* **159**: 540-554

Clayton R.K. (1966) *Photochem. Photobiol.* **5**: 669-677

Clayton R.K. (1963) in "*Bacterial Photosynthesis*" (Gest H., Pietro A. and Vermon L.P. Eds.) pp. 501-510 The Anthioc press Yellow Spring, OH

Cogdell R.J., Isaacs N.W., Freer A.A., Howard T.D., Gardiner A.T., Prince S.M., Papiz M.Z. (2003) *FEBS Letters* **555**: 35-39

Colaço C., Sen S., Thangavelu M., Pinder S. and Roser B. (1992) *Nature Biotechnol.* **10**: 1007-1011.

Comayras F., Jungas C., Lavergne J (2005a) *J. Biol. Chem.* **280**: 11203-11213

References

Comayras F., Jungas C., Lavergne J (2005b) *J. Biol. Chem.* **280**: 11214-11223

Conrad P.B., de Pablo J.J. (1999) *J. Phys. Chem. A* **103**: 4049-4055

Cordone L., Cottone G., Giuffrida S., Palazzo G., Venturoli G., Viappiani C. (2005) *Biochim. Biophys. Acta* **1749**: 252-281

Cottone G., Giuffrida S., Cicciotti G., Cordone, L. (2005) *Proteins* **59**: 291-302

Cottone G., Ciccotti G., Cordone L. (2002) *J. Chem. Phys.* **117**: 9862-9866

Cottone G., Cordone L., Cicciotti, G. (2001) *Biophys. J.* **80**: 931-938

Cramer W.A., Knaff D.B. (1990) in *"Energy Transduction in Biological Membranes"*, Springer-Verlag, New York.

Crofts A.R. (2000a) *Trends Microbiol.* **8**: 106-107

Crofts A.R. (2000b) *Trends Microbiol.* **8**: 107-108

Crofts A.R., Guergove-Kuras M., Hong S. (1998) *Photosyn. Res.* **55**: 357-362

Crofts A.R. (1986) *J. Bioenerg. Biomembr.* **18**: 437-445

Crofts A.R., Wraight C.A. (1983) *Biochim. Biophys. Acta* **726**: 149-185

Crofts A.R., Meinhardt S.W., Jones K.R., Snozzi M. (1983b) *Biochim. Biophys. Acta* **723**: 202-218

Crowe L.M. (2002) *Comp. Biochem. Physiol. A.* **132**: 505-513

Crowe J.H., Carpenter J.F., Crowe L.M. (1998) *Ann. Rev. Physiol.* **60**: 73-103

Crowe L.M., Reid D.S., Crowe J.H. (1996) *Biophys. J.* **71**: 2087-2093

Crowe J.H., Crowe L.M. (1984) *Science* **223**: 701-703

Crowe J.H., Crowe L.M. and Jackson S.A. (1983) *Arch. Biochem. Biophys.* **220**: 477-484

D'Alfonso L., Collini M., Cannone F., Chirico G., Campanini B., Cottone G., Cordone L. (2007) *Biophys. J.* **93**: 284-293

Das R., Kiley P.J., Segal M., Norville J., Yu A.A., Wang L.Y., Trammell S.A., Reddick L.E., Kumar R., Stellacci F., Lebedev N., Schnur J., Bruce B.D., Zhang S.G., Baldo M. *Nano Lett.* (2004) **4**: 1079-1083

Davidson E., Cogdell R. (1981) *FEBS Letters* **132**: 81-84

Decher, G., Schlenoff, J. B., Eds. *Multilayer Thin Films: Sequential Assembly of Nanocomposite Materials*; Wiley-VCH: Weinheim, Germany, 2003

Deisenhofer J., Michel H. (1989) *EMBO J.* **8**: 2149-2170

References

Deisenhofer J.; Epp O.; Miki K.; Huber R.; Michel H. *Nature* (1985) **31**: 618-624

Dezi M., Francia F., Mallardi A., Colafemmina G., Palazzo G., Venturoli G: (2007) *Biochim. Biophys. Acta* **1767**: 1041-1056

Ditta G., Schmidhauser T., Yakobson E., Lu P., Liang X.W., Finlay D.R., Guiney D., Helinski D.R. (1985) *Plasmid* **13**: 149-153.

Draber W., Tietjen K., Kluth J.F., Trebst A. *Angew. Chem., Int. Ed. Engl.* (1991) **3**: 1621-1633

Drachev L.A., Mamedov M.D., Mulkidjanian A.Ya, Semenov A. Yu., Shinkarev V.P., Verkhovsky M.I. (1989) *FEBS Lett.* **245**: 43-46

Dutton P.L., Petty K.M., Bonner H.S., Morse S.D. (1975) *Biochim. Biophys. Acta* **387**: 536-556

Donohue T.J., Cain B.D., Kaplan S. (1982) *J. Bacteriol.* **152**: 595-606

Ediger M.D. (2000) *Annu. Rev. Phys. Chem.* **51**: 99-128

Ekdawi-Sever N.C., Conrad P.B., de Pablo J.J. (2001*) J. Phys. Chem. A* **105**: 734-742

Engelman D.M. (2005) *Nature* **438**: 578-580

Ermler U., Fritzsch G., Buchanan S.K., Michel H. (1994) *Structure* **2**: 925-936

Eroglu A., Toner M., and Toth T.L. (2002) *Fertil. Steril.* **77**, 152-158

Eroglu A., Russo M.J., Bieganski R., Fowler A., Cheley S., Bayley H. & Toner M. (2000) *Nature Biotechnol.* **18**, 163-167

Farchaus J.W., Grünberg H., Oesterhelt D. (1990a) *J. Bacteriol.* **172**: 977-985

Farchaus J.W., Barz W.P., Grünberg H., Oesterhelt D. (1992) *EMBO J.* **11**: 2779-2788

Feher G., Allen J.P., Okamura M.Y., Rees D.C. (1989) *Nature* **339**: 111-116

Feher G., Okamura M.Y. (1978) in *The photosynthetic Bacteria* Clayton R.K., Sistrom W.R: Eds; Plenum Press: New York pp. 349

Fenimore P.W., Frauenfelder H., McMahon B.H., Parak F.G. (2002) *Proc. Natl. Acad. Sci.* **99**: 16047- 16051

Fernandez-Velasco J., Crofts A.R. (1991) *Biochem. Soc. Trans.* **19**: 588-593

Fotiadis D., Qian P., Philippsen A., Bullough P.A., Engel A., Hunter C.N. (2004) *J. Biol. Chem.* **279**: 2063-2068

Fraker P.J., Kaplan S. (1971) *J. Bacteriol.* **108**: 465-473

Francia F., Dezi M., Rebecchi A., Mallardi A., Palazzo G., Melandri B.A., Venturoli G.

(2004) *Biochemistry* **43**: 14199-14210

Francia F., Giachini L., Palazzo G., Mallardi A., Boscherini F., Venturoli G. (2004b) *Bioelectrochemistry* **63**: 73-77

Francia F., Palazzo G., Mallardi A., Cordone L., Venturoli G. Biochim. (2004c) *Biophys. Acta* **1658**: 50-57

Francia F., Palazzo G., Mallardi A., Cordone L., Venturoli G. (2003) *Biophys. J.* **85**: 2760-2775

Francia F., Wang J., Venturoli G., Melandri B.A., Barz W.P., Oesterhelt D. (1999) *Biochemistry* **38**: 6834-6845

Francia F., Turina P., Melandri B.A., Venturoli G. (1998) in "*Biophysics of Electron Transfer and Molecular Bioelectronics*" Nicolini C., Ed. Plenum Press, New York pp 103-116

Freer A., Prince S., Sauer K., Papiz M., Lawless A.H., McDermott G., Cogdell R., Isaacs N.W. (1996) *Structure* **4**:449-462

Frese R.N., Pàmies J.C., Olsen J.D., Bahatyrova S., van der Weij-de Wit C.D., Aartsma T.J., Otto C., Hunter C.N., Frenkel D., van Grondelle R. (2007) *Biophys. J.* Epub ahead of print

Frese R.N., Siebert C.A., Niederman R.A., Hunter C.N., Otto C., van Grondelle R. (2004) *Proc. Natl. Acad. Sci.* **101**: 17994-17999

Frese R.N., Olsen J.D., Branvall R., Westerhuis W.H.J., Hunter C.N., van Grondelle R. (2000) *Proc. Natl. Acad. Sci.* **97**: 5197-5202

Frauenfelder H., Wolynes P.G. (1994) *Phys. Today* **47**: 58-64

Frauenfelder H., Sligar S.G., Wolynes P.G. (1991) *Science* **254**: 1598-1603

Frauenfelder H., McMahon B. (1998) *Proc. Natl. Acad. Sci.* **95**: 4795-4797

Fyfe P.K., Isaacs N.W., Cogdell R.J., Jones M.R. (2004) *Biochim. Biophys. Acta* **1608**: 11-22

Fyfe P.K., McAuley K.E., Roszak A.W., Isaacs N.W., Cogdell R.J., Jones R.J. (2001) *Trends Biochem. Sci.* **26**: 106-112

Gafert J., Pschierer H., Friedrich J. (1995) *Phys. Rev. Lett.* **74**: 3704-3707

Gall A., Cogdell R.J., Robert B. (2003) *Biochemistry* **42**: 7252-7258

References

Garcia A.F., Venturoli G., Gad'on N., Fernandez-Velasco J.G., Meandri B.A., Drews G.(1987) *Biochim. Biophys. Acta* **890**: 335-345

Gast P., Hemedrijk P.W., Van Gorkom H.J., Hoff A.J. (1996) *Eur. J. Biochem.* **239**: 805-809

Gast P., Hemelrijk P., Hoff A.J. (1994) *FEBS Lett.* **337**: 39-42

Giardi M.T., Pace E. (2005) *Trends Biotechnol.* **25**: 253-267

Gill I., Ballesteros A. (2000) *Trends Biotechnol.* **18**: 282-296

Gill I., Ballesteros A. (2000) *Trends Biotechnol.* **18**: 469-473

Giuffrida S., Cottone G., Cordone, L. (2006) *Biophys. J.* **91**: 968-980

Giuffrida S., Cottone G., Cordone L. (2004) *J. Phys. Chem. B* **108**: 15415-15421

Giuffrida S., Cottone G., Librizzi F., Cordone L. (2003) *J. Phys. Chem. B* **107**: 13211-13217

Giustini M., Castelli F., Husu I., Giovini M., Maliardi A., Palazzo G. (2005) *J. Phys. Chem. B* **109**: 21187- 21196

Giustini M., Palazzo G., Colafemmina G., Della Monica M., Giomini M., Ceglie A. (1996) *J. Phys. Chem.* **100**: 3190-3198

Gomez B., Robinson N.C., (1999) *Biochemistry* **38**: 9031-9038

Gonçalves R.P., Bernadac A., Sturgis J.N., Scheuring S. (2005) *J. Struct. Biol.* **152**: 221-228

Grafton A.K., Wheeler R.A., (1999) *J. Phys. Chem. B* **103**: 5380-5387

Graige M.S., Feher G., Okamura M.Y. (1998) *Proc. Natl. Acad. Sci. USA* **95**: 11679-11684

Gray K.A., Farchaus W., Wachtveitl J., Breton J., Oesterhelt D. (1990) *EMBO J.* **9**: 2061-2070

Gubellini F., Francia F., Busselez J., Venturoli G., Levy D. (2006) *Biochemistry* **45**: 10512-10520

Hampp, N. *Chem. Rev.* (2000) **100**: 1755-1176

Harris R.D., Luff B.J., Wilkinson J.S:, Piehler J., Brecht A., Gauglitz G., Abuknesha R.A. (1999) *Biosens. Bioelectron.* **14**: 377-386

Herek J.L., Wohlleben W., Cogdell R.J., Zeidler D., Motzkus M. (2002) *Letters to nature* **417**: 533-535

Hirsh A. (1987) *Cryobiology* **24**: 214-228

Hoff A.J. (1988) Nomen est omen. A note on nomenclature. In: "T*he photosynthetic bacterial reaction center: structure and dynamic*s" pp. 98-99 (Breton J, Vermeglio A., eds) Plenum Press, New York

Hofmann C., Francia F., Venturoli G., Oesterhelt D., Köhler J. (2003a) *FEBS Letters* **546**: 345-348

Hofmann C., Aartsma T.J., Michel H., Köhler J. (2003b) *Proc. Natl. Acad. Sci.* **100**: 15534-15538

Hoffman B.M., Ratner M. A. (1987) *J. Am. Chem. Soc.* **109**: 6237-6243

Holden M.A.; Bayley H.*J. Am. Chem. Soc.* (2005) **127**: 6502-6503

Holt S.C., Marr A.G. (1965b) *J. Bacteriol.* **89**: 1421-1429

Hu X., Schulten K. (1997) *Phys. Today* **50**: 28-34

Hughes A.V., Rees P., Heathcote P., Jones M.R. (2006) *Biophys. J.* **90**: 4155-4166.

Jenney F.E., Daldal F. (1939) *EMBO J.* **12**: 1283-1292

Jockers R., Bier F.F., Schmid R.D., Wachtveitl J., Oesterhelt D. (1993) Anal. Chim. Acta **274**: 185-190

Joliot P., Vermeglio A., Joliot A. (1989) *Biochim. Biophys. Acta* **975**: 336-345

Jones M.R. (2007) *Progr. Lipid Res.* **46**: 56-87

Jorgensen R.A., Rothstein S.J., Reznikoff W.S. (1979) *Mol. Gen. Genet.* **177**: 65-72

Jungas C., Ranck J.L., Rigaud J.L., Joliot P., Vermiglio A. (1999) *EMBO J.* **18**: 534-542

Katona G., Andreasson U., Landau E.M., Andreasson L.E., Neutze R. (2003) *J. Mol. Biol.* **331**: 681-692

Klein C., Garcia-Rizo C., Bisle B., Scheffer B., Zischka, Pfeiffer F., Siedler F., Oesterhelt D. (2005) *Proteomics* **5**: 180-197

Kleinfeld D., Okamura M.Y., Feher G. (1984a) *Biochemistry* **23**: 5780-5786

Kleinfeld D., Okamura M.Y., Feher G. (1984b) *Biochim. Biophys. Acta* **766**: 126-140

Koepke J., Krammer E.M., Klingen A.R., Sebban P., Ullmann G.M., Fritzsch G. (2007) *J. Mol. Biol.* **371**: 396-409

Koepke J., Hu X.C., Muenke C., Schulten K., Michel H: (1996) *Structure* **4**: 581-597

Kong, J., Lu, Z., Lvov, Y.M., Desamero, R.Z.B., Frank, H.A., Rusling, J.F. (1998),*J.*

Am. Chem. Soc. **120**: 7371-7372

Kriegl J.M., Nienhaus U. (2004) *Proc. Natl. Acad. Sci.* **101**: 123-128

Kuglstatter A., Emler U., Michel H., Baciou L., Fritzsch G. (2001) *Biochemistry* **40**: 4253-4260

Labahn A., Bruce J.M., Okamura M.Y., Feher G. (1995) *Chem. Phys* **197**: 355-366

Lam, Y.H., Bustami, R., Phan, T. Chan, H.K. & Separovic, F. (2002) *J. Pharm. Sci.* **91**: 943-951

Lang H.P., Hunter C.N. (1994) *Biochem. J.* **298**; 197-205

Lange C., Nett J.H., Trumpower B.L., Hunte C. (2001) *EMBO J.* **20**: 6591-6600

Lavergne J., Matthews C., Ginet N. (1999) *Biochemistry* **38**: 4542-4552

Lavergne J., Joliot P. (1991) *Trends Biochem. Sci.* **16**: 129-134

Lavergne J., Joliot P., Vermeglio A. (1989) *Biochim. Biophys. Acta* **975**: 347-355

Lebedev, N., Trammell S.A., Spano A., Lukashev E., Griva I., Schnur J. (2006) *J. Am. Chem. Soc.* **128**: 12034-12348

Lilburn T.G., Haith C.E., Prince R.C., Beatty J.T. (1992) *Biochim. Biophys. Acta* **110**: 160-170

Lee A.G. (2004) *Biochem. Biophys. Acta* **1666**: 62-87

Lin X., Murchison H.A., Nagarajan V., Parson W.W., Allen J.P., Williams J.C. (1994) *Proc. Natl. Acad. Sci.* **91**: 10265-10269

López-Díez, E.C. & Bone, S. (2004) *Biochim. Biophys. Acta* **1673**: 139-148

Lvov Y.; Ariga K.; Ichinose I.; Kunitake T. *J. Am. Chem. Soc.* (1995) **117**: 6117

Mallardi A., Palazzo G., Venturoli G. (1997) *J. Phys. Chem B* **101**: 7850-7857

Mancino L.J., Dean D.P., Blankenship R.E. (1984) *Biochim. Biophys. Acta* **764**: 46-54

Maroti P., Wraight C.A. (1988) *Biochim. Biophys. Acta* **934**: 329-347

McAuley K.E., Fyfe P.K., Isaacs N.W., Cogdell R.J., Jones M.R. (1999) *Proc. Natl. Acad. Sci.* **96**: 14706-14711

McDermott G., Prince S.M., Howard T., Cogdell R.J., Isaacs N.W. (1995) *Nature* **374**: 517-521

McGlynn P., Hunter C.N., Jones M.R. (1994) *FEBS Lett.* **349**: 349-353

McLaughlin S. (1977) *Curr. Top. Membr. Transp.* **9**: 71-144

McMahon B. H., Muller J. D., Wraight C. A., Nienhaus G. U. (1998) *Biophys. J.* **74**:

2567-2587

McPherson P.H., Okamura M.Y., Feher G. (1988) *Biochim. Biophys. Acta* **934**: 348-368

Miller K.R. (1979) *Proc. Natl. Acad. Sci USA* **76**: 6415-6419

Müh F., Schulz C., Schlodder E., Jones M.R., Rautter J., Kuhn M., Lubitz W. *Photosynth. Res.* (1998) **55**: 199-205

Murgia S., Mele S., Monduzzi M. (2003) *Lipids* **38**: 585-591

Nabedryk E., Bagley K.A., Thibodeau D.L., Bausher M., Mäntele W., Breton J. (1990) *FEBS Lett.* **266**: 59-62

Nagy L., Milano F., Dorogi M., Agostano A., Laczkò G., Szebényi K., Vàrò G., Trotta M., Maròti P. (2004) *Biochemistry* **43**: 12913-12923

Nußberger S., Dorr K., Wang D.N., Kuhlbrandt W. (1993) *J. Mol. Biol.* **234**: 347-356

Oelze J., Drews G. (1972) *Biochim. Biophys. Acta* **265**: 209-239

Okamura M.Y., Paddock M.L., Graige M.S., Feher G., (2000) *Biochim. Biophys. Acta* **1458**: 148-163.

Okamura M.Y., Debus R.J., Kleinfeld D., Feher G. (1982) in "*Functiones of quinones in Energy Conserving Systems*" (Trumpower B.L., Ed.) Academic Press New York, pp. 299-317

Okamura M.Y., Isaacson R.A., Feher G. (1975) *Proc. Natl. Acad. Sci. USA* **72**: 3491-3495

O'Neill H.; Greenbaum E. *Chem. Mater.* (2005) **17**: 2654-2661

Onishi J.C., Niederman R.A. (1982) *J. Bacteriol.* **149**: 831-839

Overfield R.E., Wraight C.A:, Devault D. (1979) *FEBS Lett.* **105**: 137-142

Paddock M.L., Rongey S.H., Feher G., Okamura M.Y. (1989) *PNAS USA* **86**: 660-6606

Palazzo G., Mallardi A., Francia F., Dezi M., Venturoli G., Pierno M.,Vignati E., Piazza R. (2004) *Phys. Chem. Chem. Phys.* **6**: 1439-1445

Palazzo G., Mallardi A., Hochkoeppler A., Cordone L., Venturoli G. (2002) *Biophys. J.* **82**: 558-568

Palazzo G., Mallardi A., Giustini A:, Berti D., Venturoli G (2000) *Biophys. J.* **79**: 1171-1179

Palsodottir H., Hunte C. (2004) *Biochim. Biophys. Acta* **1666**: 2-18

Papiz M.Z., Prince S.M., Howard T., Cogdell R.J., Isaacs N.W. (2003) *J. Mol. Biol.*

326: 1523-1538

Parak F.G. (2003) *Rep. Prog. Phys.* **66**: 103-129

Piazza R., Pierno M., Vignati E., Venturoli G., Francia F., Maliardi A., Palazzo G. (2003) *Phys. Rev. Lett.* **90**: 208101 (4 pages)

Piletskaya E.V., El'skaya S.A:, Sozinov A.A:, Marty J.L., Roulillon R. (1999) *Anal. Chim. Acta* **398**: 49-56

Qian P., Hunter N., Bullogh P.A. (2005) *J. Mol. Biol.* **349**: 948-960

Rabenstein B., Ullmann G.M., Knapp E.W. (2000) *Biochemistry* **39**: 10487-10496

Rahaman A., Wheeler R.A. (2004) *Chem. Phys. Phys. Chem.* **5**: 249-252

Rauser G., Fleischer S., Yamamoto A. (1970) *Lipids* **5**: 494-496

Recchia P.A., Davis C.M., Lilburn T.G., Beatty J.T., Parkes-Loach P.A. (1998) *Biochemistry* **37**: 11055-11063

Rinyu L., Martin E.W:, Takahashi E., Maròti P., Wraight C.A. (2004) *Biochim. Biophys. Acta* **1655**: 93-101

Roberts C.J. & Debenedetti P.G. (1999) *J. Phys. Chem. B* **103**: 7308-7318

Roos Y. (1995) Phase Transitions in Foods, Academic Press Ltd., London

Roser B. (1991) *BioPharm.* **4**: 47-53

Roszak A.W., Gardiner A:T., Isaacs N.W., Cogdell R.J. (2007) *Biochemistry* **63**: 593-595

Roth M., Arnoux B., Ducruix A., Reiss-Husson F. (1991) *Biochemistry* **30**: 9403-9413

Roth M., Lewit-Bentley A., Michel H., Deisenhofer J., Huber R., Oesterhelt D. (1989) *Nature* **340**: 659-661

Rubin A.B., Shinkarev V.P. (1984) in *"Electron transfer in biological system"* Nauka, Moscow

Russel N.J., Coleman J.K., Howard T.D., Johnston E., Cogdell R.J. (2002) *Biochim. Biophys. Acta* **1556**: 247-253

Sampedro J.G. and Uribe S. (2004) *Mol. Cell. Biochem.* **256**: 319-327

Schägger H., von Jagow G. (1991) *Anal. Biochem.* **199**:223-231

Schägger H., von Jagow G. (1987) *Anal. Biochem.* **166**: 368-379

Scheuring S. (2006) *Curr. Opin. In Chem. Biol.* **10**: 387-393

Scheuring S., Gonçavales R.P., Prima V., Sturgis J.N. (2006b) *J. Mol. Biol.* **358**: 83-96

References

Scheuring S. Sturgis J.N. (2006c) *Biophys. J.* **91**: 3707-3717

Scheuring S., Busselez J., Levy D. (2005) *J. Biol. Chem.* **280**: 1426-1431

Scheuring S., Sturgis J.N. (2005b) *Science* **309**: 484-487

Scheuring S., Francia F., Busselez J., Melandri B.A., Rigaud J.L., Levy D. (2004) *J. Biol. Chem*. **279**: 3620-3626

Scheuring S., Seguin J., Marco S., Levy D., Breyton C., Robert B., Rigaud J.L. (2003) *J. Mol. Biol.* **325**: 569-580

Shinkarev V.P., Wraight C.A (1997) *Biophys. J.* **72**: 2304-2319

Shinkarev V.P., Wraight C.A: (1993) in "*The photosynthetic reaction center*" (Deisenhofer J., Norris J.R:, Eds.) Academic Press, San Diego1: 193-255

Shinkarev V.P., Kononenko A.A., Rubin A.B. (1984) *Biol. Memb. (USSR)* **1**: 640-650

Schlueserner D., Fisher F., Kruip J., Rögner M., Poetsch A. (2005) *Proteomics* **5**: 1317-1330

Schmid R., Labahn A. (2000) *J. Phys. Chem. B* **104**: 2928-2936

SchneiderP., Goodrow M.H., Gee S.J., Hammock B.D. (1994) *J. Agric. Food Chem*. **42**: 413-422

Schonhoff M. *Curr. Opin. Colloid Interface Sci.* (2003) **8**: 86-95; Schonhoff, M. *J. Phys.: Condens. Matter* (2003) **15**: R1781

Sebban P., Maròti P., Shiffer M., Hanson D. (1995) *Biochemistry* **34**: 8390-8397

Sener M.K., Olsen J., Hunter C.N., Schulten K. (2007) *Proc. Natl. Acad. Sci.***104**: 15723-15728

Singer S. J., Nicolson G. L. (1972) *Science* **175**: 720–731

Skl'adal P. (1999) *Biosens. Bioelectron.* **14**: 257-263

Slooten L. (1972) *Biochim. Biophys. Acta* **275**: 208-218

Steffen M.A., Lao K., Boxer S.G. (1994) *Science* **264**: 810-816

Stein R.R., Castellvi A.L, Bogacz J.P, Wraight C.A., (1984) *J. Cell. Biochem.* **24**: 243-259

Stowell M. H. B., McPhillips T. M., Rees D. C., Soltis S. M., Abresch E., Feher G. (1997) *Science* **276**: 812-816

Straley S.C., Parson W.W., Mauzerall D.C., Clayton R.C. (1973) *Biochim. Biophys.*

Acta **305**: 597-609

Stuart, J. A.; Marcy, D. L.; Wise, K. J.; Birge, R. R. *Synth. Met.* (2002) **127**: 3-15

Sturgis J.N., Niederman R.A. (2007) *Photosyn. Res*. Oct 9 Epub ahead of print

Sun W.Q. and Davidson P. (1998) *Biochim. Biophys. Acta* **1425**: 235-244

Takamiya K.I., Dutton P.L. (1979) *Biochim. Biophys. Acta* **546**: 1-6

Tunnicliffe R.B., Ratcliffe E.C., Hunter C.N., Williamson M.P. (2006) *FEBS Lett.* **580**: 6967-6971

Uritani M., Takai M. and Yoshinaga K. (1995) *J. Biochem.* **117**: 774-779

Van der Rest M. & Gringas G. (1974) *J. Biol. Chem.* **249**: 6446-6453

Van Mourik F., Reus M., Holzwarth A.R. (2001) *Biochim. Biophys. Acta* **1504**: 311-318

Varanesi L., Mills D., Murphree A., Gray J., Purser C., Baker R., Hosler J. (2006) *Biochemistry* **45**: 14896-14907

Venturoli G., Fernandez-Velasco J.G., Crofts A.R., Melandri B.A. (1986) *Biochim. Biophys. Acta* **851**: 340-352

Vermeglio A., Joliot P. (2000) *Trends Microbiol.* **8**: 106-107

Vermeglio A., Joliot P., Joliot A. (1993) *Biochim. Biophys. Acta* **1183**: 352-360

Vermeglio A., Klayton R.K. (1977) *Biochim. Biophys. Acta* **461**: 159-165

Walden S.E., Wheeler R.A. (2002) *J. Phys. Chem. B* **106**: 3001-3006

Walkers W.F., Walker N.J., Tamari Y., Tablin, F. and Crowe, J.H. (2003) *Cell Preservation Technol.* **1**, 175-188

Walz T., Jamieson S.J., Bowers C.M., Bullough P.A., Hunter C.N. (1998) *J. Mol. Biol.* **282**: 833-845

Wang H., Lin S., Allen J.P., Williams J.C., Balnkert S., Laser C., Woodbury N.W. (2007) *Science* **316**: 747-750

Wang S., Lin S., Lin X., Woodbury N.W., Allen J.P. (1994) *Photosyn. Res.* **42**: 203-215

Woese C.R. (1987) *Bacterial evolution. Microbiol. Rev.* **51**: 221-271

Wraight C.A. (1981) *Israel J. Chem.* **21**: 348-354

Wraight C.A., Stein R.R. (1983) in "The oxygen Evolving System of Photosynthesis" (Inoue Y., Crofts A.R., Govindjee, Murata N., Renger G., Satoh K., eds.) Academic press Tokyo, pp. 383-391

Wraight C.A. (1977) *Biochim. Biophys. Acta* **459**: 525-531

References

Wraight C.A. Cogdell R.J., Clayton R.K. (1975) *Biochim. Biophys. Acta* **396**: 242-249

Xu Q., Gunner M.R. (2002) *Biochemistry* **41**: 2694-2701

Xu Q., Baciou L., Sebban P., Gunner M.R. (2002b) *Biochemistry* **41**: 10021-10025

Zhao J., Liu B., Zou Y., Xu C., Kong J. (2002) *Electrochim. Acta* **47**: 2013-2017

Acknowledgements

Questa tesi non è solo il riassunto dei tre anni di lavoro svolto durante il PhD, ma anche una parte importante degli ultimi tre anni della mia vita. Per questo vorrei sinceramente ringraziare tutte le persone che hanno contribuito in qualsiasi modo all'ottenimento di tanti risultati. Per questo vorrei farlo in un amichevole italiano e non in un formale inglese.

In primis, vorrei ringraziare il mio tutor Giovanni Venturoli per essere stato una guida preziosa e costante e per il suo modo di affrontare sempre i problemi con un sorriso distensivo.

Secondo a nessuno, un grazie speciale al co-tutor, oltre che amico, Francesco Francia, insostituibile biochimico, e abilissimo "problem solver". Grazie per l'immancabile e continuo supporto morale durante questi tre anni, per le copiose consulenze tecniche e per le chiacchiere nel buio del sottomarino.

Un grazie a Lisa e alla Manu, grandi amiche e consigliere tanto dentro quanto fuori dal laboratorio. Un grazie ad Albert per la costanza nel creare ordine laddove l'ordine si pensava non potesse esistere. Un ringraziamento sincero va anche a tutti quelli che mi hanno prestato consigli, protocolli e strumenti (ahimè) mai resi e a quelli sempre disponibili per una chiacchiera, un conforto, un aperitivo o un terribile caffè della macchinetta, al sole (o all'ombra per alcuni) sulle scale del dipartimento.

Chiaramente mille grazie alla pazienza di Danilo, che volente o nolente ha condiviso interamente con me le gioie e i dolori di queti tre anni, oltre che la crescita di svariati litri di batteri nei fine settimana passati facendo "un salto" all'orto.

Per finire vorrei dedicare questi tesi anche a tutti i miei insostituibili amici (ci siete tutti, vicini e lontani), molti dei quali ancora si chiedono come sia possibile allevare batteri, per non avermi fatto diventare un topo di laboratorio.

Grazie alla mia famiglia che ha contribuito al raggiungimento di questo importante risultato, con stima e fiducia incommensurabili (e non solo).

In ultimo, grazie anche agli ostacoli e ai contrattempi perché anche loro sono stati fonte di stimoli e di reazioni inattese.

<div align="right">...grazie a tutti di cuore!</div>